Oceanic tides: A response to differential force throughout the earth's history

Oceanic tides arise from a differential force on the earth due to the moon and sun, as the earth and moon revolve about their common center of mass. I discuss how differential force arises in an object and then address the earth–moon system. I examine tides at a global scale, an ocean scale, and a coastal scale. Finally I show how sedimentary rock layers preserve ancient tidal cycles and provide insight into the earth–moon distance over the course of the earth's history.

Carl H. Tape
Advisor: Professor William Titus
Physics Senior Integrative Exercise
May 17, 2001

Submitted in partial fulfillment of the requirements for a
Bachelor of Arts degree from Carleton College, Northfield, Minnesota

Author's note

I decided to transfer my physics undergraduate thesis from Microsoft Word into Latex, in order to have an easily accessible version. I also added the reference *Tape et al.* (2003).

A PDF of this document can be downloaded from here:

http://www.gps.caltech.edu/~carltape/research/pubs/thesis/tides_CHT_thesis.pdf

A supplemental set of notes can be downloaded from here:

http://www.gps.caltech.edu/~carltape/research/pubs/thesis/tides_CHT_thesis_supplement.pdf

I would appreciate advice for improvements or any corrections.

Carl Tape

August 2005

carltape@gps.caltech.edu

Table of Contents

List of Figures

List of Tables

1 Introduction

The rise and fall of the ocean tides in coastal areas is as commonplace as the sight of the moon in the sky (Figure 1A). Why does the water rise and fall? We see two tides a day at equal intervals, so we might infer that the earth is spinning under two "bulges" of water on opposite sides of the earth (Figure 1B). Intuitively, one might expect a bulge on the side facing the moon, since it seems to be pulling the ocean toward it, but why the bulge on the opposite side? Most people have a sense that the tides are related to the moon and gravity, but few can offer an adequate explanation for the twice-a-day tides. One physicist remarked, "Many teachers are still not satisfied with the clarity of existing explanations, and students, when their guard is down, profess to be unable to discriminate it from black magic" (*Arons*, 1979).

The subject of tides is all-encompassing. Tides are an aspect of several fields of science, including astronomy, hydrodynamics, oceanography, climatology, geophysics, and sedimentology. Tides have been present throughout the earth's history — preserved in the geologic record by layers in sedimentary rocks, and preserved in the written record by writers and scientists alike.[1] Tides on the earth are not limited to the rise and fall of the sea; the solid earth and the atmosphere experience tides as well.[2] An understanding of the mechanism behind tides allows one to understand, and greater appreciate, the response of the earth. I will begin by describing the forces that cause tides, which will provide a basis for analyzing the tides of the oceans. I will finish by examining how layers in sedimentary rocks can record ancient tidal cycles and provide insights into the history of the earth–moon system.

2 Tidal force

2.1 Newton, gravity, and centripetal acceleration

In 1687 Isaac Newton published the consequences of gravitation in *Principia*, which included an explanation of the observed tides in terms of mechanics. Analyzing celestial observations, Newton discovered the universal law of gravitation, which states that the gravitational force between two objects is directed along their line of centers and has a magnitude given by

$$F = \frac{G\, m_1\, m_2}{r^2} \tag{1}$$

where m_1 and m_2 are masses of each object, r is the distance of separation of the centers of masses, and $G = 6.67 \times 10^{-11}$ N m^{-2} kg^{-2} is the gravitational constant.[3] Thus, at the surface of the earth, a spherically symmetric object of mass m is attracted to the earth's center of mass

---

[1] *Darwin* (1898, Ch. 4) contains an excellent review of the history of tides. Aristotle noted a relation between tides and the moon in 350 B.C. (*Strahler*, 1971, p. 129). The Roman historian Pliny the Elder (A.D. 23–79), discussing the work of "clever researchers," remarked on the period of the tides (*French and Greenaway*, 1986, p. 179–180).

[2] There are several books treating earth tides and atmospheric tides: see Appendix D.

[3] We will assume that the objects have spherically symmetric mass distributions, so we can treat all of the mass as being concentrated at the object's center of mass (e.g., *Fowles*, 1962, p. 112–118).

with a force

$$F = \frac{G\,M_e\,m}{r_e^2} = m\,g \tag{2}$$

where $g \equiv G\,M_e/r_e^2 \approx 9.81$ m s^{-2} (Figure 2) (see Table 1 for a table of constants).

Centripetal acceleration is the inward directed acceleration due to an object moving in circular motion.[4] Any object moving in a circular orbit has a centripetal acceleration directed toward the center of the circle with magnitude $a = v^2/r$, where v is the speed of the object and r is the radius of the circular orbit. Circular orbits occur due to (1) the gravitational attraction between objects (Eq. 1) and (2) the specific initial conditions (velocity and position) that allow two objects to reach an equilibrium of circular motion. In other words, the gravitational attraction between two objects will cause them to *deviate from linear motion* and possibly come into a circular orbit about each other. For instance, at each instant in time, the earth deflects the moon from its projected linear trajectory. Two objects in circular orbits are attracted by a gravitational force alone (Eq. 1); thus, by Newton's 2nd Law ($\mathbf{F_{net}} = m\,\mathbf{a}$), the net force is in the direction of centripetal acceleration, which is parallel to the line connecting the center of masses of the two objects. Similarly, two objects moving toward each other in linear trajectories are attracted by a gravitational force in the same direction, the line connecting the center of masses of the two objects. Each case is an example of two objects accelerating toward each other under the influence of gravity alone, a scenario known as free fall.

2.2 Differential, or tidal, force defined

A body of finite extent located in a gravitational field is subject to a differential force. The gravitational force varies over the extent of the body, since different parts of the object are at different distances to the source of the gravitational field. Because one of the most apparent consequences of a differential force are the tides, the term *tidal force* is used interchangeably with *differential force*. A rod falling vertically (Figure 3A) experiences a differential force; thus, assuming a non-rigid rod, the top of the rod will accelerate downward less than the center of the rod, which in turn will accelerate less than the bottom of the rod. Relative to the center, the top accelerates upward, the bottom accelerates downward, and the rod tends to pull apart.

The example of the object in free fall illustrates the concept of differential force, and it is analogous to the tide-producing situation on the earth. It is helpful to first consider the simplest scenario — a fixed mass with an object in free fall toward it. The effects of the water, the moon, the sun, the earth's rotation, and circular orbits are necessary to understand the observed tidal patterns on the earth, but they tend to complicate the understanding of differential force.

---

[4]The object doesn't have to be moving in a closed circular orbit to have centripetal acceleration; any nonlinear path of motion will have a component of centripetal acceleration (e.g., *Tipler*, 1991, p. 69).

2.3 A laboratory in free fall

Our laboratory for conducting experiments is an object — for example, a rod, a sphere, or a spaceship — that is accelerating vertically in free fall toward the center of the earth.[5] In each example, we would not expect Newton's laws to hold, since our reference frame is accelerating and is thus non-inertial. We first extend the example of the falling rod to a falling, rigid, spherical laboratory having uniform mass, and we focus only on the points within the lab in the line of center to the earth (Figure 3B). As with the rod, the force at the point nearest the earth is greatest at the bottom of the lab and smallest at the top. Using Equation (2), the force on a test mass m near the top (A), center (B), and bottom (C) are given by

$$f_A = \frac{F_A}{m} = \frac{G\,M_e}{(d+r_0)^2} \tag{3}$$

$$f_B = \frac{F_B}{m} = \frac{G\,M_e}{d^2} \equiv g_0 \tag{4}$$

$$f_C = \frac{F_C}{m} = \frac{G\,M_e}{(d-r_0)^2} \, . \tag{5}$$

Simplification, followed by a first-order binomial expansion, leads to

$$f_A = \frac{g_0}{\left(1 + \frac{r_0}{d}\right)^2} = g_0\left(1 - \frac{2r_0}{d} + \cdots\right) \approx g_0 - \frac{2r_0\,g_0}{d} \tag{6}$$

$$f_B = g_0 \tag{7}$$

$$f_C = \frac{g_0}{\left(1 - \frac{r_0}{d}\right)^2} = g_0\left(1 + \frac{2r_0}{d} + \cdots\right) \approx g_0 + \frac{2r_0\,g_0}{d} \, . \tag{8}$$

We now conduct our experiments inside the accelerating lab. We release three balls, one at each point. The ball released near the top (A) has an *upward* acceleration $-2r_0\,g_0/d$ relative to the center of the spaceship ($f_A - f_B$); therefore, it accelerates toward the top of the ship. The ball released at the center (B) has the same acceleration as the spaceship and remains stationary. The ball released near the bottom (C) has a *downward* acceleration $2r_0\,g_0/d$ relative to the center of the spaceship ($f_C - f_B$); therefore, it accelerates toward the bottom of the ship.

Although it is not obvious, this system is roughly analogous to the differential (tidal) force on the earth (Figure 4). Replace the earth with the moon and replace the spherical lab with the earth; the earth is now accelerating toward the fixed moon. The point facing the moon (C) accelerates toward the moon, relative to the earth's center (B); this corresponds to the tidal bulge facing the moon. The point facing opposite the moon (A) accelerates away from the moon relative to the earth's center; this corresponds to the tidal bulge opposite the moon. The previous example shows that circular motion is not required to explain the origin of differential force. Figure 5 compares the differential force due to free fall in linear motion and that due to free fall in circular motion. The "laboratory" in this case is an initially spherical water droplet that is stretched in a radial direction toward and away from the earth, which occurs for both linear and circular

---

[5]The free-falling laboratory approach is presented for linear motion in *Arons* (1979, p. 934–935), and for orbital motion in *Ohanian* (1976, p. 26–32).

motion.[6]

2.4 The earth–moon system: A vector approach to the two-body general case

In discussing the earth's motion, we will assume that it is not rotating about its spin axis once every 24 hours; this daily rotation of the earth will be considered in Section 2.8. We will analyze three systems: the earth by itself, the earth–moon system, and the earth–moon-sun system. So far we have examined differential force in a one-body,[7] one-dimensional analogy of the tides. The general case, utilizing three dimensions and the two-body approach, is presented well in *Barger and Olsson* (1973), which will serve as the basis for this section.

Figure 6 shows the configuration for determining the differential force on a particle (P, mass m) with small mass on the surface of the earth. Our inertial reference frame is oriented in space some distance r_2 from the center of a reference frame centered at the earth (E, mass M_e), such that the axes of both reference frames are parallel. Point M is a distant body (we'll call it the moon, mass M_m) that exerts a gravitational force on the earth. The equations of motion are described with respect to the inertial reference frame in terms of the position vectors $\mathbf{r}_1$, $\mathbf{r}_2$, and $\mathbf{r}_3$, which can be used to form a coordinate system relative to the earth:

$$
\begin{aligned}
\mathbf{r} &= \mathbf{r}_1 - \mathbf{r}_2 \\
\mathbf{R} &= \mathbf{r}_1 - \mathbf{r}_3 \\
\mathbf{d} &= \mathbf{r}_2 - \mathbf{r}_3 \; .
\end{aligned}
\tag{9}
$$

We are concerned with the equations of motion for the earth (E, M_e) and for a mass on the earth's surface (P, m). The force on P is due to the attraction of the earth (in the $\hat{\mathbf{r}}$-direction) and to the attraction of the moon (M, M_m). Thus,

$$
\mathbf{F}_m = m\,\ddot{\mathbf{r}}_1 = -\frac{G\,m\,M_e}{r^2}\,\hat{\mathbf{r}} - \frac{G\,m\,M_m}{R^2}\,\hat{\mathbf{R}}
\tag{10}
$$

$$
\mathbf{F}_{M_e} = M_e\,\ddot{\mathbf{r}}_2 = -\frac{G\,M_e\,M_m}{d^2}\,\hat{\mathbf{d}} \; .
\tag{11}
$$

Dividing Equation (10) by m, Equation (11) by M_e, and then taking the difference, we find

$$
\ddot{\mathbf{r}}_1 - \ddot{\mathbf{r}}_2 = -\frac{G\,M_e}{r^2}\,\hat{\mathbf{r}} - \frac{G\,M_m}{R^2}\,\hat{\mathbf{R}} - \frac{G\,M_m}{d^2}\,\hat{\mathbf{d}} \; ,
\tag{12}
$$

---

[6]Since in the absence of external forces, the surface tension would make the drop into a spherical shape, we could use the elliptical shape of the droplet to verify that the ship is a non-inertial reference frame (*Ohanian*, 1976, p. 27). As time progresses, the force on the orbiting droplet remains constant (as does the acceleration); the ellipsoidal drop is in equilibrium with the earth's gravity field. As the "falling" droplet approaches the earth (d decreasing), both the force (Eq. 1, $F \propto d^{-2}$) and the differential force (Eq. 39, $dF/dx \propto d^{-3}$) on the drop increase, and the drop is stretched in the d direction (Figure 5).

[7]See Appendix B for a one-body vs. two-body discussion.

which, using the second derivative of Eq. 9.1 with respect to time, gives

$$\ddot{\mathbf{r}} = -\left(\frac{G\,M_e}{r^2}\right)\hat{\mathbf{r}} - G\,M_m\left(\frac{\hat{\mathbf{R}}}{R^2} - \frac{\hat{\mathbf{d}}}{d^2}\right). \tag{13}$$

We now have an equation for the force per unit mass for a particle on the earth's surface, at relative coordinate $\mathbf{r}$ (Eq. 13). A qualitative analysis of the equation can provide insights into the nature of the tide-producing forces. The first term is the force per unit mass due to the earth's gravity (see Figure 2). The second term is a differential force — the tide-generating force per unit mass — representing the difference between the gravitational force due to the moon on the surface and at the center of the earth. The first component $(-\hat{\mathbf{R}}\,G\,M_m/R^2)$ is directed from the surface of the earth to the moon (P to M); the second component $(\hat{\mathbf{d}}\,G\,M_m/d^2)$ is always directed away from the moon in a line parallel to the earth–moon axis (M to E).[8]

It is important to keep in mind the generality of the scenario in Figure 6: the sphere labeled earth could be any mass (e.g., a water droplet or the moon), the particle does not have to be "on the surface" (the spherical mass could have any radius), and the distant mass labeled moon could be any body (e.g., the sun).

2.5 The earth–moon system: An extension of the vector approach and a return to the free fall examples

Now we simplify the general case (Figure 6) to the earth–moon system in two dimensions (Figure 7A). Our coordinate system is centered at the earth, we are looking down on the x'-y' plane, the moon is orbiting the earth in a circular orbit with radius d, and we take $\theta = 90°$ so that the mass (P, mass m) is in the x'-y' plane. Point P is thus a particle on the periphery of the cross-section cut through the earth by the orbital plane of the moon, as shown in Figure 7A.[9]

We neglect the gravitational attraction at P due to the earth, since it is not part of the tide-producing force presented in Equation (13).[10] The force-per-unit-mass at P due to the moon is given by

$$\mathbf{f}_P = \frac{\mathbf{F}_P}{m} = \left(\frac{G\,M_m}{R^2}\right)\hat{\mathbf{R}}, \tag{15}$$

where $\hat{\mathbf{R}}$ points from the moon to P (see Figure 7B and Figure 6). This force can be resolved

---

[8]The fictitious force term is anticipated, since we are in a non-inertial reference frame.

[9]This scenario is presented in *Arons* (1979, p. 934–935).

[10]The reason we can neglect the force on the particle due to the earth becomes evident in the potential energy approach (Section 2.6). There we can set the gravitational potential equation equal to any convenient value, such as the gravitational potential at the earth's surface. This effectively subtracts the potential field at the earth's surface.

into components perpendicular and parallel to the earth's surface (Figure 7A):

$$f_r = \left(\frac{G\,M_m}{R^2}\right)\cos(\phi+\alpha) \tag{16}$$

$$f_\phi = \left(\frac{G\,M_m}{R^2}\right)\sin(\phi+\alpha)\ . \tag{17}$$

Using the Law of Cosines on triangle PEM in Figure 7, we have

$$R^2 = d^2 + r_e^2 - 2r_e\,d\cos\phi\ , \tag{18}$$

which can be rearranged to give

$$\frac{1}{R^2} = \frac{1}{d^2}\left(\frac{1}{1 - 2\left(\frac{r_e}{d}\right)\cos\phi + \left(\frac{r_e}{d}\right)^2}\right)\ . \tag{19}$$

Noting that $r_e/d \approx 1/60$ (see Table 1 or Figure 8A), we expand $1/R^2$, $\sin\alpha$, and $\cos\alpha$ to first order in (r_e/d):[11]

$$\frac{1}{R^2} = \frac{1}{d^2}\left(1 + \frac{2r_e}{d}\cos\phi + \cdots\right) \tag{20}$$

$$\begin{aligned}\frac{1}{R} &= \frac{1}{d}\left[1 - 2\left(\frac{r_e}{d}\right)\cos\phi + \left(\frac{r_e}{d}\right)^2\right]^{-1/2}\\ &\approx \frac{1}{d}\left[1 + \frac{1}{2}\left[2\left(\frac{r_e}{d}\right)\cos\phi - \left(\frac{r_e}{d}\right)^2\right]\right]\\ &= \frac{1}{d}\left[1 + \left(\frac{r_e}{d}\right)\cos\phi - \frac{1}{2}\left(\frac{r_e}{d}\right)^2\right]\end{aligned}$$

$$\sin\alpha = \frac{r_e}{R}\sin\phi = \frac{r_e}{d}\sin\phi\left[1 + \left(\frac{r_e}{d}\right)\cos\phi - \frac{1}{2}\left(\frac{r_e}{d}\right)^2\right] \approx \frac{r_e}{d}\sin\phi \tag{21}$$

$$\cos\alpha = \sqrt{1 - \sin^2\alpha} = \sqrt{1 - \left(\frac{r_e}{R}\sin\phi\right)^2} \approx \sqrt{1 - \left(\frac{r_e}{d}\right)^2\sin^2\phi} \approx 1\ . \tag{22}$$

Using these expansions in Equations (16) and (17), we obtain (see Appendix C, p. 41)

$$f_r = \left(\frac{G\,M_m}{d^2}\right)\left[\cos\phi - \left(\frac{r_e}{d}\right)\left(1 - 3\cos^2\phi\right) + \cdots\right] \tag{23}$$

$$f_\phi = \left(\frac{G\,M_m}{d^2}\right)\left[\sin\phi + \left(\frac{r_e}{d}\right)\left(\frac{3}{2}\sin 2\phi\right) + \cdots\right]\ . \tag{24}$$

These are the radial and tangential gravitational field strengths, to first-order approximation, due to the moon at any point on the earth's surface. We can represent this force in vector form as the sum of the zero- and first-order components, being careful to note the sign convention, as

---

[11] From Eq. 19 to Eq. 20, we ignore the $(r_e/d)^2$ term and then use a binomial expansion, just as shown in Eqs. 6–8, which were derived for the free-falling laboratory.

shown in the inset of Figure 7A.

$$\mathbf{f}_{01} = \mathbf{f}_{r01} + \mathbf{f}_{\phi 01} = f_r\,\hat{\mathbf{r}} - f_\phi\,\hat{\boldsymbol{\phi}}$$

$$
\begin{aligned}
\mathbf{f}_{01} &= \frac{G\,M_m}{d^2}\left(\left[\cos\phi - \left(\frac{r_e}{d}\right)\left(1 - 3\cos^2\phi\right)\right]\hat{\mathbf{r}} - \left[\sin\phi + \left(\frac{r_e}{d}\right)\left(\frac{3}{2}\sin 2\phi\right)\right]\hat{\boldsymbol{\phi}}\right) \\
&= \frac{G\,M_m}{d^2}\left(\left[(\cos\phi)\hat{\mathbf{r}} - (\sin\phi)\hat{\boldsymbol{\phi}}\right] + \left[\left(\frac{r_e}{d}\left(3\cos^2\phi - 1\right)\right)\hat{\mathbf{r}} - \left(\frac{r_e}{d}\frac{3}{2}\sin 2\phi\right)\hat{\boldsymbol{\phi}}\right]\right)
\end{aligned}
$$
(25)

$$\equiv \mathbf{f}_0 + \mathbf{f}_1$$
(26)

where $\mathbf{f}_{01}$ is the force due to the zero-order terms ($\mathbf{f}_0$) and first-order terms ($\mathbf{f}_1$), which are given by

$$\mathbf{f}_0 = \frac{G\,M_m}{d^2}\left[(\cos\phi)\hat{\mathbf{r}} - (\sin\phi)\hat{\boldsymbol{\phi}}\right]$$
(27)

$$\mathbf{f}_1 = \frac{G\,M_m}{d^2}\frac{r_e}{d}\left[\left(3\cos^2\phi - 1\right)\hat{\mathbf{r}} - \left(\frac{3}{2}\sin 2\phi\right)\hat{\boldsymbol{\phi}}\right] .$$
(28)

Before we examine the zero- and first-order components of the tide-producing force, we take a look at the motion of the earth and the moon, which form a two-body system (Figure 8). (We will continue to assume that the earth is not spinning about its axis.) The two bodies share a common center of mass, and they are locked into circular orbits *about their common center of mass.* As shown in Figure 8B2, each point within the earth circles the earth–moon center of mass (C.M.) with an equal radius, a motion described as "revolution without rotation".[12] The centripetal acceleration is directed to the center of each earth-point's (P$_1$, P$_2$, and C in Figure 8) circle of revolution. It is not sufficient to say that the earth revolves about the earth–moon center of mass; that would suggest that the particles throughout the earth transcribe circles of unequal radii.

Following the advice of *Arons* (1979, p. 935), we examine the zero- and first-order vector-components of $\mathbf{f}_{01}$ separately. We can write $\mathbf{f}_0$ in terms of the x-y coordinates by substituting

$$
\begin{aligned}
\hat{\mathbf{r}} &= \cos\phi\hat{\mathbf{x}} + \sin\phi\hat{\mathbf{y}} \\
\hat{\boldsymbol{\phi}} &= -\sin\phi\hat{\mathbf{x}} + \cos\phi\hat{\mathbf{y}} .
\end{aligned}
$$
(29)

into $\mathbf{f}_0$ (Eq. 27), which gives (see Appendix C)

$$\mathbf{f}_0 = \left(\frac{G\,M_m}{d^2}\right)\hat{\mathbf{x}} .$$
(30)

Figure 9 shows a graphical view of the $\mathbf{f}_0$ vectors at the earth's surface; the key is that they always

---

[12]This type of motion — "revolution without rotation" — is described in several treatments of tides: *Arons* (1979, p. 935), *Tsantes* (1974, p. 330), *Strahler* (1971, p. 130). I corresponded with White (*White et al.*, 1993), who felt that this type of explanation was more harmful than helpful, since the earth does indeed rotate (once every 24 hours).

point in a direction parallel to the earth–moon axis. This corresponds to a free-fall acceleration of the entire rigid earth. In the two-body problem (Figure 8), the $\mathbf{f}_0$ force is the centripetal force, which is equal in magnitude and direction at every point within the earth at any "snapshot" in time.

To examine the consequence of the zero-order force, we consider a hypothetical one-body problem: a fixed, rigid, spherical earth, with the moon at a distance. To see the effects of the zero-order force in this scenario, we add an ocean covering that is free to move under the zero-order force. Now, note that $\mathbf{f}_0$ is an order of magnitude (d/r_e) greater than $\mathbf{f}_1$. If $\mathbf{f}$ were the only force acting on the earth's surface, then $\mathbf{f}_0$ would dominate: the water covering would tend to pile up on the side facing the moon, forming one, not two, tidal bulges (Figure 10). If we were on the earth, rotating under the tidal bulge, we would experience a single, enormous, tide each day. The fact that we typically see two tides per day is evidence that the earth is part of a two-body system, as it is itself revolving about a common center of mass.

Arons (1979, p. 935–6) addressed some of the confusion of the centripetal force term $\mathbf{f}_0$: "In most developments of tidal theory, as soon as the $\mathbf{f}_0$ term appears, it is dropped with some cryptic comment such as 'this is shared by the entire earth' or ... 'we subtract the centrifugal force.' Such remarks avoid the physics and are unintelligible to most students." The term is indeed dropped, because it is a *free fall* acceleration of the entire rigid earth. This is precisely what we did with the free-falling (rigid) laboratory in Figure 3B (and Figure 4). In that case, we subtracted the free fall acceleration of the lab from the acceleration of each ball, since we were interested in the motion of the ball from the reference frame of the lab. In the present case, we will subtract the free fall acceleration of the rigid earth from the acceleration of each particle of water, since we are interested in the motion of the ocean from the reference frame of the earth.

We now focus on the remaining lunar force-per-mass terms relative to the ocean-covered earth, the first-order terms $\mathbf{f}_1$ (Eq. 28). Figure 11 shows a plot of the $\mathbf{f}_1$ vectors at the surface and center of the earth. The tangential component $\mathbf{f}_{\phi 1}$ — horizontal with respect to the earth's surface — is responsible for moving the water, since it is orthogonal to the earth's gravitational field (Figure 12). This "ocean-moving" $\mathbf{f}_{\phi 1}$-component will pull the water from the sides of the earth (Figure 12). The water will pile up in the regions facing toward and away from the moon (Figure 13). The radial component $\mathbf{f}_{r 1}$ — vertical with respect to the earth's surface — cannot shift water around; it can only change the apparent weight of each particle of mass very slightly.[13]

---

[13]We can calculate this effect. Using Eq. 23, the maximum radial (with respect to the earth) force occurs when $\phi = 0$:

$$\mathbf{f}_{r1} \;=\; \frac{G\,M_m}{d^2}\left[\frac{r_e}{d}\left(3\cos^2 0 - 1\right)\hat{\mathbf{r}}\right] \;=\; \frac{2\,G\,M_m\,r_e}{d^3}\,\hat{\mathbf{r}}\,,$$

which can be compared to the force-per-mass due to the earth (Eq. 2), which is constant for all ϕ:

$$\frac{f_{r1}}{f_G} \;=\; \left(\frac{2\,G\,M_m\,r_e}{d^3}\right)\Big/\left(\frac{G\,M_e}{r_e^2}\right) \;=\; \frac{M_m\,r_e^3}{M_e\,d^3} \;\approx\; 10^{-5}\,.$$

2.6 Equilibrium tide: A potential energy approach to the earth–moon system

The differential force due to gravity can be examined from a potential energy standpoint (Appendix A). I find that the potential energy approach, when used alone in deriving the differential force (e.g., *Kibble*, 1985), lacks the "visual" confirmation that the vector approach provides (e.g., Figure 6 and Eq. 13). But in understanding how the water behaves under the influence of the differential force and thus in explaining what we observe each day, the potential energy approach is helpful.[14]

As Newton first articulated,[15] a shell of water covering the earth will form a surface that is in equilibrium with the net gravitational field. In other words, the equipotential water surface will be orthogonal to the net gravitational field, and there will be no tangential force on the surface (Figure 14A). This equipotential surface is referred to as the *equilibrium tide*. Appendix A contains a derivation of the equilibrium tide; this section contains some of the consequences.

Based on the general 3D case depicted in Figure 6, we can show (Appendix A) that the gravitational potential (potential energy per unit mass) at point $P(r, \theta, \phi)$ on the (distorted) earth's surface is given by

$$\Phi(\mathbf{r}) = -\frac{G M_e}{r} - \frac{G M_m r^2}{d^3} \left(\frac{3}{2} \sin^2 \theta \cos^2 \phi - \frac{1}{2} \right) , \tag{31}$$

Since this is an equipotential surface, we may set it equal to any constant, since adding a constant to the potential does not affect the force. We choose $\Phi(\mathbf{r}) = -G M_e/r_e$, where r_e is the radius of the undistorted (spherical) earth:[16]

$$-\frac{G M_e}{r_e} = -\frac{G M_e}{r} - \frac{G M_m r^2}{d^3} \left(\frac{3}{2} \sin^2 \theta \cos^2 \phi - \frac{1}{2} \right) , \tag{32}$$

which can be rearranged to give

$$r - r_e = \frac{M_m}{M_e} \frac{r_e r^3}{d^3} \left(\frac{3}{2} \sin^2 \theta \cos^2 \phi - \frac{1}{2} \right) . \tag{33}$$

We define $h(\theta, \phi) \equiv r - r_e$ to be the height of the water displacement due to tides (see Figure 14). Since $h \ll r_e$, we use a zeroth-order approximation[17] to obtain

$$h(\theta, \phi) = \frac{M_m}{M_e} \frac{r_e^4}{d^3} \left(\frac{3}{2} \sin^2 \theta \cos^2 \phi - \frac{1}{2} \right) . \tag{34}$$

---

[14] *Tsantes* (1974) treats the equilibrium tide theory using vectors. He incorporates a "reaction force resulting from the earth's rigidity" (p. 331) that is perpendicular to the equilibrium surface.

[15] See Book 1, Proposition 66, Corollaries 19 and 20 of Newton's *Principia* (*Newton*, 1687, p. 582–583).

[16] This choice of this constant effectively eliminates the gravitational force due to the earth on the particle.

[17] By definition, $r = r_e + h$. Then we can approximate the term in Eq. 33 as follows:

$$r_e r^3 = r_e (r_e + h)^3 = r_e^4 \left(1 + \frac{h}{r_e} \right)^3 = r_e^4 \left(1 - 3\frac{h}{r_e} + \cdots \right) \approx r_e^4 .$$

For simplicity, we'll look at the 2D case with $\theta = 90°$, a view looking down on the orbital plane of the moon, as in Figure 14B.[18] The tidal range as a function of "longitude"[19] is then

$$h(\theta, \phi) = \frac{M_m}{M_e} \frac{r_e^4}{d^3} \left(\frac{3}{2} \cos^2 \phi - \frac{1}{2} \right) , \tag{35}$$

which we can use to plot the equilibrium tide (equipotential water surface). Figure 14 shows the equilibrium tide and how it depends on astronomical parameters (e.g., earth–moon distance). The tidal range is the difference between the high tide (height $h > 0$), which occurs parallel to the earth–moon axis at $\phi = 0°$ and $\phi = 180°$, and the low tide (height $h < 0$), which occurs perpendicular to the earth–moon axis at $\phi = 90°$ and $\phi = 270°$. Therefore, using Equation (35), the maximum tidal range[20] on an earth covered with water (and void of continents) is predicted to be

$$\begin{aligned} range_M &= h(0°) - h(90°) = \frac{3}{2} \frac{M_m}{M_e} \frac{r_e^4}{d^3} \\ &\approx 0.36\,\mathrm{m} - (-0.18\,\mathrm{m}) = 0.54\,\mathrm{m} . \end{aligned} \tag{36}$$

To make the shape of the equilibrium tide distinguishable from a circle,[21] we must either increase the mass of the moon or bring the moon closer to the earth. As shown in Figure 14E, the equilibrium tide is noticeable if the moon's mass is increased to $M_m = 10,000 M_e$; the tidal range in this scenario would be (a catastrophic) 436 km.

2.7   The tidal effect due to the sun

The "tidal effect" at body A due to a body i with mass M_i at distance x_i from A is defined as

$$T_i = \frac{M_i}{x_i^3} . \tag{37}$$

This is found by analyzing Equation (35) and extracting the terms due to the tide-producing body (the moon, in that case). It can also be found by differentiating Equation (1),

$$F = \frac{G\,M_i\,M_A}{x_i^2} . \tag{38}$$

to find the change in force over distance:

$$\frac{dF}{dx_i} = -\frac{2G\,M_i\,M_A}{x_i^3} . \tag{39}$$

---

[18] Any cross-section of the earth that contains the earth–moon axis would give the same results, because the problem has cylindrical symmetry about the earth–moon axis. For example, we could take a vertical cross-section of the earth.

[19] If the spin axis were perpendicular to the plane of the diagrams in Figure 14, then we could call ϕ the longitude. However, we haven't specified where the spin axis is yet.

[20] The maximum tidal range will occur at the point on the earth closest to the moon, which, in the 3D example (Figure 6), occurs when $\phi = 0°$ and $\theta = 90°$. In the 2D treatment we have already set $\theta = 90°$. The plane of the lunar orbit, shown in Figure 7fig14, will show the maximum tidal ranges.

[21] The spherical ocean covering would result from the earth at rest, without the moon (Figures 2 and 10a).

Moving the dx_i to the right-hand side, we get

$$dF = \frac{2G\,M_i\,M_A}{x_i^3}\,dx_i\,, \tag{40}$$

where dF is the magnitude of the differential gravitational force directed along x_i, and dx_i is the diameter of body A.[22] The tidal effect at body A includes only the body-i-terms, M_i/x_i^3.[23]

So far we have not considered the sun. The case presented in Section 2.6 can be easily extended to consider the effects of the sun. Since the general case (Figures 6 and 7) considers differential force induced by any single astronomical body, we can replace the moon with the sun. Replacing the moon constants in Equation (36) by the sun constants, we find that the maximum tidal range at the earth due to the sun is given by

$$
\begin{aligned}
range_s &= \frac{3}{2}\frac{M_s}{M_e}\frac{r_e^4}{D^3} \\
&\approx \frac{3}{2}\frac{(3.33\times10^5\,M_e)}{M_e}\frac{r_e^4}{(23460\,r_e)^3} = \frac{3}{2}\frac{(3.33\times10^5)}{23460^3}\,r_e \approx 0.24\,\mathrm{m}\,,
\end{aligned}\tag{41}
$$

where M_s is the mass of the sun and D is the distance from the earth to the sun.

It is an interesting coincidence that the tidal effect due to the sun is of the same order of magnitude as the effect due to the moon (Eqs. 36 and 41). In fact, it is a unique occurrence in our solar system (*Kibble*, 1985, p. 130). It implies that the sun should be able to enhance or weaken the tidal effects on the earth due to the moon, depending on the relative positions of the bodies. The moon will produce bulges that are parallel to the earth–moon axis; the sun will produce weaker bulges parallel to the earth-sun axis. Figure 16 shows how these effects can interfere constructively to produce spring tides and destructively to produce neap tides. We should expect the highest tides (spring tides) and the lowest tides (neap tides) to occur twice each lunar cycle (Figure 16C). This fortnightly cycle is known as the neap-spring-neap tidal cycle.

We can predict the tidal ranges on the earth due to the combined effect of the moon and the sun (Figure 17). The equilibrium tidal range during spring tides (syzygy) is 0.78 m and during neap tides (quadrature) is 0.30 m. Theoretically, you could determine the relative tidal effects of the moon and sun by measuring the tidal ranges (Figure 17):

$$\frac{T_m}{T_s} = \frac{range_m}{range_s} = \frac{0.54}{0.24} \approx 2.25\,. \tag{42}$$

Another interesting calculation can be derived based on the observation that the sun and the moon appear as the same size when viewed from the earth (think of a total solar eclipse) (*Good*, 2000). Because the angle subtended by each body as seen from the earth is approximately equal ($\theta_m \approx \theta_s$), it turns out that the relative tidal effects depend on only the densities (ρ) (see

---

[22] Or dx_i could be the separation between two bodies close together, as shown in Figure 43.

[23] The preceding calculations appear in most treatments of tides in introductory astrophysics texts (e.g., *Zeilik and v. P. Smith*, 1987, p. 46).

Appendix C, p. 42):

$$\frac{T_m}{T_s} = \frac{M_m\, d^{-3}}{M_s\, D^{-3}} \approx \frac{\left(\frac{4}{3}\pi r_m^3 \rho_m\right)\left(\frac{2\,r_m}{\theta_m}\right)^{-3}}{\left(\frac{4}{3}\pi r_s^3 \rho_s\right)\left(\frac{2\,r_s}{\theta_s}\right)^{-3}} = \frac{\rho_m}{\rho_s}\frac{\theta_s^3}{\theta_m^3} \approx \frac{\rho_m}{\rho_s}\ . \tag{43}$$

Thus the relative tidal effects, which can (in theory) be measured from the tidal ranges (Figure 17), also give the relative densities of the moon and sun. The actual density ratio is $\rho_m/\rho_s \approx (3340\,\mathrm{kg\,m^{-3}})/(1400\,\mathrm{kg\,m^{-3}}) \approx 2.38$, which is in agreement with Equation (42).

One final point regarding the sun is that it, too, experiences a tidal force due to the planets revolving around it (*Olson and Lytle*, 2000). The variation in the solar tide over time is complicated but predictable (Figure 18). When the planets and moon are clustered together in the night sky, we would expect the greatest tidal effect at the sun.[24]

2.8 The effects of the earth's rotation

As we have shown, the differential force on the earth results from the earth's revolution about the earth–moon center of mass, and it has nothing to do with the rotation of the earth about its spin axis. But to understand the consequences of the differential force based on our daily observations of tides, we must consider the earth's spin.

Our coordinate system, shown in Figure 19, is now centered at the earth (E), which has a vertical spin axis, such that θ angles correspond to latitude and ϕ angles correspond to longitude. The moon is at position $M(\phi_m, \theta_m, d)$, where d is the fixed distance to the earth. A particle is on the surface at position $P(\phi_p, \theta_p, r_e)$, where r_e is the fixed radius of the earth.

Using this coordinate system, we now focus on the equilibrium tide-producing term,

$$\tfrac{1}{2}\left(3\cos^2\psi - 1\right)\ , \tag{44}$$

which is presented in Equation (35) (see Figures 11 and 14). The angle ϕ or ψ is the angle between the direction of the particles and the direction of the moon (angle between EP and EM). In the 2D case, the angle is labeled ϕ (Figure 14B); in the 3D case here, ψ is found from the relationship (see Appendix C, p. 43)

$$\cos\psi = \cos\theta_p\cos\theta_m + \sin\theta_p\sin\theta_m\cos\left(\phi_p - \phi_m\right)\ , \tag{45}$$

Incorporating this into the equilibrium tide-producing term (Eq. 44), we find, after simplification

---

[24]We would also expect a tidal effect on the earth due to all the planets: see inset figure in *Olson and Lytle* (2000, p. 109).

(see Appendix C, p. 44),

$$\frac{1}{2}\left(3\cos^2\psi - 1\right) = \frac{3}{4}\sin^2\theta_p \ \sin^2\theta_m \ \cos\left[2\left(\phi_p - \phi_m\right)\right]$$
$$+ \frac{3}{4}\sin 2\theta_p \ \sin 2\theta_m \ \cos\left(\phi_p - \phi_m\right)$$
$$+ \left(\frac{3\cos^2\theta_p - 1}{2}\right)\left(\frac{3\cos^2\theta_m - 1}{2}\right) . \tag{46}$$

The three quantities of interest in this expression are (1) the latitude of point P, θ_p, which remains constant as the earth spins; (2) the longitude of point P, ϕ_p, which goes from 0° to 360° in each daily rotation of the earth, irrespective of the location of P; and (3) the angular coordinates of the moon, ϕ_m and θ_m, which vary over the course of a month, as the moon orbits around the earth: ϕ_m goes from 0° to 360° in ~28 days.

Each of the three parts of the expanded tide-producing term in Equation (46) produces an interesting, observable periodic variation (*Cook*, 1969, p. 73–74). The first term (Eq. 46.1), with $\cos 2\phi_p$, has a maximum twice over a 360° rotation;[25] this is the *semidiurnal tide* component, the tide that occurs twice a day, with a period of approximately 12 hours. The second term (Eq. 46.2), with $\cos\phi_p$, has a maximum once over a 360° rotation; this is the *diurnal tide* component, the tide that occurs once a day, with a period of approximately 24 hours. The third term (Eq. 46.3), with $\cos^2\theta_m$, has a maximum twice over the period of one lunar revolution; these maxima occur when θ_m is closest to θ_p, that is, when the declination of the moon (θ_m) is closest to the latitude of P (θ_p).

Thus, if the earth did not spin, we would observe a tidal range due to two effects: (1) the revolution of the earth–moon system in the gravitational field of the sun, which causes the fortnightly neap-spring-neap cycle, and (2) the fortnightly cycle of the declination moon with respect to the earth, as shown by the Eq. 46.3 component (see Section 4.3).

2.9 Analogies to other two-body systems: Balls on a turntable and the Bohr atom

Differential force is not unique to an accelerating mass in a gravitational field. Differential force will arise in any object of finite extent over which the force varies. For instance, a charged object accelerating in an electric field is subject to a differential force as well. Field lines — whether gravitational, electric, or magnetic — are curves that indicate the direction of the force. By definition, they are perpendicular to the equipotential surfaces (see Figure 15). Electric fields, like gravitational fields, obey an inverse-square law. One consequence of this is that two-body motion may arise due to the Coulomb force between charged particles, which occurs with the proton and electron in the Bohr atom (Appendix B). A comparison of the gravitational and electric fields is shown in Table 2.

It is possible to demonstrate the tidal bulges in an experiment using magnetic fields (*White*

---

[25]This is assuming that ϕ_m is roughly constant over the earth's 24-hour rotation (ϕ_p); in other words, the moon doesn't move very much over the course of a day.

et al., 1993, G. White, 2001, personal communication). Under certain conditions, the magnetic field between two bar magnets will obey an inverse-square law, just as the gravitational field and electric field do (Figure 20A-B). The configuration of the experiment is shown in Figure 20C. Two cylindrical magnets are positioned symmetrically about the center of a turntable, separated by distance x, such that an attractive force F_m exists between the magnets. Two large steel balls, each with mass M, situated on a plate balanced above the ends of the cylindrical magnets will "polarize" in the manner shown in Figure 20C. Four small steel balls with situate themselves between the large (magnetized) balls. This is analogous to the zero-order, one-body force of the earth–moon system (Figures 9 and 10).[26]

The turntable is turned on and spins with angular velocity ω. The four small balls are free to move, while the two large balls are essentially fixes. The reduced mass of the two large balls is $m = M/2$ (Figure 20D). At a particular angular velocity (see Figure 20B), the attractive magnetic force between the two large steel balls will equal the centripetal acceleration of the two-body system (two large steel balls) times the reduced mass: $F_m = x\,m\,\omega^2$.[27] At this angular velocity, two of the small balls swing to the opposite sides of the large balls (Figure 20D). At greater angular velocities, the four small balls will swing to the outside of the large balls and, at higher velocities, will fly off the plate. At a still higher angular velocity, the two large balls will fly off.

This experiment is easier to understand, having discussed the earth–moon system: each large ball represents the earth or moon; the smaller balls represent the tidal bulges of the ocean (Figure 20E). With the earth–moon system, the centripetal acceleration of the earth is due to the gravitational attraction between the earth and moon. The moon exerts a greater pull on the water on earth facing it than on the water facing away from it. Acceleration relative to the earth's center of mass causes water to bulge on both sides. In the turntable experiment, the moon-ball exerts a greater magnetic force on the ocean-ball in front of the earth-ball than the ocean-ball in back of the earth (Figure 20E). Centripetal acceleration of the ocean-balls relative to the acceleration of the center of mass of the earth-ball causes the two ocean-balls to swing to the front and back of the earth-ball.

---

[26]A better one-body analogy would be to have one cylindrical magnet at the center of the turntable and the other at distance x. Then one large steel ball (earth) would remain fixed while the other (moon) revolved around it.

[27]The magnetic force between the large steel balls is assumed to be the same as the magnetic force between cylindrical magnets on the turntable. The balls extend the effective length of the cylindrical magnets.

3 The behavior of oceanic tides

The motion of the water on the earth — whether on a continent-less earth, in an ocean, or in an estuary[28] — is best approached using principles of hydrodynamics. A hydrodynamic approach must incorporate the global-scale effects of the differential force (equilibrium tide), as well as the rotation of the earth about its spin axis. We will analyze the consequence of these two aspects, using hydrodynamic principles only qualitatively.[29]

3.1 Differential force at the global scale

So far we have dealt with the equilibrium tide: the behavior of a thin water covering over a completely rigid, spherical (i.e., no continents) earth that is under the influence of a differential force. At the global scale, the differential force on this ideal ocean due to an astronomical body would cause the ocean to be deeper in the regions of the earth facing toward and away from the body and shallower on the sides of the earth, as shown in Figure 13. The earth's daily rotation under the tidal bulges will cause the water level to change by a maximum of 0.78 m (Figure 17). This equilibrium tidal range turns out to be a reasonable prediction for places in the ocean far from the coast and in deep water, where the water level fluctuates on the order of one meter. But this 1-m estimate differs by an order of magnitude from the observed tidal ranges from certain areas on the earth.[30] Also, the equilibrium tide does not take into account how the water moves in the ocean. The equilibrium tide treatment, while helpful in understanding the nature of tidal forces, does not adequately explain the tidal patterns that we observe on earth. It is helpful to think of the tidal effects at the scale of an ocean and at the scale of an estuary or an inlet near the coast.

3.2 Tides at the ocean scale

The differential force on the earth due to the sun and moon create the tidal bulges on the earth. The rotation of the earth under these bulges is the driving frequency of the daily tides. The components of this driving frequency can be seen in Equations 46.1 and 46.2, which depend on the 24-hour rotation about the earth's spin axis (360° cycle of angle ϕ_p). The first component generates a *semidiurnal tide*, the tide that occurs twice a day, which is typical of most coastal systems. The second component generates a *diurnal tide*, the tide that occurs once a day, which occurs in some coastal systems. The semidiurnal and diurnal components can interfere with each other to produce more complicated tide known as a *mixed tide*. All three types of tides — not just

---

[28]An *estuary* is defined as "a body of water partially surrounded by land where fresh water from a river mixes with ocean water..." (*Garrison*, 1998, p. 531).

[29]*Lamb* (1945) is a classic text for hydrodynamics. Introductory oceanography texts, like *Garrison* (1998), are nice to get an introduction to how the water behaves, but they use minimal mathematics and physics in their discussions.

[30]Some of the largest tidal ranges in the world are found in the Bay of Fundy, Nova Scotia, and in Bristol Channel, England (*Desplanque and Mossman*, 2001; *Archer and Hubbard*, 2003).

the twice-a-day semidiurnal tide — are found in coastal systems around the world (Figures 21 and 22).

Another consequence of the earth's rotation is the Coriolis effect.[31] The Coriolis effect can be observed in the propagation of the tidal wave in the oceans (Figure 23). An ocean, such as the Atlantic, is confined by continents. The tidal wave, for both the semidiurnal and diurnal components, follows a very complicated path, which is governed in part by the shape of the ocean basin and in part by the Coriolis force. The direction of propagation of the tidal wave is counterclockwise in the northern hemisphere (two cases) and clockwise in the southern hemisphere (three cases).[32] In the North Sea (Figure 24), at the next scale down, the propagation of the tide is complex but remains consistent with the (Coriolis-influenced) counterclockwise motion observed in the North Atlantic.

3.3   Tides at the coastal scale

Having discussed tides at an astronomical level and at an ocean level, we now turn to the coasts, where almost everyone first becomes familiar with tides. We begin with a qualitative discussion of the concept of flux. The flux of water is the volume of water passing through a given cross-sectional area over a given time.[33] The flux at an interface, such as that between a large-diameter pipe and a small-diameter pipe, is constant. If we decrease the cross-sectional area (water enters small pipe), then the velocity of the water will increase. Consider the mouth of a river that flows into the ocean. A tidal wave, with a particular volume and velocity, approaches the mouth (= small pipe) from the ocean (= large pipe). Part of the tidal wave enters the mouth of the river, and, since the flux at the mouth remains constant, the velocity of the tidal wave increases. The addition of volume at the mouth causes the water level to increase. Thus, by passing through the mouth, the tidal wave increases its velocity (i.e., the "particle velocity") and raises the height of water.

What is a tidal wave exactly? It is not just any large wave, such as a tsunami, as is commonly believed. In discussing the propagation of a tidal wave in the ocean basin, we are referring to the changing position of the approximate crest of the high tide water level. This tidal wave, with an

---

[31]Because the earth rotates with an angular velocity, a particle mass, such as a volume of water, moving on the surface will experience the Coriolis force. The Coriolis force deflects horizontally moving masses in the northern hemisphere to the right and deflects masses moving in the southern hemisphere to the left. As a result, ocean-scale surface currents in the Atlantic and Pacific move in a clockwise direction in the northern hemisphere and counterclockwise in the southern hemisphere (*Garrison*, 1998, p. 207). (It is actually quite a bit more complicated than this. Winds, salinity, and temperature are major factors that determine ocean circulation patterns.) In the reference frame of the particle, the force appears to be "real." From the earth's non-inertial (rotating) reference frame, it is an apparent force, the consequence of the rotation. If the earth's angular velocity is ω, and the velocity of the particle relative to a coordinate system at rest on the earth's surface is $d^*\mathbf{r}/dt$, then the Coriolis force is given by $-2m\omega \times d^*\mathbf{r}/dt$. The Coriolis force is treated in any classical mechanics text (e.g., *Symon*, 1961, p. 278–280).

[32]This is the *opposite* direction that one might expect, based on the Coriolis force. One explanation (*Garrison*, 1998, p. 270) for this is that the incoming tidal wave is deflected to the right by the Coriolis force in the northern hemisphere and "wraps around" the ocean basin in a counterclockwise fashion. In fact, I think it is quite a bit more complicated, having to do with the superposition of two Kelvin waves, which gives rise to amphidromic circulation (*Marchuk and Kagan*, 1989, p. 118–122).

[33]We're assuming water is incompressible, which is a good approximation.

amplitude of less than a meter and a wavelength greater than 1,000 km, would not be noticeable. But if the tides generated in the ocean are confined into narrow, shallow regions — such as those near coasts — then the tidal wave will reach an appreciable velocity. In this case, the incoming tide may actually take the form of an observable wave, in which case the tidal wave is called a *tidal bore*. Figure 26 shows a tidal bore from Cook Inlet, south-central Alaska. In southwest England, people commonly surf *up* River Severn when anomalously large tidal bores come in from Bristol Channel. The Bay of Fundy in Nova Scotia has a configuration (Figure 25) that produces the largest tides on record: a 16.8 m (54.6 ft) tidal range (*Archer and Hubbard*, 2003)! The enormous tidal range in the Bay of Fundy is due in part to the geometry of the basin, which has a resonance frequency approximately equal to the frequency of the lunar tide (*Desplanque and Mossman*, 2001).[34]

---

[34]A simple rectangular basin will have a resonance period for the "sloshing" mode given by

$$T \;=\; \frac{\pi\,L}{\sqrt{3\,g\,h}} \;,$$

where L is the length of the basin, h is the depth, and g is the gravity (*Crawford Jr.*, 1968, p. 45). Higher resonant periods will be equal to the sloshing period divided by the number of nodes in the harmonic (*Korgen*, 1995, p. 443). The basin geometry — not just the cross-sectional area — is fundamental in determining how the tide behaves in a coastal area. See *Garrison* (1998) or *Marchuk and Kagan* (1989) for more on water wave propagation.

4 The preservation of oceanic tides and tidal cycles in the rock record

The massive tidal ranges in places like the Bay of Fundy or Cook Inlet provide a sense of awe and appreciation for the tides. Tidal currents in these local settings are on the order of meters per second and are substantial enough to float boats up the mouths of rivers. These currents also transport and deposit sediment. In certain tidal systems, the periodic ebb and flood of the tide can be recognized as a pattern of alternating layers of deposited sediment. Identifying these patterns in sedimentary deposits of modern systems allows one to apply the same techniques to layering patterns in sedimentary rock, in hopes of determining the history of oceanic tides over geologic time.

4.1 A brief background in physical sedimentology

Sediment, such as sand or mud, is carried by water.[35] When the sediment is deposited, it forms a sedimentary structure, which is either removed by other currents or is buried by additional sediment, which would allow it to be preserved in the rock record. Three mechanisms for transporting sediment and forming sedimentary structures are currents, waves, and storms. Sedimentary structures associated with currents tend to be asymmetric in shape (due to unidirectional water motion), structures associated with waves tend to be symmetric (due to oscillatory water motion), and structures associated with storms tend to be erosional surfaces (removal of sediment) or massive sediment deposits. Currents, including those generated by tides, will give rise to asymmetric sedimentary structures. The most common current sedimentary structure is called cross-bedding. At an outcrop of sandstone, cross-bedding looks like a series of tilted, near-parallel lines, which are bounded into near-horizontal sets (Figure 27). Cross-bedding is the preservation of underwater sand dunes migrating across the sea floor. Figure 27 illustrates how a series of sand dunes on the sea floor might be preserved in the rock record.

4.2 Tidal cycles in the rock record I: The ebb-flood cycle and the neap-spring-neap cycle at Homer, Minnesota

Figure 28 shows a roadside outcrop of sandstone near Homer, Minnesota.[36] The Homer outcrop contains several sets of cross-bedding, several of which contain thick layers of mud interspersed in the sandy layers. This feature of cross-bedded sand with mud is one characteristic of deposits in tidal settings (*Nio and Yang*, 1991). I will present the results of the Homer study as an introduction to the ebb-flood cycle and to how tides can be identified in the rock record.

A spatial and temporal context is helpful. The sands at Homer were deposited in a shallow sea[37] covering much of North America approximately 480 million years ago (Ma) (Figure 29).

---

[35]To be precise, sediment is carried by a fluid, which may be water or air. In the context of tides, we are concerned with sediment transport due to water, i.e., ocean currents.

[36]I spent part of the summer of 2000 studying this outcrop, which became a source of motivation for this paper.

[37]The term "shallow" is vague because there is very limited information to constrain the depth. The term used

The notion that tides may have been present at Homer implies that the tidal wave traveled from the ocean basin over the continent for more than 1,000 km.[38]

The ebb-flood cycle refers to the familiar rise-and-fall of the water level in a tidal setting. The ebb current is the outgoing tide; the flood current is the incoming tide. In most systems, one or the other tidal current will dominate. Figure 30 explains the stages of an (ebb-dominated) ebb-flood cycle and the corresponding migration of a sand dune during each stage. Our chief observation is that the volume of sand transported is proportional to the current speed; thus, currents with the greatest speeds will deposit the most amount of sediment. In reverse, the thickness of the deposited sand layer should be proportional to the magnitude of the tide. Another observation is that most sand is transported during the ebb current, little sand is deposited during the flood current, and only mud — particles much finer than sand — is deposited during the slackwater period between the ebb and flood. Recall that the ebb-flood cycle may occur once a day, twice a day, or have a more complicated behavior, depending on the coastal setting (Figures 21 and 22).

The neap-spring-neap cycle may also be preserved in sedimentary deposits. This cycle corresponds to the fortnightly variation in the overall strength (tidal range) of the tides (i.e., of the individual ebb-flood cycles). Figures 31 and 32 show the consequence of this cycle on the sedimentation. A *tidal bundle* is the sediment deposited by a migrating dune during one complete ebb-flood tidal cycle (about 12 to 24 hours). A *tidal bundle sequence* (Figures 32A and 31B) is the sediment deposited by a migrating dune during one complete neap-spring-neap tidal cycle (about a fortnight). The tidal bundles therefore normally vary in thickness (Figure 32D); relatively thin bundles — thin sandy layers with mud (Figure 32B) — are deposited during neap tides; relatively thick bundles (Figure 32C) are deposited during spring tides.

Sedimentary structures — composite mud drapes as well as indicators for both an ebb current and a flood current[39] — together with the variation in tidal bundle thickness, are diagnostic of tidal deposits (*Nio and Yang*, 1991). Therefore, the cross-bedding at the Homer outcrop preserves the record of tides in the layers left by the migration of a dune under tidal currents. Each tidal bundle sequence is the product of a single fortnightly neap-spring-neap cycle, and the 26 bundle sequences in the study section (see Figure 32D) therefore represent approximately thirteen Cambrian months. There is an average of 20 tidal bundles per sequence (corresponding to the number of ebb-flood cycles per neap-spring-neap cycle), which falls within the expect range

---

for the shallow sea in the literature is "epeiric" sea, which is short for "epicontinental" sea, literally, a sea above the continent. The depth was probably at most on the order of a couple hundred meters.

[38]Whether tides could have reached the interior portions of the continent is controversial, at least in the literature. Irwin's model of epeiric sedimentation, which contains no mathematical basis whatsoever, suggests that tides would have been dampened in the (presumably) shallow seas (*Irwin*, 1965). A more mathematical treatment of the topic can be found in *Wells et al.* (2005); *Keulegan and Krumbein* (1949); *Clark* (1982). *Tape et al.* (2000, 2003) document evidence of ocean tidal currents in the continental interior.

[39]To convince yourself that the dune migrated under reversing currents (ebb and then flood), you would ideally like to find evidence for both directions. Large dunes migrated — presumably under the ebb current (see Figure 29) — in a southerly direction, and this migration is preserved as the layers seen in Figure 28. I also observed smaller dunes (called ripples) in portions of the cross-bedding set. These smaller dunes probably formed during the flood current, as shown in Figure 30. It is difficult to explain reversely dipping layers without having reversing currents. The flood current dunes provide substantial support to the case for tides at Homer.

of 14–28 for tidal systems, although the standard deviation is is large (20 ± 7).

4.3 Tidal cycles in the rock record II: Three monthly lunar cycles, the semi-annual cycle, and the lunar nodal cycle

The examples in Section 4.2 show how a sand dune migrating in a coastal tidal channel may preserve tidal cycles in its daily depositional sedimentary layers (Figure 30B). Sediment may also be deposited by tidal currents in water further offshore (Figure 33). This form of deposition leaves a pattern of very thin, horizontal layers known as rhythmites.[40] Just as was the case with the cross-bedding layers (tidal bundles), the thickness of the rhythmite layer corresponds to the magnitude of the tide. Measuring the thickness of these layers in a continuous section may reveal cycles that may or may not be attributable to tides.

The orbital patterns of astronomical bodies in space give rise to the tidal cycles. Tides record the passage of time in the reference frame of the earth. This reference frame is known as the celestial sphere, which can be thought of as a projection of the earth's latitude-longitude coordinate system into space.[41] Consider describing the position of a particle on the earth's surface and a body in space. On the earth's surface, the particle's polar angle is expressed by its latitude; in space, the body's polar angle is given by its *declination* angle on the celestial sphere. Several orbital parameters influence the declination of astronomical bodies. Two of these are the *inclination* of the earth and the *inclination* of the moon's orbital plane. As Figure 34 shows, the earth is inclined 23° with respect to its orbital plane (the Ecliptic), and the lunar orbital plane is inclined 6° with respect to the Ecliptic. As a result, the declination of the sun varies over the course of the year (think of the seasons), and the declination of the moon varies over the course of the month.

I will outline six tidal cycles from two spectacular studies of tidal rhythmites (*Williams*, 2000; *Kvale et al.*, 1999). Each tidal cycle is explained using three approaches: the orbital configuration that causes the cycle, the resultant cycle in modern tidal charts, and the evidence of the cycle in the rock record (see Figures 35–40). The periods of the tidal cycles listed here are based on modern-day values in sidereal time, that is, time measured with respect to the (fixed) stars.

Figures 35 and 36 show the ebb-flood cycle and the neap-spring-neap cycle, which we introduced already. However, here we invoke the changing declination of the moon. When the lunar declination is zero, the moon is in the equatorial plane (i.e., on the celestial equator), and every point on the spinning earth will experience two equal bulges. When the lunar declination is nonzero, every point on the earth will experience two unequal bulges. Thus for a semidiurnal tidal system (two ebb-flood cycles per day), one ebb-flood cycle will have a greater tidal range than the other, a feature known as the *diurnal inequality* ("dominant tide" vs. "subordinate tide"

---

[40]The thickness of rhythmite neap-spring-neap cycles are a few centimeters, whereas the thickness of the sand dune neap-spring-cycles are up to 100 cm. See *Alexander et al.* (1998) for a collection of rhythmite studies.

[41]The celestial equator is the plane (or projection) of the earth's Equator, and the celestial pole is an extension of the earth's spin axis.

in Figure 35).[42] The neap-spring-neap cycle is due changes in the lunar phase and is termed the synodic month (29.53 days).

Two other monthly lunar cycles can be observed in the behavior of modern tides and in patterns in the rock record. The second lunar cycle, which causes the tropical month (27.32 days), is attributed to the inclination of the lunar orbit (Figures 37 and 34). This cycle was anticipated from the tide-producing term due to the rotating earth (Section 2.8, Eq. 46.3). The third lunar cycle, which causes the anomalistic month (27.55 days), is attributed to the eccentricity of the lunar orbit (Figure 38).[43]

Several tidal cycles longer than a month can be identified in both modern tide charts and in the rock record. The changing declination of the sun produces the semiannual cycle (182.6 days), which occurs twice each year (Figure 39). A longer cycle, the lunar apsides cycle (8.85 years), is due to the 360° rotation of the line of apsides (Figure 38A) and can be calculated using monthly and annual tidal cycle periods.[44] An even longer tidal is the lunar nodal cycle (18.6 years), which is due to the regression of the line of nodes, the line formed by the intersection of the lunar orbital plane with the earth's orbital plane (Ecliptic) (Figure 40).

The tidal rhythmite studies, which reveal that daily events can be preserved consecutively for several years, provide a new appreciation and perspective of geologic time and the rock record. The tidal studies in the rock record preserve sediment deposited on the time scale of our daily lives, not geologic time.

---

[42]The diurnal inequality (*Fenies et al.*, 1999) depends on latitude, which can be seen in Figure 37A.

[43]The plots of modern tidal heights in Figure 38B and Figure 39B are the same. But I invoke two different mechanisms to explain the ∼6-month fluctuation: one when the line of apsides points to the sun (Figure 38A), the other due to the declination of the sun (Figure 38A). Probably both of these mechanisms are contributing to the ∼6-month cycle in these particular data.

[44]The lunar apsides cycle was 9.7 ± 0.1 years at 620 Ma, according to tidal rhythmite layers (*Williams*, 2000, p. 48). Also see *Kaufmann III and Freedman* (1999), p. 56–57.

5 The history of the earth–moon system

The tides on earth are ultimately due to the gravitational attraction between the earth and moon, which depends on their distance of separation. If the distance of separation changes, then the differential force on the earth will change, and the tides on the earth should respond accordingly. The earth–moon distance has not remained constant over the course of the earth's history. With the use of lasers, scientists have measured that the moon is retreating from the earth at a rate of 3.82 ± 0.07 cm/yr (*Dickey et al.*, 1994). Therefore, today the differential force on the earth, and thus the magnitude of the tides, is getting weaker.

The history of the earth–moon distance is an important debate in science, since it has a direct bearing on the origin of the moon. If the current lunar retreat rate is projected back in time, then the moon would have been too close to the earth to maintain its orbit, within a distance known as the Roche limit (see Section 5.2). A chief question then becomes, "How can we determine the lunar retreat rate at different times in the earth's history?"

5.1 Conservation of angular momentum

The magnitude of the oceanic tides is getting weaker due to the oceans themselves. In simplest terms, the spinning earth "carries" the bulging oceans in front of their preferred position, which is along the earth–moon axis (Figure 42). This creates an enormous amount of friction between the oceans and the solid earth. To compensate for the energy loss dissipated by the friction of the oceans, the earth's rotation must slow down at the rate of 4.4×10^{-8} s per rotation, which results in a cumulative loss of time of about 28 seconds per century.[45]

Conservation of angular momentum explains the relationship between the earth's rotation and the earth–moon distance. The angular momentum of the earth–moon system, which is centered at the earth–moon center of mass, remains constant. The slowing of the earth's rotation — the loss of rotational angular momentum — must be accompanied by an equal increase of the angular momentum of the earth–moon system.

The angular momentum for a mass m orbiting in a circle of radius d with velocity v is given by

$$\mathbf{L} = \mathbf{d} \times \mathbf{p} \tag{47}$$

$$L = dmv \sin \phi = dmv \, , \tag{48}$$

where $\phi = 90°$ is the angle between $\mathbf{d}$ and $\mathbf{p}$ for the circular orbit. This one-body derivation can be extended to the two-body case, using the reduced mass concepts presented in Appendix B.

---

[45]This interesting fact is from *Barger and Olsson* (1973); introductory astrophysics texts typically show some basic figures for the earth's decreasing rotational rate (some figures are inconsistent over different texts, but they give the same order of magnitude). The fact explains why eclipses run systematically 28 s ahead of the calculations based on observations a century ago.

We find that the net orbital angular momentum of the earth–moon system is

$$L = d\mu v \tag{49}$$

where μ is the reduced mass of the system, $\mathbf{d} = \mathbf{d}_m - \mathbf{d}_e$ is the relative coordinate, and $\mathbf{v} = \mathbf{v}_m - \mathbf{v}_e$ is the relative velocity (Figure 42). Assuming circular orbits, the gravitational and centrifugal forces balance:

$$\frac{G M_e M_m}{d^2} = \frac{\mu v^2}{d} . \tag{50}$$

Combining Equations (49) and (50), we find

$$L^2 = (G M_e M_m \mu)d . \tag{51}$$

Thus, if the earth's *rotational* angular momentum decreases, then the net *orbital* angular momentum L must increase by increasing the distance of separation d. As the earth's rotation slows, the moon retreats.

A quote from George Gamow (*Gamow*, 1962, p. 91) nicely illustrates several concepts of the earth–moon–sun–ocean interactions.

> As a result of gradual recession, the moon will eventually get so far away from the earth that it will become rather useless as a substitute for lanterns at night. In the meantime solar tides [tides on earth due to the sun] gradually will slow down the rotation of the earth (provided the oceans do not freeze up),[46] and there will come the time when *the length of a day will be greater than the length of a month*.[47] The friction of lunar tides will then tend to accelerate the rotation of the earth,[48] and, by the law of conservation of angular momentum, the moon will begin to return to the earth. . .

Of course, by this time, the sun will probably have burned out, which would make those lanterns necessary again.

---

[46] Now the sun is exerting a torque on the bulges: see Figure 42, only replace the moon by the sun.

[47] In other words, the period of the moon's revolution about the earth (or earth–moon center of mass), presently about 28 days, will some day be greater than the period of the earth's daily rotation, which is presently 24 hours. Computer calculations show that this should occur at an earth–moon distance of 6.45×10^5 km $\approx 101 \, r_e$ (*Zeilik and v. P. Smith*, 1987, p. 51).

[48] Now the moon is *pulling* on the bulge, so the earth's rotation increases (see Figure 42).

5.2 The Roche limit

In 1850, Edouard Roche (1820–1883) demonstrated that a satellite with mass m and radius $r_m \geq 500$ km orbiting a planet with mass $M \gg m$ and radius r_M would be torn apart by differential force if it approached the planet within distance of

$$x_R \; = \; 2.44 \left(\frac{\rho_M}{\rho_m} \right)^{1/3} r_M \; , \tag{52}$$

where ρ_m and ρ_m are the average densities of the planet and satellite, and x_R is the Roche limit. We can derive an approximation of the Roche limit based on the configuration in Figure 43.[49] The "moon" is depicted as two spherical masses, each with mass m and radius r, that are separated by a distance $dx = 2r$. There is a mutual gravitational attraction (Eq. 2) between the two masses given by

$$F \; = \; \frac{G\,m\,m}{dx^2} \; . \tag{53}$$

The earth causes a differential force (Eq. 40) between the two moon-balls given by[50]

$$
\begin{aligned}
dF \; &= \; \frac{2\,G\,M_e\,m}{(x-r)^3} dx \; = \; \frac{2\,G\,M_e\,m}{x^3} \left(1 - \frac{r}{x} \right)^{-3} dx \\
&\approx \; \frac{2\,G\,M_e\,m}{x^3} \left(1 + \frac{3\,r}{x} \right) dx \; \approx \; \frac{2\,G\,M_e\,m}{x^3} dx \; .
\end{aligned}
\tag{54}
$$

This force causes the two moon-balls to separate, as the earth pulls more on the near-ball than on the far-ball, just as in the example in Figure 4. At the Roche limit, the differential force between the two balls equals their mutual gravitational attraction:

$$\frac{2\,G\,M_e\,m}{x_R^3} dx \; = \; \frac{G\,m\,m}{dx^2} \; , \tag{55}$$

where x_R is the Roche limit. Solving for x_R, we find

$$x_R^3 \; = \; \frac{2M_e}{m} dx^3 \; . \tag{56}$$

Substituting $dx = 2r$, $m = \rho_m \frac{4}{3}\pi r^3$, and $M_e = \rho_e \frac{4}{3}\pi r_e^3$, we get

$$
\begin{aligned}
x_r^3 \; &= \; \frac{2\,\rho_e \frac{4}{3}\pi r_e^3}{\rho_m \frac{4}{3}\pi r^3} (2r)^3 \; = \; \frac{2^4 \rho_e r_e^3}{\rho_m} \\
x_r \; &= \; \left(\frac{2^4 \rho_e}{\rho_m} \right)^{1/3} r_e \; \approx \; 2.5 \left(\frac{\rho_e}{\rho_m} \right)^{1/3} r_e \; \approx \; 2.9\,r_e \; .
\end{aligned}
\tag{57}
$$

---

[49]See *Stacey* (p. 129–133 1992) for a more rigorous treatment of the Roche limit.

[50]This is admittedly a bit "hand-wavy," but it is standard in most introductory derivations (e.g., *Hartmann*, 1999, p. 60). In the derivation we assume that the two moon-balls are sufficiently far from the earth so that $r/x \ll 1$, and then we keep only the leading coefficient of the binomial expansion (zeroth-order).

Thus, we have derived Equation (52) and we have shown that for the earth–moon system, the Roche limit is $2.9\,r_e$, which is about 18,500 km. If our moon were to come within this distance, it would be torn into smaller fragments by the differential force.

5.3 Calculating earth–moon distance from tidal cycles preserved in the rock record

How are the tidal cycles (Figures 35–40) detected in the rock record and how can they be determined to an accuracy of two decimal places? First, the thickness of each rhythmite layer in the rock record is measured (see Figure 41E-F). The lamina thickness is then plotted as a histogram (such as in Figure 32D), which can be examined using Fourier analysis to extract the cycles. Figure 41 shows the results from 1580 neap-spring-neap cycle thickness measurements from the layers in a 600-Ma (Precambrian) rock core from Australia. This particular record preserved an astounding 60 consecutive (Precambrian) years of daily tidal cycle deposits.[51]

The periods of the tidal cycles shown in Figure 41 can be used to determine the length of the number of days per synodic month and the number of days per year at the time the sediment was deposited (620 Ma). These values can provide an estimate for the earth's rotational rate and the distance to the moon. Because the tidal cycles record the time in the earth's reference frame, it is necessary to convert the paleoastronomical tidal cycle periods into sidereal times. Using different tidal cycles (sidereal time), one can make multiple calculations of the earth–moon distance,[52] and these values can be checked with Kepler's laws for internal consistency.[53]

5.4 Evidence of lunar retreat from the rock record

Knowing the age of the rock in which the tidal cycle is preserved, one may conclude that ocean tides were present on the earth at the time the sediment was deposited.[54] The presence of ocean tides can be found throughout the rock record. The oldest evidence of tides is from a sandstone formation in South Africa dated 3.2 Ga (3.2 billion of years before present).[55] (For comparison, the earth formed about 4.6 Ga.) Evidence of ocean tides has also been recognized in sedimentary

---

[51]Although some of the daily tidal events were probably not preserved in the record, the peaks in Figure 41 are sharp and indicate the lack of "noise" in the data.

[52]This calculation is usually straightforward, from period to radius (or semi-major axis) of orbit. However, one must be careful to keep track of what reference frame the cycle is recorded in.

[53]*Williams* (2000) is the only rhythmite study that does this check.

[54]The age of rocks are determined by measuring the amount of radioactive material (e.g., K, Ar, U) in a sample of rock. There are several other methods for constraining the age of rocks, but the isotopic dating method is the most accurate, especially for Precambrian and older rocks.

[55]Moodies Group formations of *Eriksson and Simpson* (2000).

rocks with ages 2.4 Ga,[56] 2.3 Ga,[57] 0.9 Ga,[58] 0.62 Ga,[59] 0.48 Ga,[60] and 0.30 Ga,[61] among others; only four studies, however, have a data set good enough (i.e., 'clean' and long) to calculate the earth–moon distance (Figure 44). It is not unreasonable to assume that ocean tides have been present continuously throughout the earth's history, at least as far back as 3.2 billion years.

Geological studies can help constrain the lunar retreat rate over the course of the earth's history. If every tidal study listed above could provide an earth–moon distance value, then we could plot one point for each study on a plot of earth–moon distance versus time. This is shown for four studies in Figure 44. Derivations of tidal energy dissipation[62] provide an equation for the earth–moon distance at an earlier time in the earth's history:

$$ d_t \; = \; d_0 \left(1 - \frac{13}{2} \frac{\left\langle \dot{d_t} \right\rangle}{d_0} \right)^{2/13} , \tag{58} $$

where $d_0 = 3.82 \times 10^{10}$ cm is the present-day earth–moon distance and $\left\langle \dot{d_t} \right\rangle$ is the mean lunar retreat rate at a time t, which is based on the calculation from the geologic study and the present day value d_0 (*Walker and Zahnle*, 1986). Although there are few data points, this plot is one of the only lines of evidence for the lunar retreat rate over the earth's history. One important note is that the best-constrained curve (D) suggests that the moon was not within the Roche limit in the past four billion years, as suggested by the others. Further studies of tidal rhythmite deposits should help to constrain the lunar retreat rate curve.

---

[56] Weeli Wolli banded iron formation of *Williams* (2000).

[57] Chaibas formation of *Bose et al.* (1997).

[58] Big Cottonwood formation of *Chan et al.* (1994); *Sonett et al.* (1996); *Sonett and Chan* (1998). *Sonett et al.* (1996) contains several mistakes with published corrections (e.g., *Science*, v. 100, p. 1325), which ultimately led to a re-analysis of the dataset (*Sonett and Chan*, 1998).

[59] Elatina formation of *Williams* (1989b, 2000). See footnote in Appendix D.

[60] Jordan Formation (Uppermost Cambrian) of *Tape et al.* (2000, 2003).

[61] Brazil formation of *Kvale and Archer* (1990); *Kvale et al.* (1999). The Mansfield Formation underlies the Brazil Fm. and also records tidal cycles (*Kvale et al.*, 1989).

[62] The lunar retreat rate curves are based on energy dissipation due to the friction of the ocean tides. The equations are discussed in *Walker and Zahnle* (1986). See also *Lambeck* (1980).

6 Summary

I have found it very difficult to understand tides — from the physics of differential force, to the propagation of the tidal wave in the ocean, to the astronomical variations that give rise to tidal cycles. Looking at tides from different perspectives — the physicist, the oceanographer, the sedimentologist — provides perhaps the best approach to understanding tides. This paper has covered a large amount of material on tides. I hope that the reader may retain a few key points about tides, which I have listed below.

1. Differential force ("tidal force") arises in any object with finite extent accelerating in a gravitational field. The differential force is the difference between the force on the object's center of mass and the force on a part of the object closer or further from the source of the field. Thus, there is a differential force at the earth due to the combined effects of the moon, sun, and planets.

2. The tides on the earth are due primarily to the sun and the moon, the most apparent effect being the neap-spring-neap fortnightly cycle. The relative motion of the sun and moon with respect to the earth generates tidal cycles with periods ranging from 14 days to 18 years (and longer).

3. Circular motion is not a prerequisite for tides, but free fall acceleration is. If we stopped the earth and moon in their orbits, then "let go", they would accelerate toward each other in a catastrophic manner, and we would still get the two tidal bulges on the earth (as well as two on the moon).

4. Rotation of the earth is not a prerequisite for tides. Rotation allows us to "see" the tidal bulges on a daily period in the form of the ebb-flood cycle, which occurs once or twice per day (diurnal or semidiurnal), depending on the coastal area. Even without rotation, we would still "see" the tidal bulges that arise due to the longer-period tidal cycles.

5. On a continent-less, spherical earth, the global ocean's preferred shape is the equilibrium tide, which is an ellipsoidal equipotential water surface (i.e., it has two bulges) whose semimajor axis parallels the earth–moon axis.

6. The equilibrium tide does not account for the complex propagation of the tidal wave in the ocean basin, which is governed in part by the basin geometry and in part by the Coriolis effect.

7. The equilibrium tide does not account for the several-meter-scale tidal range in coastal areas, where the tidal wave is confined into narrow openings and may be influenced by resonance in the basin.

8. An understanding of the sedimentary deposition in modern tidal systems can be applied to the rock record to recognize ancient tidal systems in sedimentary layers. Geologic studies

indicate that oceanic tides have been present for the majority of the earth's history (at least over the past three billion years).

9. The sedimentary rock record records tidal cycles with a wide range of periods: 12 hours, 24 hours, 14 days, 28 days, 183 days, 8.8 years, and 18.6 years. The length of the period of the cycles is limited by the length of the uninterrupted record of tidally-deposited sedimentary layers.

10. Friction of the oceans due to tides is slowing the earth's rotation. The decrease in the earth's rotational angular momentum is accompanied by an increase in the net orbital momentum of the earth–moon system, which is evidenced by an increasing earth–moon distance.

11. Lunar laser ranging shows that the moon is retreating from the earth at about 4 cm per year (with an error of ± 0.07 cm/yr). Geologic studies provide constraints for the lunar retreat over the course of the earth's history.

7   Acknowledgments

A   The potential energy approach to the 3D case

In this section we derive Equation (31), the starting point for Section 2.6.

Gravitational force, like an electric field force, is a central force, "a force whose line of action passes through a fixed point or center of force" (*Fowles*, 1962, p. 80). The work done by a central force in moving an object does not depend on the path; every central force is thus conservative. Because gravitational force is conservative, the change in potential energy in moving an object from point a to point b can be expressed as the negative integral of the work

$$\Delta U_{ab} \;=\; -\int_a^b \mathbf{F}_G \cdot \mathbf{ds} \;, \tag{59}$$

where $\mathbf{F}_G$ is the gravitational force on the object and $\mathbf{ds}$ is an infinitesimal displacement vector. Here we use a potential energy argument based on *Barger and Olsson* (1973) to supplement the general case (two bodies, three dimensions) treated in Section 2.4. Rewriting Equation (59) using vectors, the change in potential energy in moving the object from position $\mathbf{r}_s$ to position $\mathbf{r}$ is defined as the negative integral of the work:

$$\Delta V_{\mathbf{r}_s\,\mathbf{r}} \;=\; -\int_{\mathbf{r}_s}^{\mathbf{r}} \mathbf{F}_G \cdot \mathbf{dr} \;, \tag{60}$$

where, if we take $\mathbf{r}_s$ to be sufficiently far away such that $V(\mathbf{r}_s) = 0$, we can express the potential energy at a point as

$$V(\mathbf{r}) \;=\; -\int_{\mathbf{r}_s}^{\mathbf{r}} \mathbf{F}_G \cdot \mathbf{dr} \;, \tag{61}$$

Our "tidal equation" (Eq. 13) is expressed in terms of force per unit mass. We therefore define a gravitational potential as the potential energy per unit mass:

$$\Phi(\mathbf{r}) \;=\; \frac{V(\mathbf{r})}{m} \;=\; -\int_{\mathbf{r}_s}^{\mathbf{r}} \frac{\mathbf{F}(\mathbf{r})}{m} \cdot \mathbf{dr} \;, \tag{62}$$

Rewriting this expression and using Equation (13), we have

$$-\nabla\Phi(\mathbf{r}) \;=\; \frac{F(\mathbf{r})}{m} \;=\; \ddot{\mathbf{r}} \;=\; -\frac{G\,M_e}{r^2}\,\hat{\mathbf{r}} \;-\; \frac{G\,M_m}{R^2}\,\hat{\mathbf{R}} \;+\; \frac{G\,M_m}{d^2}\,\hat{\mathbf{d}} \;. \tag{63}$$

We can find the gravitational potential function $\Phi(\mathbf{r})$ corresponding to the force $\mathbf{F}(\mathbf{r})$ by using Equation (62) and integrating Equation (63) over a convenient path $\mathbf{dr}$. As *Barger and Olsson* (1973) suggest, it is simpler to guess $\Phi(\mathbf{r})$ and then verify that it gives the correct force (by Eq. 63). We'll take the scenario shown in Figure 6, with the moon situated on the x'-axis at a fixed distance d from the earth. We have the vector relationship (see Figure 6) $\mathbf{R} = \mathbf{d} + \mathbf{r}$, where $\mathbf{d}$ is now constant, even as the position of particle P is varied. The gravitational potential that

gives the correct force is (*Barger and Olsson*, 1973)

$$\Phi(\mathbf{r}) = -\frac{G\,M_e}{r} - \frac{G\,M_m}{R} + \frac{G\,M_m\,x}{d^2} \ . \tag{64}$$

The distance R between the moon (point M, mass M_e) and the particle on the earth's surface [point $P(x, y, z)$, mass m] is

$$R^2 = (d-x)^2 + y^2 + z^2 = d^2 - 2dx + x^2 + y^2 + z^2 = d^2 - 2dx + r^2 \ , \tag{65}$$

which can be rewritten as

$$\frac{1}{R} = \frac{1}{(d^2 - 2dx + r^2)^{1/2}} = \frac{1}{d\left(1 - \frac{2x}{d} + \left(\frac{r}{d}\right)^2\right)^{1/2}} \ . \tag{66}$$

We can expand $1/R$ in powers of $r/d \approx 0.017 \ll 1$ by using the binomial expansion

$$(1+\beta)^n = 1 + n\beta + \frac{n(n-1)}{2}\beta^2 + \cdots \tag{67}$$

with $n = -1/2$ (then $n(n-1)/2 = 3/8$) and

$$\beta = -\frac{2x}{d} + \frac{r^2}{d^2} \ , \tag{68}$$

as follows:

$$
\begin{aligned}
\frac{1}{R} &= \frac{1}{d}\left[1 - \frac{2x}{d} + \left(\frac{r}{d}\right)^2\right]^{-1/2} \\
&= \frac{1}{d}\left[1 - \frac{1}{2}\left(-\frac{2x}{d} + \frac{r^2}{d^2}\right) + \frac{3}{8}\left(-\frac{2x}{d} + \frac{r^2}{d^2}\right)^2 + \cdots\right] \\
&= \frac{1}{d}\left[1 + \frac{x}{d} + \frac{(3x^2 - r^2)}{2d^2} - \frac{3xr^2}{2d^3} + \frac{3r^r}{8d^4} + \cdots\right] \\
&\approx \frac{1}{d} + \frac{x}{d^2} + \frac{(3x^2 - r^2)}{2d^3} \ .
\end{aligned}
\tag{69}
$$

In this expansion we retain only the powers of r/d (or x/d) through $(r/d)^2$; the higher order terms shown are removed in the last step. Using this expansion, the potential (Eq. 64) is approximated by

$$
\begin{aligned}
\Phi(\mathbf{r}) &\approx -\frac{G\,M_e}{r} + \frac{G\,M_m\,x}{d^2} - G\,M_m\left[\frac{1}{d} + \frac{x}{d^2} + \frac{(3x^2 - r^2)}{2d^3}\right] \\
\Phi(\mathbf{r})\left(+\frac{G\,M_m}{d}\right) &= -\frac{G\,M_e}{r} - \frac{G\,M_m}{d^3}\left[-dx + dx + \frac{3}{2}x^2 - \frac{1}{2}r^2\right] \\
&= -\frac{G\,M_e}{r} - \frac{G\,M_m\,r^2}{d^3}\left[\frac{3}{2}\left(\frac{x}{r}\right)^2 - \frac{1}{2}\right] \ .
\end{aligned}
\tag{70}
$$

Note that we have moved the constant $G\,M_m/d$ to the left side, since the definition of the potential allows for an arbitrary constant. Transformation from Cartesian to spherical coordinates is defined by

$$\mathbf{r} \;=\; x\,\hat{\mathbf{x}} + y\,\hat{\mathbf{y}} + z\,\hat{\mathbf{z}} \;=\; (r\sin\theta\cos\phi)\hat{\mathbf{x}} + (r\sin\theta\sin\phi)\hat{\mathbf{y}} + (r\cos\theta)\hat{\mathbf{z}}\;, \tag{71}$$

where $r^2 = x^2 + y^2 + z^2$, θ is the polar angle, and ϕ is the azimuthal angle. Thus, we have $x/r = \sin\theta\cos\phi$, and Equation (70) becomes

$$\Phi(\mathbf{r}) \;=\; -\frac{GM_e}{r} - \frac{GM_m r^2}{d^3}\left[\frac{3}{2}\sin^2\theta\cos^2\phi - \frac{1}{2}\right]\;. \tag{72}$$

Setting this equation equal to a constant will give an equipotential surface known as an equilibrium tide. See Section 2.6.

B   The one-body and two-body problem

The two examples used in the paper to explain differential force and the nature of the earth–moon system are the one-body problem — the earth fixed with the moon revolving around it (or vice versa) — and the two-body problem — the earth and moon both revolving about a common center of mass. As an example of the differences, we will derive the period of revolution for the moon in both cases. For simplicity we assume circular orbits in both cases.

In the **one-body** case, the moon revolves about earth with a circular orbit of radius d. (In other words, we are assuming the earth is infinitely massive.) The moon's velocity is equal to its circumference of orbit, divided by its period: $v_1 = 2\pi\, d/T_1$. The net force on the moon is equal to the earth's gravity. Thus, we equate Newton's second law, using centripetal acceleration and the velocity in terms of period,

$$F_{net} \;=\; M_m\, a \;=\; M_m\, \frac{v_1^2}{d} \;=\; \frac{M_m}{d}\left(\frac{2\pi d}{T_1}\right)^2 \;=\; \frac{4\pi^2\, d\, M_m}{T_1^2}\;. \tag{73}$$

with the gravitational attraction:

$$F_{net} \;=\; F_G$$

$$\frac{4\pi^2 d\, M_m}{T_1^2} \;=\; \frac{G\, M_e\, M_m}{d^2}$$

$$(T_1)^2 \;=\; \frac{4\pi^2\, d^3}{G\, M_e}\;. \tag{74}$$

Equation (74) is an expression of Kepler's third law. Note that the period of the moon's orbit does not depend on its mass, but only on the mass of the central body and the distance to the central body.

The **two-body** problem for the earth–moon system is outlined in Figure 45, where the inertial reference frame — the earth–moon center of mass — is assumed to be fixed. The moon and the earth make one revolution about the earth–moon center of mass in time T_2, with circular orbits of radii d_m and d_e, respectively. The equation of motion for the moon is (*Symon*, 1961, p. 178–181)

$$\mathbf{F}_G \;=\; \mu\, \ddot{\mathbf{d}}\;, \tag{75}$$

where $\mathbf{F}_G$ is the gravitational force between the earth and moon (the net force), μ is the reduced mass of the earth–moon system,

$$\mu \;=\; \frac{M_m\, M_e}{M_m + M_e}\;, \tag{76}$$

and $\mathbf{d}$ is the relative coordinate (see Figure 45). Substituting the gravitational force and the

centripetal acceleration into Equation (75), we get

$$\frac{G\,M_m\,M_e}{d^2} = \mu \left(\frac{v^2}{d}\right) . \tag{77}$$

Substituting the reduced mass (Eq. 76) and the velocity $v = 2\pi d/T_2$ into Eq. 77, we get

$$\frac{G}{d} = \frac{1}{M_m + M_e}\left(\frac{2\pi d}{T_2}\right)^2 . \tag{78}$$

After simplification, we find that the period of lunar revolution in the two-body problem is given by

$$(T_2)^2 = \frac{4\pi^2\,d^3}{G\,(M_m + M_e)} . \tag{79}$$

This period is slightly shorter than in the one-body case (Eq. 74):

$$\frac{T_2}{T_1} = \sqrt{\frac{\frac{d^3}{M_m+M_e}}{\frac{d^3}{M_e}}} = \sqrt{\frac{M_e}{M_m + M_e}} = \left(1 + \frac{M_m}{M_e}\right)^{-1/2} .$$

Plugging in the constants (Table 1) into Equations (74) and (79), the one-body lunar period is about 27.4 days and the two-body period is about 27.3 days. The earth will have the same period of revolution about the earth–moon center of mass as that of the moon (Figure 8).

The Bohr model of the hydrogen atom offers an analogy to the orbital motion in the earth–moon system. In the Bohr model, a single electron with negative charge $-e$ and mass m_e orbits a single proton with positive charge $+e$ and mass $m_p \approx 1800\,m_e$. The Coulomb force on the electron, $F = ke^2/r^2$ (Table 2), allows it to maintain a circular orbit of radius r. The Bohr derivation[63] yields an expression for the allowed energy levels for the electron

$$E_n = -E_R/n^2 . \tag{80}$$

where n is the energy level and E_R is the Rydberg energy constant given by

$$E_R = \frac{\left(ke^2\right)^2}{2\left(\frac{h}{2\pi}\right)^2}\,m_e = \left(\frac{2\pi^2 k^2 e^4}{h^2}\right)m_e , \tag{81}$$

where h is Plank's constant. Because the mass of the proton is much greater than the mass of the electron ($m_p \approx 1800\,m_e$), the Bohr model is approximated as a one-body problem, with the proton fixed in space. In actuality, the proton and electron revolve about a common center of mass (two-body problem).[64] To find the Rydberg energy in the two-body problem the mass

---

[63]This analogy is suggested in *Arons* (1979, p. 936). The Bohr model is treated in almost any physics text (e.g., *Taylor and Zafiratos*, 1991, p. 130–139).

[64]The resultant energy levels of the hydrogen atom are therefore reduced by about 1 part in 1800 as a result of this correction. The discrepancy is small but detectable on a spectrometer (*Taylor and Zafiratos*, 1991, p. 138).

of the electron must be replaced with the reduced mass, which gives a corrected, "two-body" Rydberg energy constant (Eq. 81) of

$$E_R = \left(\frac{2\pi^2 k^2 e^4}{h^2}\right) \frac{m_e \, m_p}{m_e + m_p} \; . \tag{82}$$

Just as the two-body lunar revolution period was a more accurate description of the moon's behavior, the two-body Rydberg energy constant should predict the energy values of the hydrogen atom better than the "one-body" Rydberg energy constant (Eq. 80).

C   Selected equation derivations

Taylor series for a few selected functions

The tides literature is filled with Taylor series expansions; although the language may come in many forms — "small-angle approximation", "binomial expansion/series/approximation", "Taylor series/approximation" — but they can be easiest understood in terms of Taylor series[65].

A one-dimensional Taylor series is a series expansion of a real function $f(x)$ about a point $x = x_0$ is given by

$$f(x) = f(x_0) + f'(x_0)\,(x - x_0) + \frac{f''(x_0)}{2!}\,(x - x_0)^2 + \frac{f^{(3)}(x_0)}{3!}\,(x - x_0)^3 + \cdots . \tag{83}$$

A Maclaurin series is a Taylor series expansion of a function $f(x)$ about $x_0 = 0$. For example, the Maclaurin series for $\sin x$, $\cos x$, and $\tan x$ are given by

$$\sin x \;=\; x - \frac{x^3}{3!} + \frac{x^5}{5!} - \cdots \qquad \text{for all x} \tag{84}$$

$$\cos x \;=\; 1 - \frac{x^2}{2!} + \frac{x^4}{4!} - \cdots \qquad \text{for all x} \tag{85}$$

$$\tan x \;=\; x + \frac{x^3}{3} + \frac{2x^5}{15} + \cdots \qquad \text{for } |\mathrm{x}| < \frac{\pi}{2} \tag{86}$$

Note that, to first order,

$$\sin x \approx \tan x \approx x, \tag{87}$$

which is known as the "small-angle approximation".

From the binomial theorem, we have the Maclaurin series

$$(1 + x)^r \;=\; 1 + rx + \tfrac{1}{2}r(r - 1)x^2 + \tfrac{1}{6}(r - 1)(r - 2)x^3 + \cdots \qquad \text{for } |\mathrm{x}| < 1 \tag{88}$$

$$(1 - x)^{-r} \;=\; 1 + rx + \tfrac{1}{2}r(r + 1)x^2 + \tfrac{1}{6}(r + 1)(r + 2)x^3 + \cdots \qquad \text{for } |\mathrm{x}| < 1 \tag{89}$$

Note that, to first order, these series are both equal to $1 + rx$.

---

[65]In fact, only special cases of the binomial series, such as Equations (88) and (89), give the Taylor series.

Equations (23) and (24)

We'll show Equation (23) first. Expanding the cosine term in Equation (16) and substituting Equations (20)–(22) gives

$$
\begin{aligned}
f_r &= \left(\frac{G\,M_m}{R^2}\right)\cos\left(\phi+\alpha\right) \\[2mm]
&= G\,M_m\left(\frac{1}{R^2}\right)(\cos\phi\cos\alpha - \sin\phi\sin\alpha) \\[2mm]
&\approx \left(\frac{G\,M_m}{d^2}\right)\left(1+\frac{2r_e}{d}\cos\phi\right)\left(\cos\phi - \sin\phi\left(\frac{r_e}{d}\sin\phi\right)\right) \\[2mm]
&= \left(\frac{G\,M_m}{d^2}\right)\left(\cos\phi - \frac{r_e}{d}\sin^2\phi + \frac{2r_e}{d}\cos^2\phi - 2\left(\frac{r_e}{d}\right)^2\cos^2\phi\sin^2\phi\right) \\[2mm]
&= \left(\frac{G\,M_m}{d^2}\right)\left(\cos\phi - \frac{r_e}{d}\left((1-\cos^2\phi) - 2\cos^2\phi\right) - 2\left(\frac{r_e}{d}\right)^2\cos^2\phi\sin^2\phi\right) \\[2mm]
&= \left(\frac{G\,M_m}{d^2}\right)\left(\cos\phi - \frac{r_e}{d}\left(1-3\cos^2\phi\right) + \cdots\right),
\end{aligned}
$$

where, in the last step, we have ignored the $(r_e/d)^2$ term (as before).

Equation (24) follows a similar derivation:

$$
\begin{aligned}
f_\phi &= \left(\frac{G\,M_m}{R^2}\right)\sin\left(\phi+\alpha\right) \\[2mm]
&= G\,M_m\left(\frac{1}{R^2}\right)(\sin\phi\cos\alpha + \sin\alpha\cos\phi) \\[2mm]
&\approx \left(\frac{G\,M_m}{d^2}\right)\left(1+\frac{2r_e}{d}\cos\phi\right)\left(\sin\phi + \left(\frac{r_e}{d}\sin\phi\right)\cos\phi\right) \\[2mm]
&= \left(\frac{G\,M_m}{d^2}\right)\left(\sin\phi + \frac{r_e}{d}\cos\phi\sin\phi + \frac{2r_e}{d}\cos\phi\sin\phi + 2\left(\frac{r_e}{d}\right)^2\cos^2\phi\sin\phi\right) \\[2mm]
&= \left(\frac{G\,M_m}{d^2}\right)\left(\sin\phi + \frac{3r_e}{d}\cos\phi\sin\phi + 2\left(\frac{r_e}{d}\right)^2\cos^2\phi\sin\phi\right) \\[2mm]
&= \left(\frac{G\,M_m}{d^2}\right)\left(\sin\phi + \frac{r_e}{d}\left(\frac{3}{2}\sin 2\phi\right) + \cdots\right),
\end{aligned}
$$

where, in the last step, we use $\sin 2\phi = 2\cos\phi\sin\phi$ and again ignore the $(r_e/d)^2$ term.

Equation (30)

We insert Equation (29) into Equation (27) and simplify:

$$
\begin{aligned}
\mathbf{f}_0 &= \frac{G\,M_m}{d^2}\left[(\cos\phi)\hat{\mathbf{r}} - (\sin\phi)\hat{\boldsymbol{\phi}}\right] \\[2mm]
&= \frac{G\,M_m}{d^2}\left[\cos\phi\left(\cos\phi\hat{\mathbf{x}} + \sin\phi\hat{\mathbf{y}}\right) - \sin\phi\left(-\sin\phi\hat{\mathbf{x}} + \cos\phi\hat{\mathbf{y}}\right)\right] \\[2mm]
&= \frac{G\,M_m}{d^2}\left[\left(\cos^2\phi + \sin^2\phi\right)\hat{\mathbf{x}} + \left(\cos\phi\sin\phi - \cos\phi\sin\phi\right)\hat{\mathbf{y}}\right] \\[2mm]
&= \left(\frac{G\,M_m}{d^2}\right)\hat{\mathbf{x}}.
\end{aligned}
$$

Equation (43)

As seen from the earth, the angle subtended by each body is given by (Table 1; Figure 8A)

$$\tan(\theta_m/2) \;=\; \frac{r_m}{d} \;\approx\; 0.0045 \qquad \text{and} \qquad \tan(\theta_s/2) \;=\; \frac{r_s}{D} \;\approx\; 0.0046 \;. \tag{90}$$

Since these values are very small, we can make the approximation $\tan\theta \approx \theta$ (Eq. 87) and rewrite them as

$$\theta_m \;\approx\; \frac{2\,r_m}{d} \qquad \text{and} \qquad \theta_s \;\approx\; \frac{2\,r_s}{D} \;, \tag{91}$$

which can be rearranged to give

$$d \;\approx\; \frac{2\,r_m}{\theta_m} \qquad \text{and} \qquad D \;\approx\; \frac{2\,r_s}{\theta_s} \;. \tag{92}$$

These expressions are used in Equation (43).

Equation (45)

See Figure 19B. The angle between $\mathbf{r}_e$ and $\mathbf{d}$ is ψ. The points P and M can be expressed in Cartesian coordinates or spherical coordinates: $P(x_p, y_p, z_p)$ or $P(r_e, \phi_p, \theta_p)$ and $M(x_m, y_m, z_m)$ or $M(d, \phi_m, \theta_m)$, where θ is the polar angle (colatitude) and ϕ is the azimuthal angle (longitude). Using the substitutions for spherical coordinates (see Figure 19A and Eq. 72), the derivation of $\cos \psi$ follows:

$$
\begin{aligned}
\cos \psi \;&=\; \frac{\mathbf{r}_e \cdot \mathbf{d}}{|\mathbf{r}_e||\mathbf{d}|} \\[2mm]
&=\; \frac{x_p x_m + y_p y_m + z_p z_m}{r_e d} \\[2mm]
&=\; \frac{(r_e \sin \theta_p \cos \phi_p)(d \sin \theta_m \cos \phi_m) \;+\; (r_e \sin \theta_p \sin \phi_p)(d \sin \theta_m \sin \phi_m) \;+\; (r_e \cos \theta_p)(d \cos \theta_m)}{r_e\, d} \\[2mm]
&=\; \cos \theta_p \cos \theta_m + \sin \theta_p \sin \theta_m \left(\cos \phi_p \cos \phi_m + \sin \phi_p \sin \phi_m \right) \\[1mm]
&=\; \cos \theta_p \cos \theta_m + \sin \theta_p \sin \theta_m \cos \left(\phi_p - \phi_m \right) \; .
\end{aligned}
$$

The angle ψ is the angle between the directions marked by (ϕ_m, θ_m) and (ϕ_p, θ_p).

Equation (46)

Following *Cook* (1969, p. 72–73), we plug Equation (45) (derived above) into Equation (44), omitting the $\frac{1}{2}$ factor for now:

$$
\begin{aligned}
&3\cos^2\psi - 1 \\
=\ & 3\left[\cos\theta_p\cos\theta_m + \sin\theta_p\sin\theta_m\cos(\phi_p - \phi_m)\right]^2 - 1 \\
=\ & 3\left[\cos^2\theta_p\cos^2\theta_m + 2\cos\theta_p\cos\theta_m\sin\theta_p\sin\theta_m\cos(\phi_p - \phi_m) + \sin^2\theta_p\sin^2\theta_m\cos^2(\phi_p - \phi_m)\right]^2 - 1 \\
=\ & 3\Big[\cos^2\theta_p\cos^2\theta_m + \tfrac{1}{2}\sin^2\theta_p\sin^2\theta_m\left[\cos 2(\phi_p - \phi_m) + 1\right] \\
& + \tfrac{1}{2}\left(2\cos\theta_p\sin\theta_p\right)\left(2\cos\theta_m\sin\theta_m\right)\cos(\phi_p - \phi_m)\Big] - 1 \\
=\ & 3\cos^2\theta_p\cos^2\theta_m + \tfrac{3}{2}\sin^2\theta_p\sin^2\theta_m\left[\cos 2(\phi_p - \phi_m) + 1\right] + \tfrac{3}{2}\sin 2\theta_p\sin 2\theta_m\cos(\phi_p - \phi_m) - 1 \\
=\ & 3\cos^2\theta_p\cos^2\theta_m + \tfrac{3}{2}\left(1 - \cos^2\theta_p\right)\left(1 - \cos^2\theta_m\right) - 1 \\
& + \tfrac{3}{2}\sin^2\theta_p\sin^2\theta_m\cos 2(\phi_p - \phi_m) \\
& + \tfrac{3}{2}\sin 2\theta_p\sin 2\theta_m\cos(\phi_p - \phi_m) \\
=\ & \tfrac{1}{2}\left(3\cos^2\theta_p - 1\right)\left(3\cos^2\theta_m - 1\right) \\
& + \tfrac{3}{2}\sin^2\theta_p\sin^2\theta_m\cos 2(\phi_p - \phi_m) \\
& + \tfrac{3}{2}\sin 2\theta_p\sin 2\theta_m\cos(\phi_p - \phi_m) \ ,
\end{aligned}
$$

where in the last step we have done the following, with $a = \cos\theta_p$ and $b = \cos\theta_m$:

$$
\begin{aligned}
3\,a^2 b^2 + \tfrac{3}{2}(1 - a^2)(1 - b^2) - 1 &= 3\,a^2 b^2 + \tfrac{3}{2}(1 - b^2 - a^2 + a^2 b^2) - 1 \\
&= 3\,a^2 b^2 + \tfrac{3}{2} - \tfrac{3}{2}b^2 - \tfrac{3}{2}a^2 + \tfrac{3}{2}a^2 b^2 - 1 \\
&= \tfrac{9}{2}a^2 b^2 - \tfrac{3}{2}a^2 - \tfrac{3}{2}b^2 + \tfrac{1}{2} \\
&= \tfrac{1}{2}\left(9\,a^2 b^2 - 3\,a^2 - 3\,b^2 + 1\right) \\
&= \tfrac{1}{2}\left(3\,a^2 - 1\right)\left(3\,b^2 - 1\right) \ .
\end{aligned}
$$

Finally, multiplying by $\frac{1}{2}$ gives Equation (46):

$$
\begin{aligned}
\tfrac{1}{2}\left(3\cos^2\psi - 1\right) =\ & \tfrac{3}{4}\sin^2\theta_p\sin^2\theta_m\cos\left[2(\phi_p - \phi_m)\right] \\
& + \tfrac{3}{4}\sin 2\theta_p\sin 2\theta_m\cos(\phi_p - \phi_m) \\
& + \left(\frac{3\cos^2\theta_p - 1}{2}\right)\left(\frac{3\cos^2\theta_m - 1}{2}\right) \ .
\end{aligned}
$$

D Selected annotated bibliography

Introduction to tides

- *Darwin* (1898). Probably the most oft-cited treatment of tides. Great historical chapter on the development of tidal theory.

- *Gamow* (1962). A layman's introduction to the basic physics of tides, highlighted by simple illustrations and interesting facts about tides (see quote on p. 20).

- *Strahler* (1971). A classic, extensive earth sciences text with a good chapter on tides (Ch. 9). The physics aren't deep, but the tidal charts, showing actual daily tidal ranges for semidiurnal, mixed, and diurnal systems, are good.

- *Garrison* (1998). It's great to have a different perspective on the tides. This looks at tides and tidal phenomena at the scale of the ocean (as opposed to and astronomical scale or a coastal scale).

- *Pugh* (1988). I will cite this as a text *not to read*. This oft-cited text is one of the sloppiest treatments of tides (Ch. 3), and the figures are terrible.

Differential force and classical mechanics

- *Newton* (1687). It's worth seeing what the founding father of tides had to say. *Prinicipia* is overwhelming and includes at least two sections on tides: Book 1, Proposition 66, Corollaries 19 and 20 (p. 582–583) and Book 3, Proposition 24, Theorem 19 (p. 835–839). The first section outlines the equilibrium tide theory, which is explained (to varying degrees of clarity) in almost every physics treatment of tides.

- *Barger and Olsson* (1973). Section 7-2, "The Tides", is *a superior description of tides*, and one that I used as a basis for several sections (e.g., Section 2.5, Appendix A). I bought the book and would be happy to pass along a photocopy of the tides section to anyone interested.

- *Marion and Thorton* (1995). The section on tides (5.5, p. 204–210) appears to be based upon that of *Barger and Olsson* (1973).

- *Ohanian* (1976). Section 1.6 (p. 26–32) is a great explanation of tidal forces, and how an astronaut in free fall can prove he is in a non-inertial reference frame by examining the distorted shape of a water droplet in the spacecraft.

- *Kibble* (1985). Excellent treatment of tides in section 6.6 (p. 129–132). Kibble approaches tides from a potential standpoint, whereas I emphasized the force approach, which uses vectors.

- *White et al.* (1993). This possibly the only article that outlines a laboratory experiment to demonstrate the origin of the tidal bulge. The inverse-square force in the experiment is magnetic, and the centripetal acceleration is due to a record player turntable. Personal communication with White clarified some points.

- *Misner et al.* (1973). The bible of gravitation. Presents the tide-producing force in Ch. 1 (p. 29–44) and introduces a treatment involving differential geometry involving the Riemann curvature tensor and the fiducial geodesic (yikes!).

- *Tsantes* (1974). Equilibrium tidal theory derivation using vectors and hydrodynamic principles.

- *Horsfield* (1976). Derives the three components of the tides due to the earth's rotation (see my Section 2.8).

- *Arons* (1979). This article is a must-have. A substantial part of this paper contains ideas from Arons. He has a unique way of presenting tides and avoids all mention of fictitious forces.

- *Olson and Lytle* (2000). This is an interesting article about how other planets in the solar system influence the tides on the sun. It ties in historical events — alignment of planets in the sky — with (relatively large) predicted solar tides (see "Conjugations that changed the wold," same issue). Also addresses tides on earth.

Ocean tides, hydrodynamics, and wave theory

- *Lamb* (1945). Classic hydrodynamics text, cited in most hydrodynamic treatments of tides.

- *Seligmann and Steinberg* (1975).

- *Symon* (1961). Standard classical mechanics text, containing a very good treatment of hydrodynamics (p. 313–337).

- *Archer and Hubbard* (2003). An overview of the 13 highest tidal areas in the world. The final rankings: (1) Bay of Fundy, (2) Bristol Channel (SW England), (3) Ungava Bay (NE Canada), (4) Gulf of St. Malo (NW France), (5) Straits of Magellan, (6) Cook Inlet (southern Alaska), (7) Sea of Okhotsk (eastern Russia), (8) eastern English Channel, (9) northwest Australia, (10) west-central England, (11) Gulf of Cambay (eastern India), (12) Gulf of Mezan (NW Russia), and (13) the Yellow Sea (China/Korea).

- *Desplanque and Mossman* (2001). A very good treatment of the Bay of Fundy tides, the largest in the world.

- *Korgen* (1995). An interesting, non-mathematical treatment of an awesome phenomenon. It addresses the concepts of the resonant frequency of a basin and of modes of oscillation. It also points out a relationship between tidal currents and seiches.

- *Dronkers* (1964); *Schureman* (1941); *Marchuk and Kagan* (1984, 1989). Here are a few sources on the harmonic analysis of ocean tides. In essence the behavior of the tidal wave in the ocean depends on the numerous driving frequencies that arise from the earth–moon system. I didn't cover much of this in the paper.

Physical sedimentology and the preservation of tidal layers in the geological record

- *Allen* (1985). Perhaps the best source on physical sedimentology. "How do bedforms move?" (Section 4.7, p. 67–71) is a great section for understanding the relationship between the process of sand dune migration and the preservation of sand dune migration in the rock record (cross-bedding sets).

- *Reineck and Singh* (1980). The preeminent text on sedimentary geology, with emphasis on clastic deposition (i.e., sand and mud, as opposed to carbonate deposition, which is from fossils). 638 figures!

- *Nio and Yang* (1991); *Dalrymple* (1992); *Visser* (1980). Three great articles on how the daily and monthly tidal cycles are preserved in sedimentary systems and how one can identify tidal patterns in the sedimentary rock record.

- *Runkel* (1994); *Byers and Dott Jr.* (1995). The two main articles on the Jordan Sandstone, which contains a 485-Ma record of tides, as found in our study.

- *Tape et al.* (2000). A more detailed description of our Jordan Sandstone study, which documents 13 months of Cambrian tides near Winona, Minnesota. Our study was formally published in *Tape et al.* (2003).

- *Irwin* (1965); *Clark* (1982). Tides are generally believed to have not been present in the shallow seas covering the Midwest during Late Cambrian time, as suggested by these two papers. Our study of the Jordan Sandstone (*Tape et al.*, 2003) suggests that tides were present. A more informative title for *Clark* (1982) might be "Epeiric tides in Lower Ordovician North America: Evidence from the Shakopee Dolomite, southern Minnesota".

Tidal cycles in the rock record and the history of the earth–moon system

- *Williams* (2000). This is one of the most amazing articles I've ever read. It reviews a landmark study site of a Precambrian (620 Ma) rhythmite sandstone that records a 60-year (continuous) record of tidal deposits. It utilizes Fourier analysis to find monthly, semiannual, annual, and 18-year cycles, and it applies Kepler's laws to verify that the cycles are internally consistent. Great references, too. The review paper extends the findings of *Williams* (1989b,a).[66]

- *Kvale et al.* (1999). Good explanations of the various 28-day tidal cycles that arise from certain parameters of the moon's orbit: eccentricity, declination with respect to earth, and phase as observed from earth. Good figures synthesizing modern tides, the rock record, and lunar cycles. Fourier analysis applied to lamina thickness patterns. However, I think their explanation for the semiannual tidal cycle (their Figure 6A, my Figure 39) is incorrect, so try to reason out the tidal cycles for yourself and don't accept their explanations on faith.

- *Rosenburg* (1997). Synthesizes the results of several geologic studies, including those discussed in the two papers above, in discussing how the lengths of the day and year have changed over time. It doesn't have much to do with dinosaurs.

- *Eriksson and Simpson* (2000). The oldest evidence of ocean tides on earth: sedimentary layers 3.2 billion years old.

- *Zeilik and v. P. Smith* (1987).

- *Hartmann* (1999). Nice, simple mathematical treatment of differential force and the Roche limit (p. 57–60).

- *Dickey et al.* (1994). A feature article on lunar laser ranging, summarizing real-time measurements of several astronomical parameters, including the present-day lunar retreat rate (3.82 ± 0.07 cm/yr).

- *Walker and Zahnle* (1986). Discusses and derives the tidal energy dissipation equations (my Eq. 58).

---

[66]The story of the Elatina Formation is an interesting one, and it contains an important lesson. Williams originally attributed the source of the the cyclic pattern in the sedimentary layers to *sunspot cyclicity* (*Williams*, 1981, 1985). The mistake highlights the importance of ascribing the time interval of each sedimentary layer, e.g., 1 layer = 12 hours. In the words of Williams: "If each lamina of the Elatina series is regarded as an annual increment, the cyclicity displayed by that series bears strong empirical similarity to sunspot cyclicity, with a lamina-cycle representing a single sunspot cycle... Nonetheless...a tidal rather than a solar-climatic control of deposition must now be preferred as it can explain not only the Elatina cyclicity but also the new evidence of more complex lamina-cycles containing up to 25 or more laminae provided by the Reynella siltstone and the Chambers Bluff tillite" (*Williams*, 1989b, p. 41).

- *Condie* (1997). Contains a very good overview of the four models of the origin of the moon (p. 250–254).

- *Stacey* (1992). A basic introduction to some geophysical concepts, including tides (Section 3.4, "Tides and Tidal Friction", p. 115–133). Contains a substantial mathematical treatment of the Roche limit. For the most part, the figures are poor.

Earth tides and atmospheric tides

- *Wilhelm et al.* (1997). A synthesis of various tidal phenomena — including earth tides, atmospheric tides, and ocean tides — based on a conference in Germany.

- *Harrison* (1985); *Melchior* (1966). Solid earth tides.

- *Chapman and Lindzen* (1970); *Volland* (1988). Atmospheric tides.

Mathematical Physics

- *Harper* (1976); *Wong* (1991); *Griffiths* (1999); *Danby* (1988); *Taff* (1985). Mathematical physics is essential for understanding the mathematics behind the development of the gravitational potential. Spherical harmonics, Legendre polynomials, and Laplace's equation are addressed in Harper (p. 172–181), Wong (p. 216–250), Griffiths (p. 137–149), Danby (p. 112–120), and Taff (p. 6–14). In some cases they discuss gravitational force between masses; other times it is the electric force between charges. In both cases, the force goes as r^{-2} and the math is essentially the same.

Table 1: Astronomical constants.

Notation	Description	Value
G	gravitational constant	6.67×10^{-11} N m^2 kg^{-2} [kg^{-1} m^3 s^{-2}]
Earth (E)		
M_e	mass	5.97×10^{24} kg = 81.3 lunar masses
r_e	mean radius	6.371×10^6 m
D	mean distance from sun	1.496×10^{11} m (= 1 AU)
ρ_e	mean density	5520 kg m^{-3}
Moon (M)		
M_m	lunar mass	7.35×10^{22} kg = 1 lunar mass
r_m	mean radius	1.738×10^6 m
d	distance to earth	3.844×10^8 m = 60.3 earth radii
Sun (S)		
S_m	solar mass	1.99×10^{30} kg = 333,000 earth masses
r_s	radius	6.96×10^8 m
ρ_s	mean density	1400 kg m^{-3}
Earth–Moon Center of Mass (C.M.)		
$M_{CM} = M_e + M_m$	mass	6.044×10^{24} kg = 1.012 earth masses
	mean distance to center of earth	4.671×10^6 m = 0.73 earth radii
	mean distance to center of moon	3.7973×10^8 m = 59.54 earth radii

Table 2:   A comparison of the gravitational and electric force.

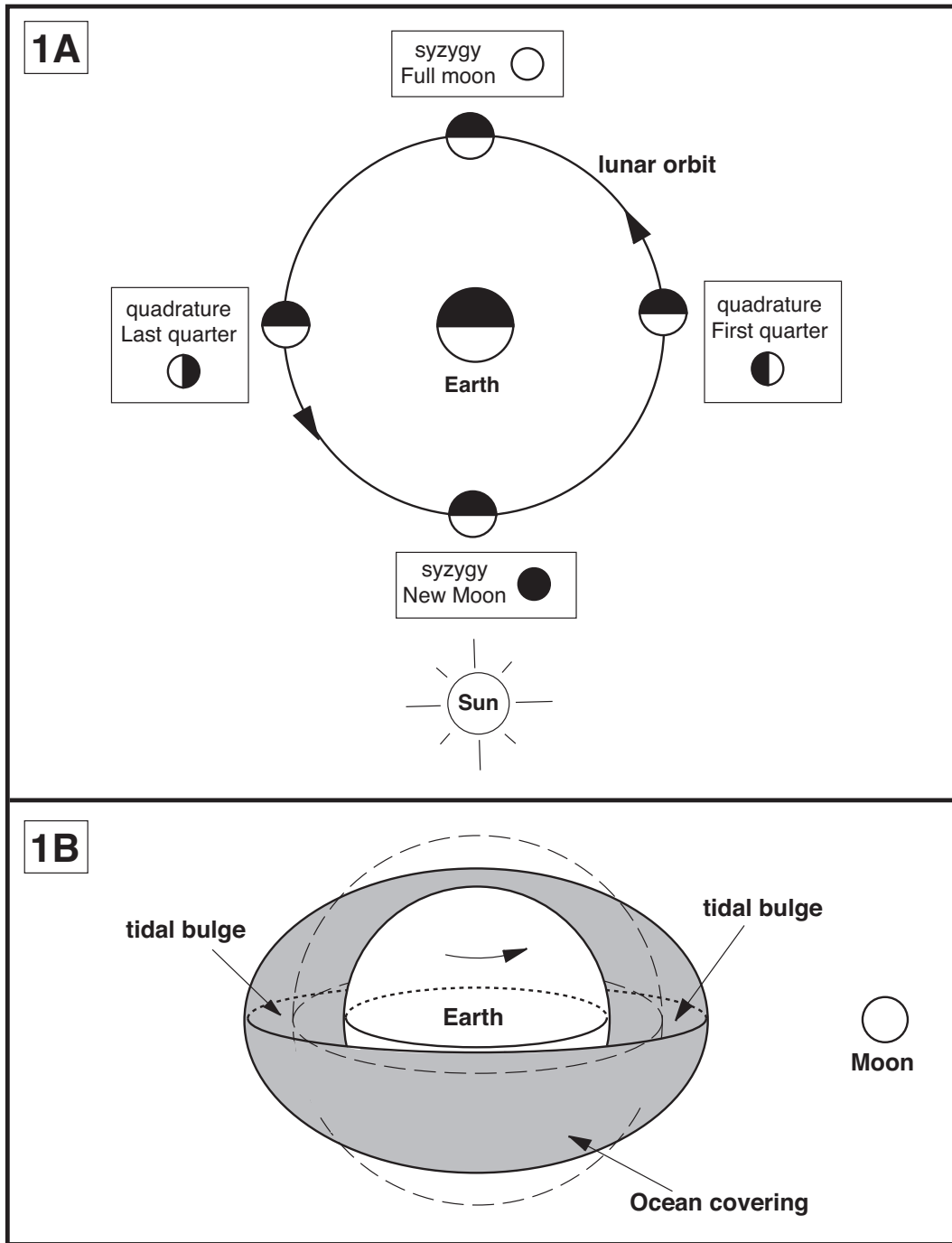|	Gravitational	Electrical
Particle	mass m_1 and m_2 test mass m	charge q_1 and q_2 test charge q
Force Equation	$\mathbf{F}_{G_{12}} = -\left(\dfrac{G\,m_1\,m_2}{r^2}\right)\hat{\mathbf{r}}_{12}$	$\mathbf{F}_{E_{12}} = \left(\dfrac{k\,q_1\,q_2}{r^2}\right)\hat{\mathbf{r}}_{12}$
Field Equation	$\mathbf{G} = \dfrac{\mathbf{F}_G}{m}$	$\mathbf{E} = \dfrac{\mathbf{F}_E}{q}$
Conservative Force	curl $\mathbf{F}_G = \mathbf{0}$	curl $\mathbf{F}_E = \mathbf{0}$
Potential Energy	$V_G(\mathbf{r}) = -\displaystyle\int_{\mathbf{r}_s}^{\mathbf{r}} \mathbf{F}_G \cdot d\mathbf{r}$	$V_E(\mathbf{r}) = -\displaystyle\int_{\mathbf{r}_s}^{\mathbf{r}} \mathbf{F}_E \cdot d\mathbf{r}$

Figure 1: An introduction to tides. **A.** The lunar cycle, showing the position of the moon at four different times and the corresponding view of the moon from the earth (the lunar phase). Syzygy is a generic term for the alignment of three bodies; quadrature is a generic term for the three bodies forming a right angle. **B.** Because we see two rise-and-falls of the tides each day, we might infer that the earth is spinning through two bulges of water on opposite sides. Dotted sphere is an undistorted ocean covering.
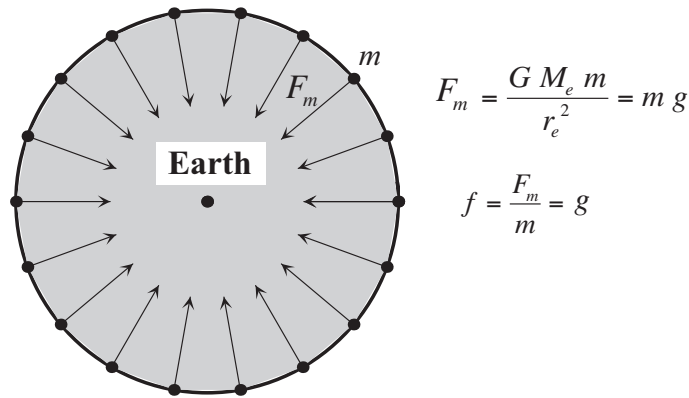
Figure 2: The earth at rest, without the moon. All the forces at the surface of the (perfectly spherical) earth are equal in magnitude and directed toward the center of mass of the earth. F_m is the force on a particle of mass m, which can also be expressed as f, the force per mass, which is equivalent to acceleration, in this case.
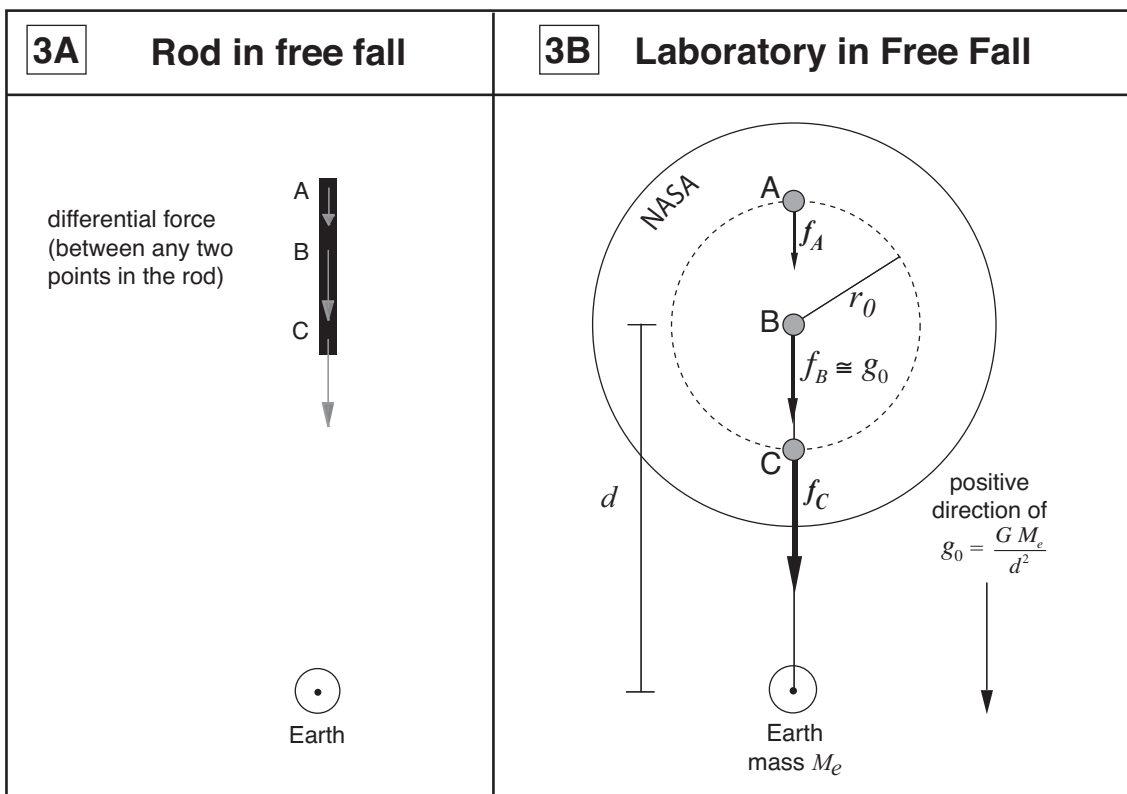

Figure 3: Free fall toward the (stationary) earth. **A.** The earth will exert a greater gravitational pull at point C of the rod than at point B or A. Thus, a differential force arises in the rod and tends to stretch the rod away from its center (point C) in both directions. **B.** A free-falling, rigid-shelled, spherical laboratory, in which we run a series of experiments. We drop a ball at points A, B, and C, and interpret what happens (see Section 2.3) After *Arons* (1979).

ocean tidal bulge

entire Earth (lab)
in free fall to moon
(linear motion)

Earth (lab)
center of
mass

ocean tidal bulge

arrows =
acceleration relative
to center of Earth (lab)

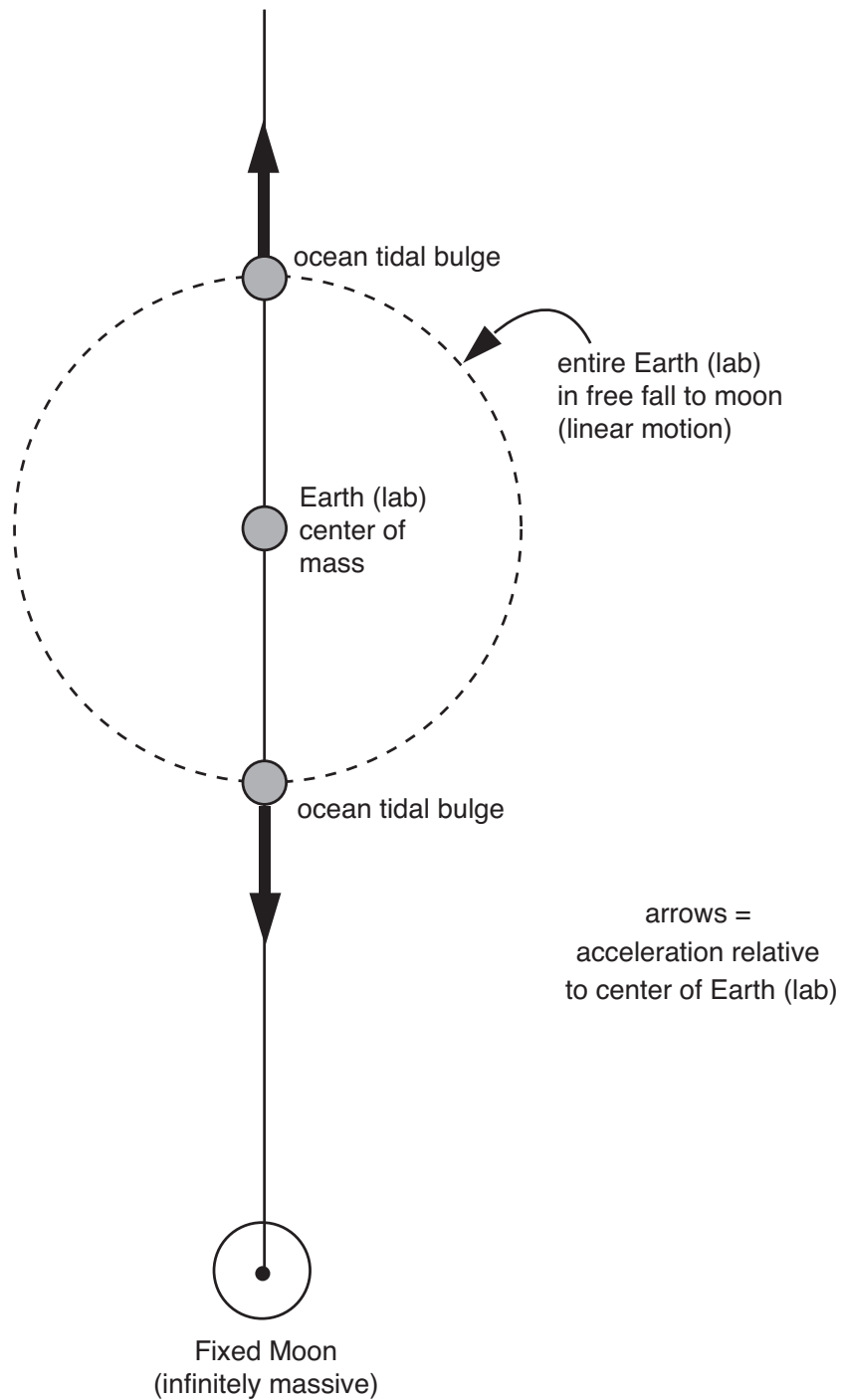Fixed Moon
(infinitely massive)

Figure 4:   Free-falling laboratory analogy to the earth–moon system. The laboratory in Figure 3B is replaced by the earth, and the earth is replaced by the moon. The acceleration of the balls relative to the center of mass of the lab (Figure 3B) corresponds to the acceleration of the oceans relative to the earth. The relative acceleration of the oceans causes the tidal bulges.

Case 1: LINEAR MOTION
("dropping" the spaceship from height d)

Case 2: CIRCULAR MOTION
(spaceship orbiting at radius d)

drop of water

drop of water

$$f = \frac{G\,M_e}{d^2} = \frac{v^2}{d}$$

constant in time

$$f = \frac{G\,M_e}{d^2}$$
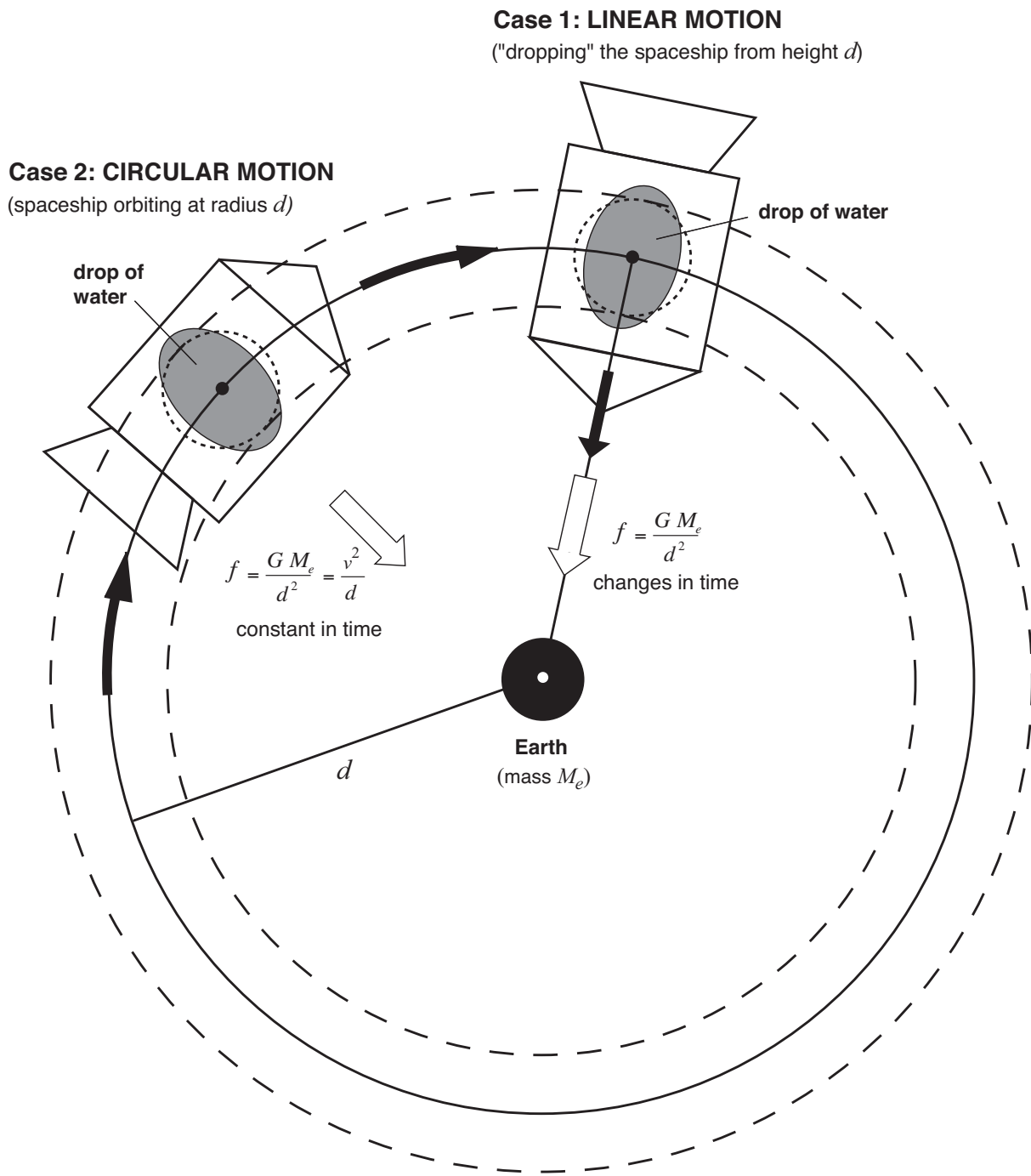
changes in time

Earth
(mass M_e)

d

Figure 5: Differential force due to linear motion versus circular motion. Our scenario is a water droplet in a spaceship in the gravitational field of the earth, which is at rest. (In other words, the mass of the earth is much, much greater than the mass of the spaceship). For each case, the solid arrows indicate the direction of the spaceship's motion, and the open arrows indicate the direction of the acceleration of the spaceship and water droplet (i.e., the direction of the force-per-mass due to earth). At time $t = 0$, the Case 1 spaceship is released from rest, and the Case 2 spaceship orbits the earth with speed v at distance d. The shape of the drop in Case 2 will remain constant in time. The shape of the drop in Case 1 will elongate in time (see Section 2.3).
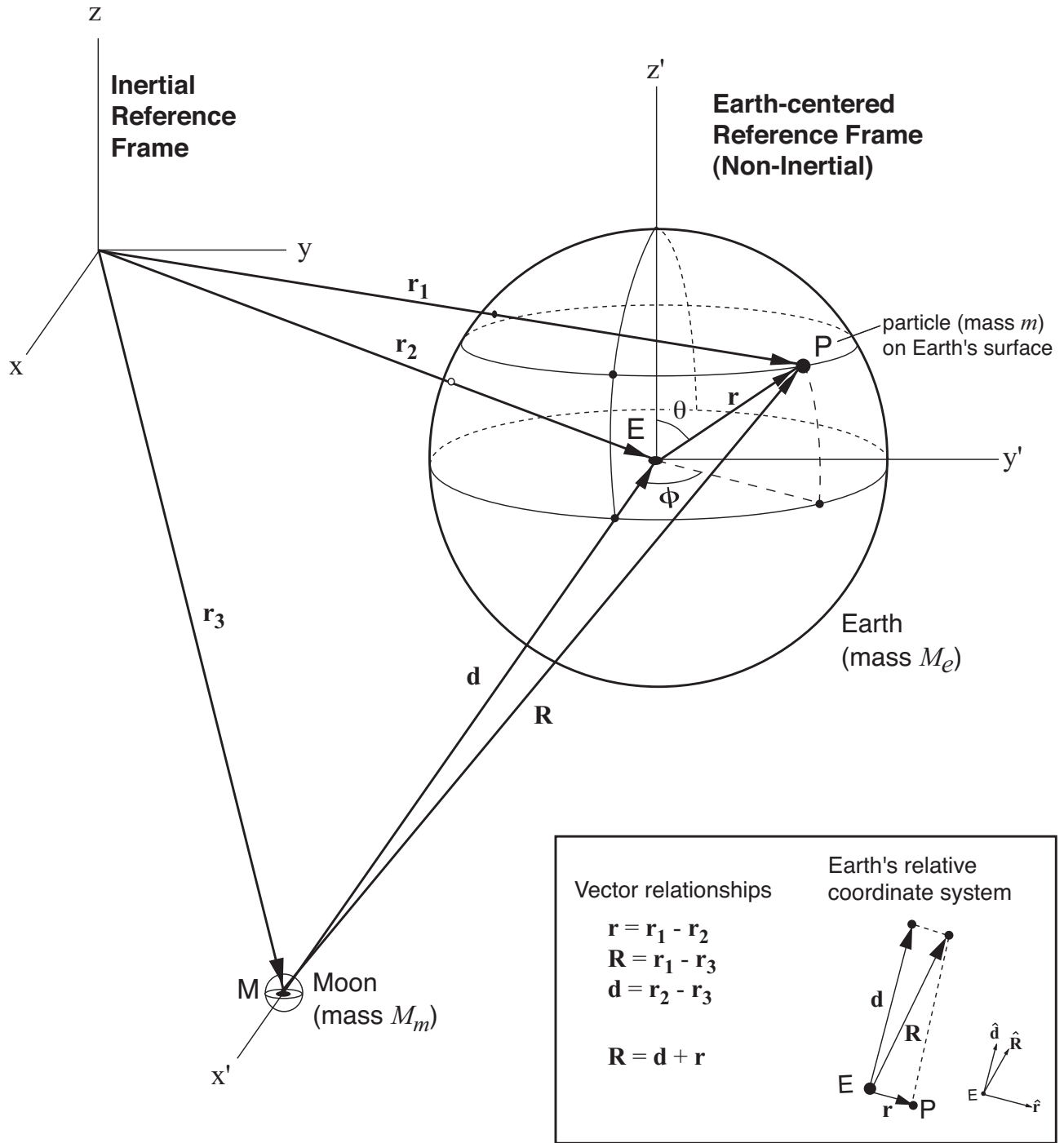
Figure 6: Configuration for the vector approach to the 3D treatment of the earth–moon system (after *Barger and Olsson*, 1973). The labeling system is specific to the earth–moon system, although the configuration applies to a general case: M and E could be any bodies, and P could be any point in space (not necessarily the "surface" of body E). The earth's coordinate system $(\mathbf{r}, \mathbf{d}, \mathbf{R})$ is non-inertial, since the earth (E, at position $\mathbf{r}_2$) could be accelerating with respect to the inertial reference frame.
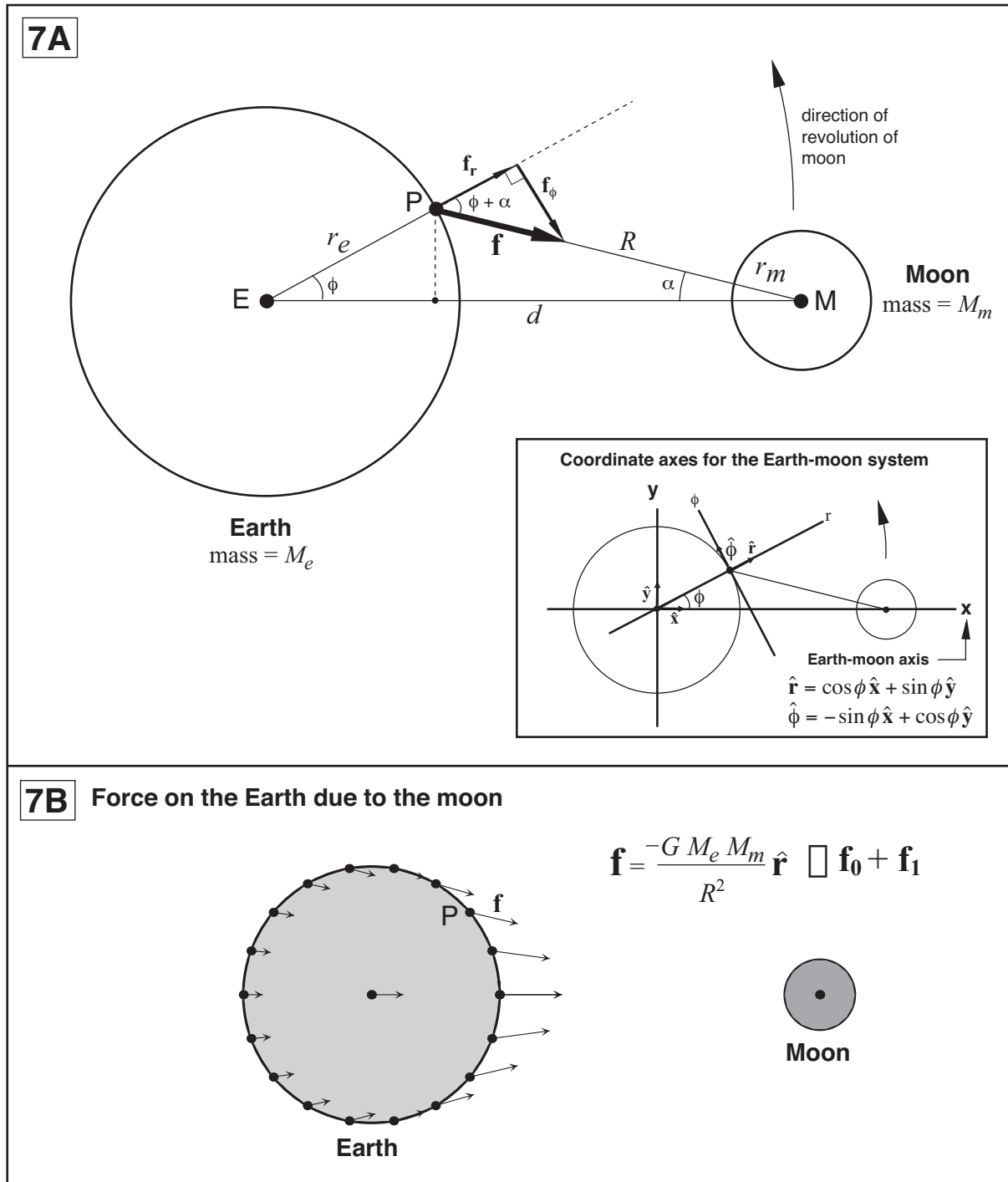
7A

$\mathbf{f_r}$

$\mathbf{f}_\phi$

direction of revolution of moon

P

$\phi + \alpha$

r_e

$\mathbf{f}$

R

ϕ

α

r_m

Moon
mass $= M_m$

E

d

M

Earth
mass $= M_e$

Coordinate axes for the Earth-moon system

y

ϕ

r

$\hat{\phi}$ $\hat{r}$

$\hat{y}$

ϕ

$\hat{x}$

x

Earth-moon axis

$\hat{r} = \cos\phi\,\hat{x} + \sin\phi\,\hat{y}$
$\hat{\phi} = -\sin\phi\,\hat{x} + \cos\phi\,\hat{y}$

7B **Force on the Earth due to the moon**

$$\mathbf{f} = \frac{-G\,M_e\,M_m}{R^2}\,\hat{r} \ \square\ \mathbf{f_0} + \mathbf{f_1}$$

P

$\mathbf{f}$

Moon

Earth

Figure 7: The force on the (non-rotating) earth due to the moon (2D). This view of the earth–moon system is looking down on the orbital plane of the moon and the cross-section this plane cuts through the earth. **A.** Configuration, variables and axes (after *Arons*, 1979). **B.** Plot of the force-per-mass at the surface and at the center of the earth. Compare with Figure 3B, which did not take into account the transverse dimension of the object with respect to the gravitational field. The force-per-mass **f** can be approximated as the sum of zero- and first-order components, which are plotted in Figures 9 and 11. Note that $\hat{\mathbf{R}}$ points from the moon to a point on the earth.
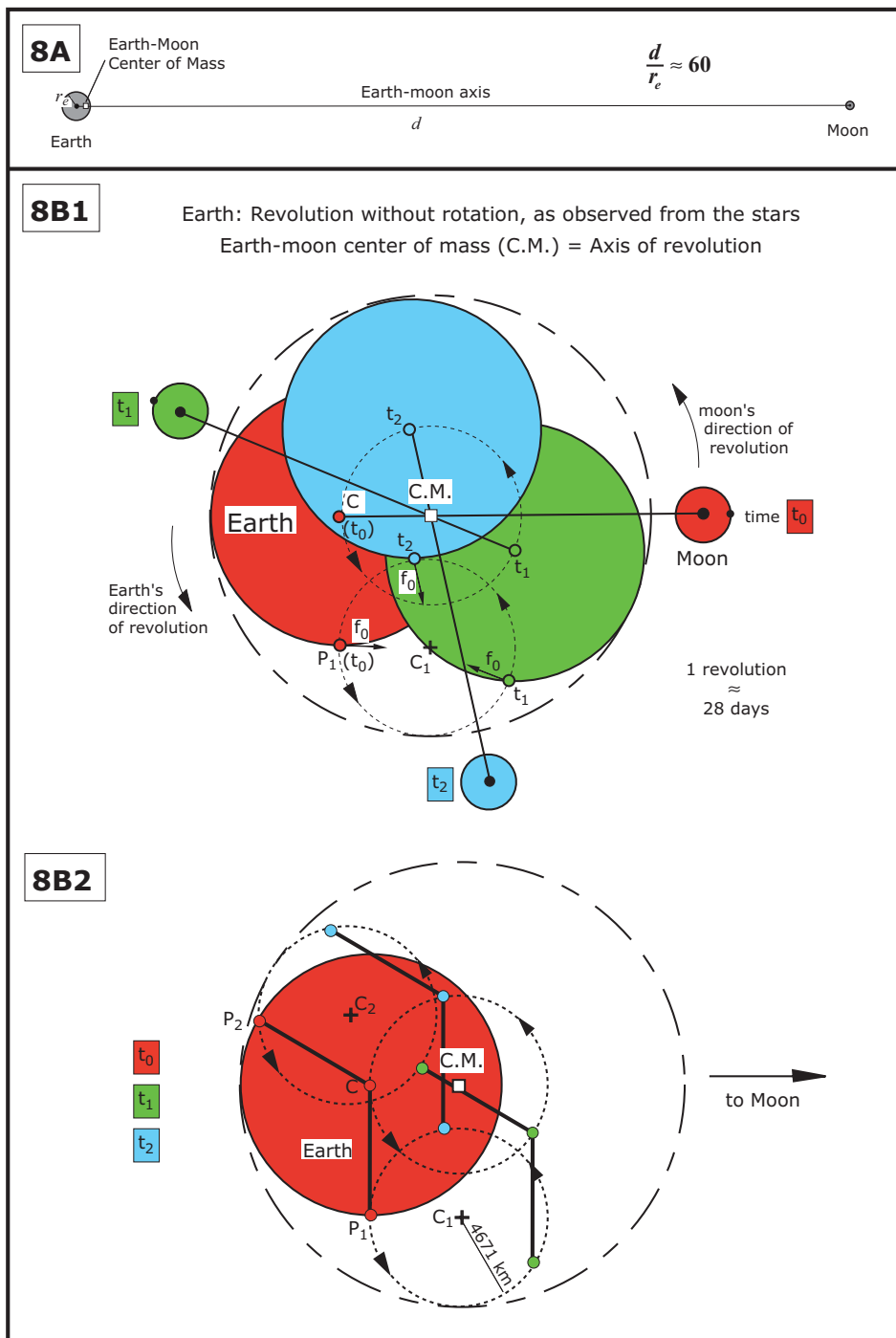
8A

Earth-Moon Center of Mass

Earth-moon axis

$\frac{d}{r_e} \approx 60$

r_e

Earth

d

Moon

8B1

Earth: Revolution without rotation, as observed from the stars
Earth-moon center of mass (C.M.) = Axis of revolution

moon's direction of revolution

Earth

C.M.

C (t_0)

t_2

f_0

t_1

Moon

time t_0

Earth's direction of revolution

f_0

P_1 (t_0)

C_1

f_0

t_1

1 revolution ≈ 28 days

t_1

t_2

8B2

t_0

t_1

t_2

P_2

C_2

C.M.

C

to Moon

Earth

P_1

C_1

4671 km

Figure 8: The two-body motion of the earth–moon system. Our reference frame is the stars, and the view is one looking down on the orbital plane of the moon and the cross-section this plane cuts through the earth. The rotation of the earth about its spin axis is neglected here. **A.** Earth–moon system, drawn to scale. **B1.** Three snapshots of the earth–moon systemat times t_0 (red), t_1 (green), and t_2 (blue). Over the course of one revolution about the earth–moon center of mass, each particle within the earth, such as P$_1$ or C, transcribes a circle about the earth–moon center of mass (C.M.). The radius of these circles is always constant as a result of the earth's revolution without rotation from the reference frame of the stars: any vector normal to the earth's surface always points in the same direction (i.e., toward the same stars). The zero-order centripetal force **f**$_0$ always points to the center of these circles, and therefore parallel to the earth–moon axis, as is shown for the circles centered at C.M. and C$_1$. **B2.** Three dotted circles show three paths followed by certain particles of the earth (P$_1$, P$_2$, C). Each particle makes a circle with a radius of 4671 km, the approximate distance from the center of the earth to the center of mass of the earth–moon system (C to C.M.). After *Arons* (1979).
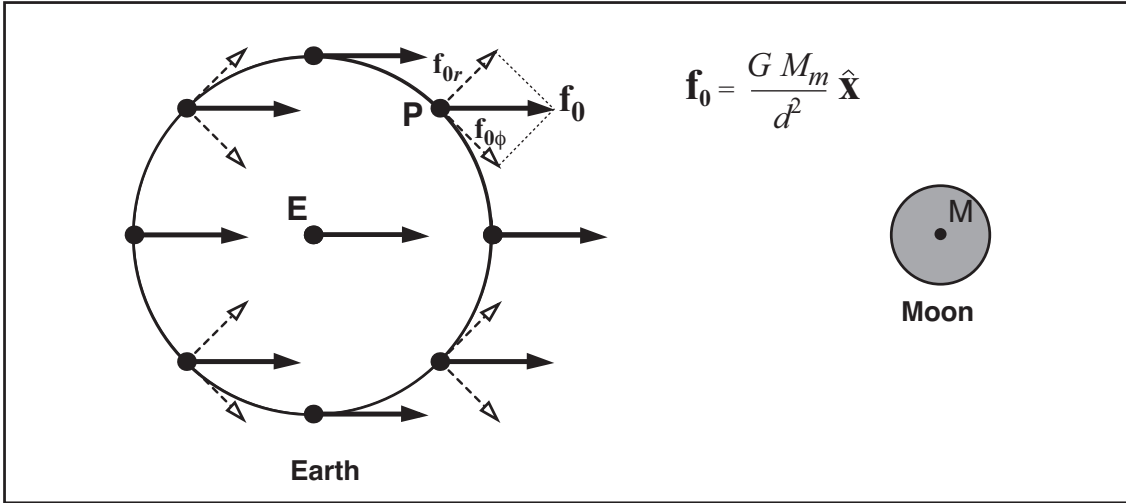
Figure 9: The zero-order term $\mathbf{f}_0$ (and components r and ϕ) of the differential force. In the two-body problem, the zero-order term of the lunar attraction is a centripetal force that is constant at every point throughout the rigid earth, as shown in Figure 8B1. Thus the entire rigid earth is in a state of free fall under this force. Imagine what would happen to a thin covering of (non-rigid) water on the surface (Figure 10).
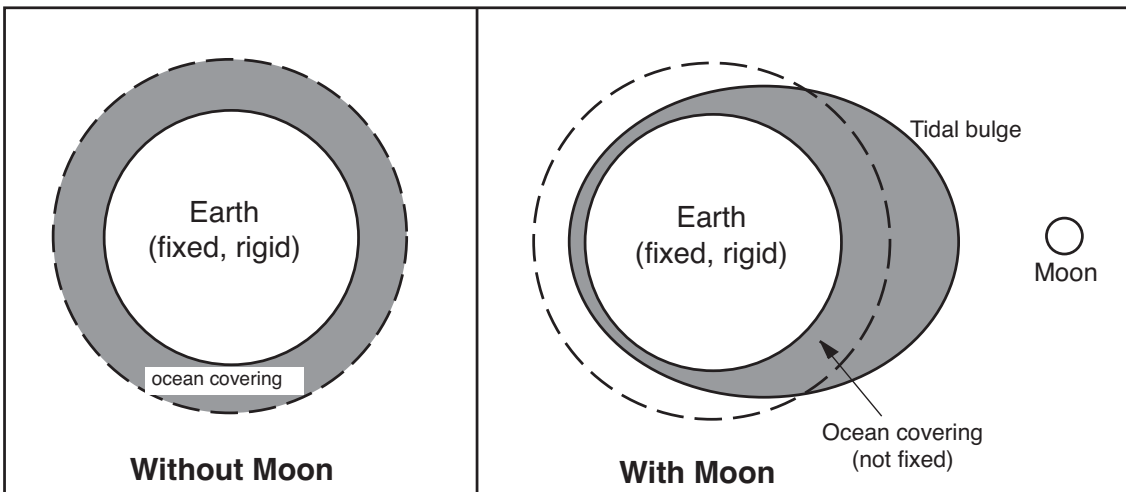

Figure 10: The fixed, rigid earth with ocean covering, under the influence of the $\mathbf{f}_0$ "free fall" term. If the earth were fixed in space (hypothetical one-body scenario), then only the free-moving ocean covering would feel the $\mathbf{f}_0$ force. Water would pile up on the side facing the moon, and we would experience a single, enormous tide per day (see Section 2.5).

$$f_1 = \frac{G\,M_m}{d^2}\,\frac{r_e}{d}\left(\left(3\cos^2\phi - 1\right)\hat{r} - \left(\frac{3}{2}\sin 2\phi\right)\hat{\phi}\right)$$
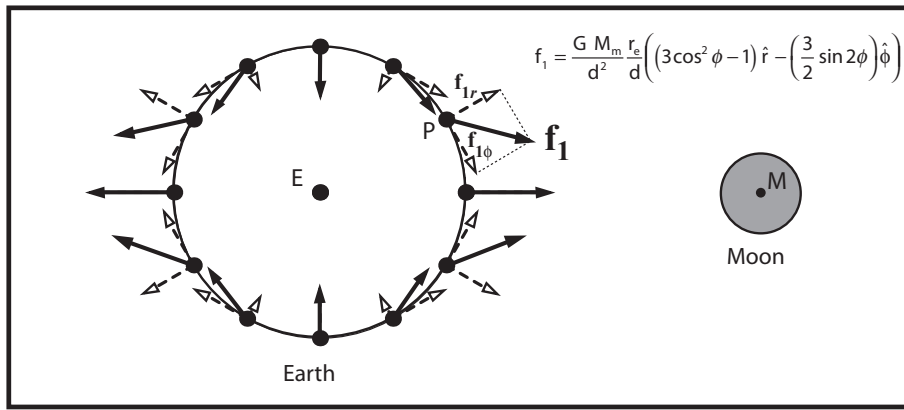
Figure 11: The first-order term $\mathbf{f}_1$ (plus components) of the differential force. The tangential component $\mathbf{f}_{1\phi}$ is responsible for shifting the water covering the earth (see Section 2.5).
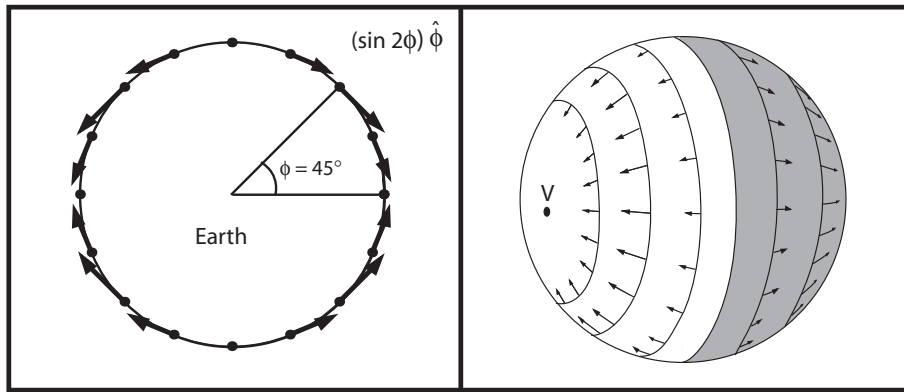

Figure 12: The "water-moving" component of the tide-producing force on the earth: $\mathbf{f}_{1\phi}$. **A**. Two-dimensional view, plotting $-(\sin 2\phi)\hat{\phi}$ on the surface. Since the earth–moon system has cylindrical symmetry about the earth–moon axis, a 2D view suffices, as long as we are not concerned with the rotation of the earth about its spin axis. **B**. Three-dimensional view of the tide-producing force. The moon illuminates half of the earth and is directly overhead at point V. After *Darwin* (1898).
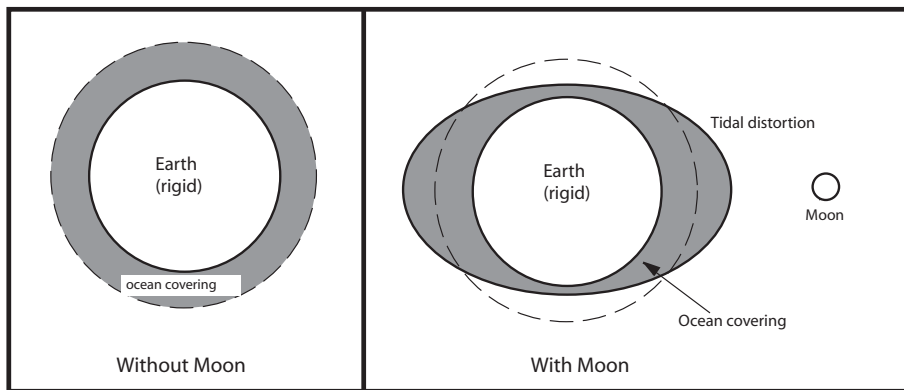

Figure 13: The rigid earth with an ocean covering, under the influence of the tide-producing force $\mathbf{f}_1$. The tide-producing force $\mathbf{f}_1$ pulls water from the sides, causing water to pile up in regions facing toward and away from the moon.

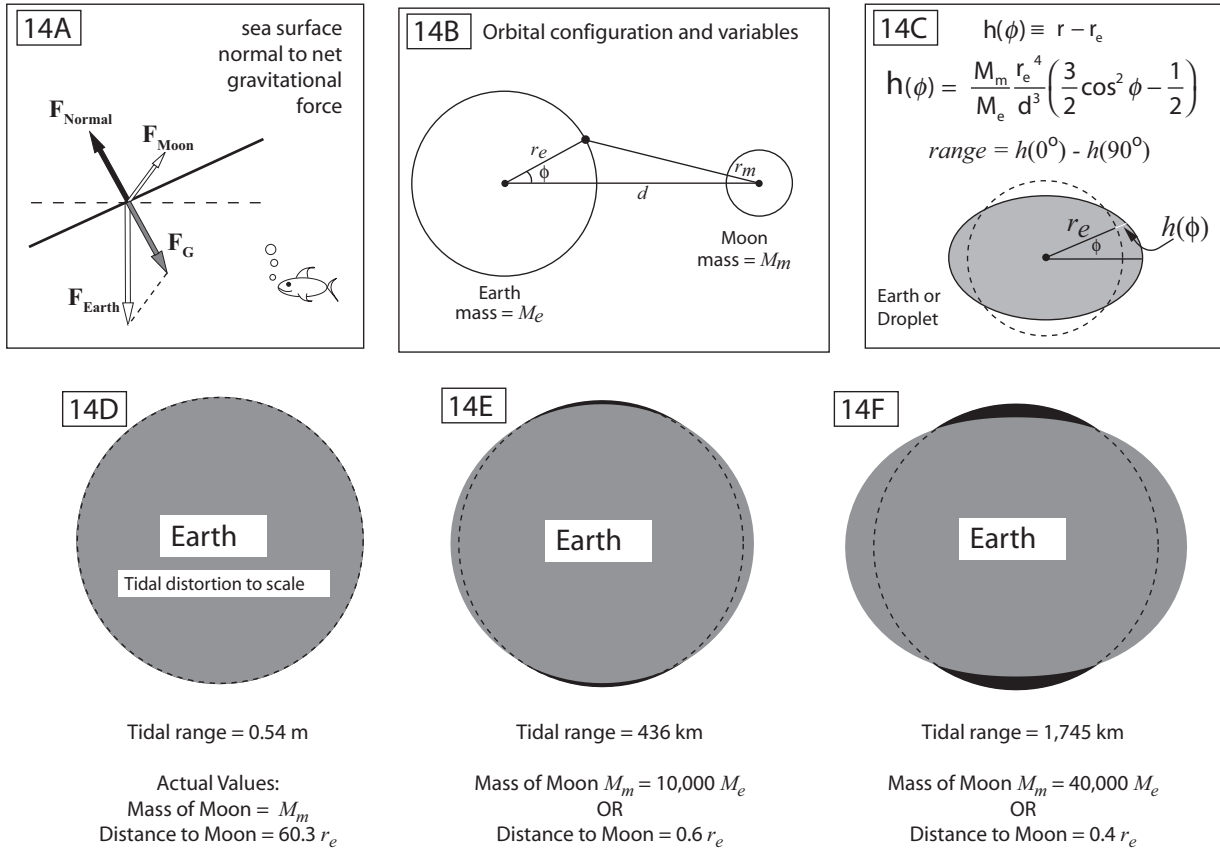**Equilibrium Tide = Equipotential Water Surface**

The Earth as a Water Droplet

14A — sea surface normal to net gravitational force

F_{Normal}, F_{Moon}, F_G, F_{Earth}

14B — Orbital configuration and variables

r_e, ϕ, d, r_m

Moon mass $= M_m$

Earth mass $= M_e$

14C

$$h(\phi) \equiv r - r_e$$

$$h(\phi) = \frac{M_m}{M_e}\frac{r_e^{\,4}}{d^3}\left(\frac{3}{2}\cos^2\phi - \frac{1}{2}\right)$$

$$range = h(0^\circ) - h(90^\circ)$$

r_e, ϕ, $h(\phi)$

Earth or Droplet

14D — Earth — Tidal distortion to scale

Tidal range = 0.54 m

Actual Values:
Mass of Moon = M_m
Distance to Moon = 60.3 r_e

14E — Earth

Tidal range = 436 km

Mass of Moon M_m = 10,000 M_e
OR
Distance to Moon = 0.6 r_e

14F — Earth

Tidal range = 1,745 km

Mass of Moon M_m = 40,000 M_e
OR
Distance to Moon = 0.4 r_e

Figure 14: The equilibrium tide: the earth as water-droplet responding to the gravitational field. See Section 2.6. **A**. The surface of water will orient itself orthogonal to the gravitational force, so as to minimize its potential. **B**. Orbital configuration and variables of the earth–moon system. **C**. Relevant equations, which are used in **D-F**. The range expression gives the difference between the highest high tide and the lowest low tide. **D-F**. Four Mathematica plots of equilibrium tide surfaces based on the equation to calculate the tidal height $h(\phi)$. The black circle and dotted line is the "water-earth" without the moon; the gray ellipse is the equipotential surface formed under the gravitational field. In **D** the parameters are to scale; the equilibrium tide range is 0.54 m, which approximates that which is observed in the deep oceans, far from coasts. This tidal distortion is of course not visible. To show the shape of the bulge, we increase the mass of the moon or bring the moon closer (decrease d).
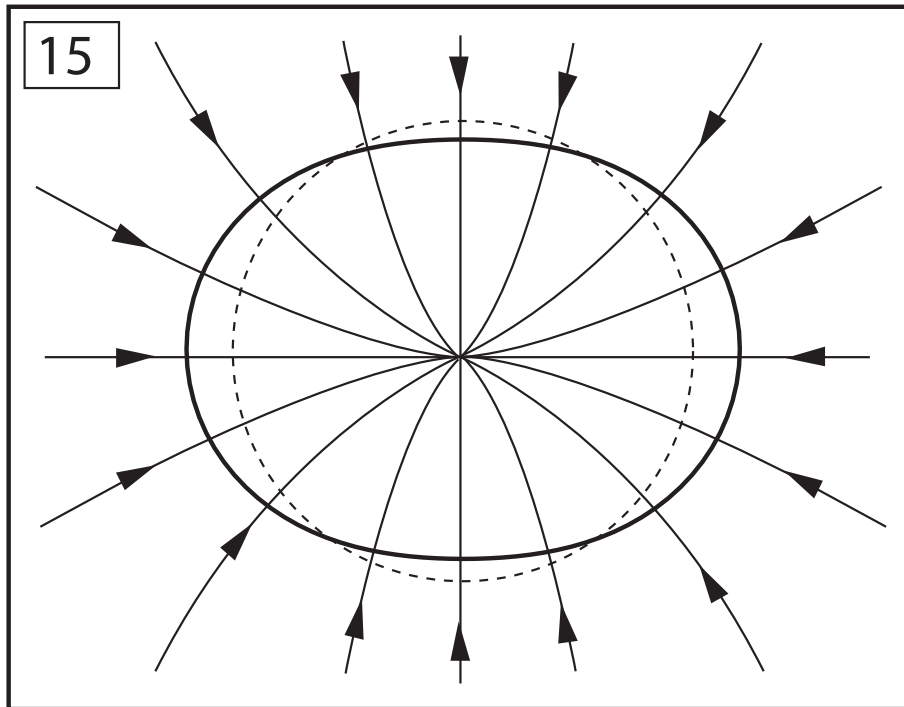
Figure 15: The vector-field equivalent of the equilibrium tide. The gravitational field lines are always perpendicular to the equipotential surfaces, as shown in Figure 14A. Field lines represent the force-per-mass on a particle and can be thought of as a vector field. Dotted circle is the undeformed earth; solid ellipse is the equilibrium tide surface in Figure 14G.
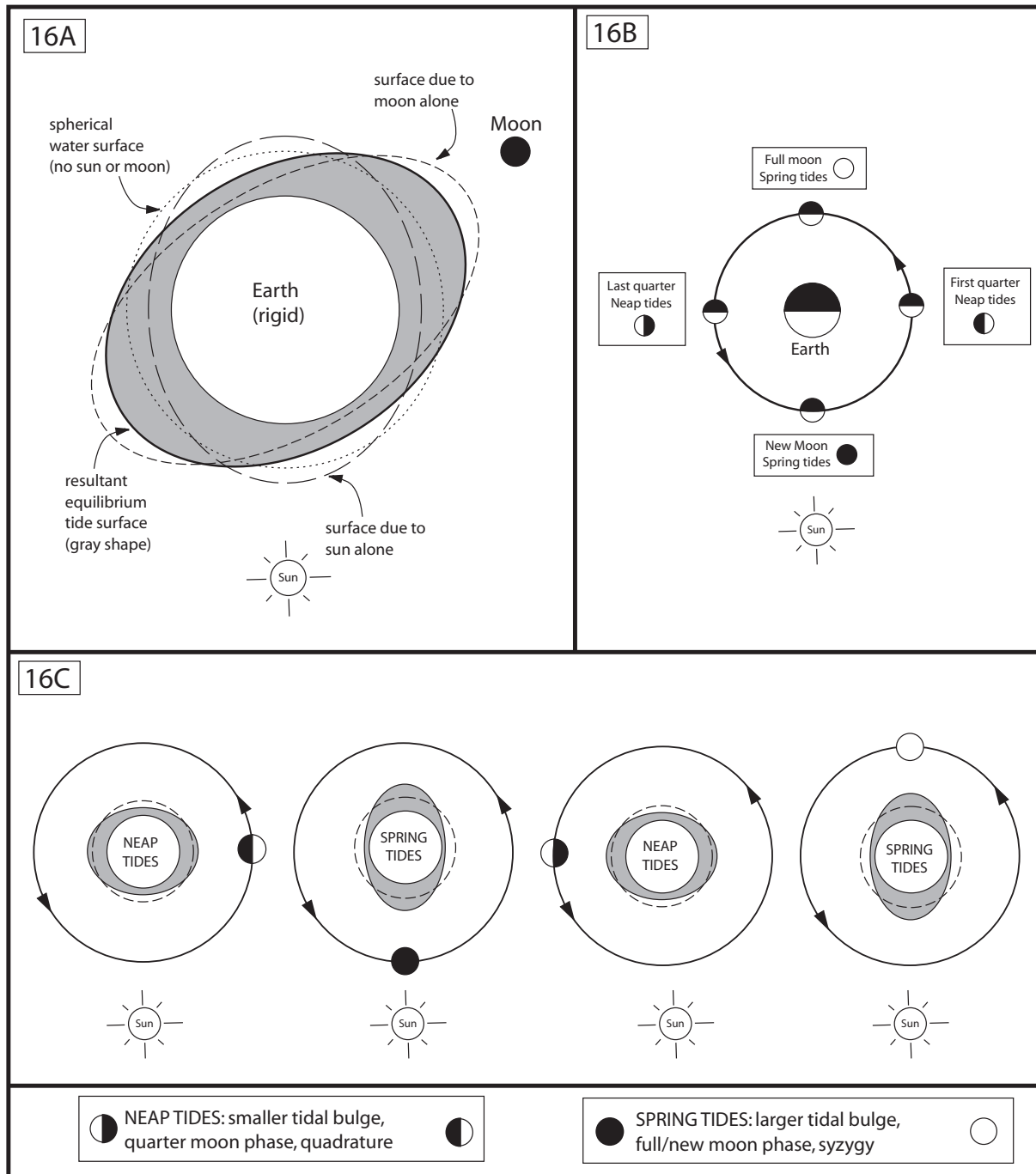
16A

spherical
water surface
(no sun or moon)

surface due to
moon alone

Moon

Earth
(rigid)

resultant
equilibrium
tide surface
(gray shape)

surface due to
sun alone

Sun

16B

Full moon
Spring tides

Last quarter
Neap tides

First quarter
Neap tides

Earth

New Moon
Spring tides

Sun

16C

NEAP
TIDES

SPRING
TIDES

NEAP
TIDES

SPRING
TIDES

Sun   Sun   Sun   Sun

NEAP TIDES: smaller tidal bulge,
quarter moon phase, quadrature

SPRING TIDES: larger tidal bulge,
full/new moon phase, syzygy

Figure 16:   The lunar cycle and the neap-spring-neap tidal cycle. **A**. The equilibrium tide on the earth is due to the combined effects of the sun and the moon. **B**. The sun and moon interfere destructively in quadrature, when the sun diminishes the tidal bulges caused by the moon, which are always parallel to the earth–moon axis. The resulting tides, with the lowest tidal range of the month, are known as neap tides. Spring tides occur in syzygy, when the sun enhances the tidal bulges parallel to the earth–moon axis. There are two neap-spring-neap tidal cycles per lunar cycle. **C**. Four stages of the lunar cycle, showing the lunar phase at each position and the resultant tidal bulge. Without the sun, there would not be a neap-spring-neap tidal cycle, since the moon would create a uniform bulge on both sides of the earth that would always be parallel to the earth–moon axis.
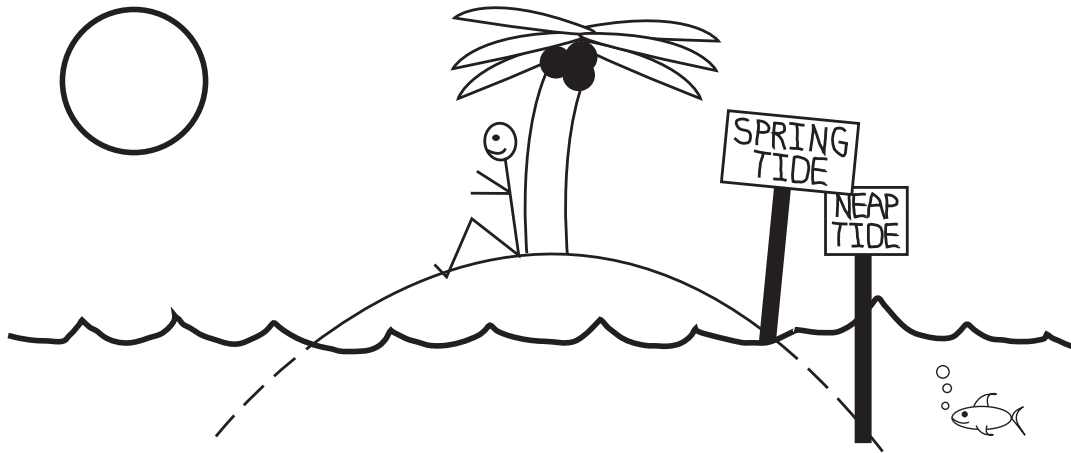
Astronomical Body	Maximum high tide height on Earth [h(0°)]	Maximum low tide height on Earth [h(90°)]	Maximum tidal range on Earth [h(0°) – h(90°)]
Moon	0.36 m	−0.18 m	0.54 m
Sun	0.16 m	−0.08 m	0.24 m
Moon – Sun (Neap tide)	0.20 m	−0.10 m	0.30 m
Moon + Sun (Spring tide)	0.52 m	−0.26 m	0.78 m

Figure 17: Relative equilibrium tide effects of the moon and the sun on the earth. The values in the table are derived from Equations (36) and (41); they can be used to calculate the relative tidal effects of the sun and the moon on the earth. One could determine the relative tidal effects of the sun and moon by measuring the spring tide tidal range and then the neap tide tidal range 14 days later. The average of these ranges $[(0.78 + 0.30)/2 = 0.54]$ is the range due to the moon; the variation from the average $[(0.78 − 0.30)/2 = 0.24]$ is the range due to the sun.
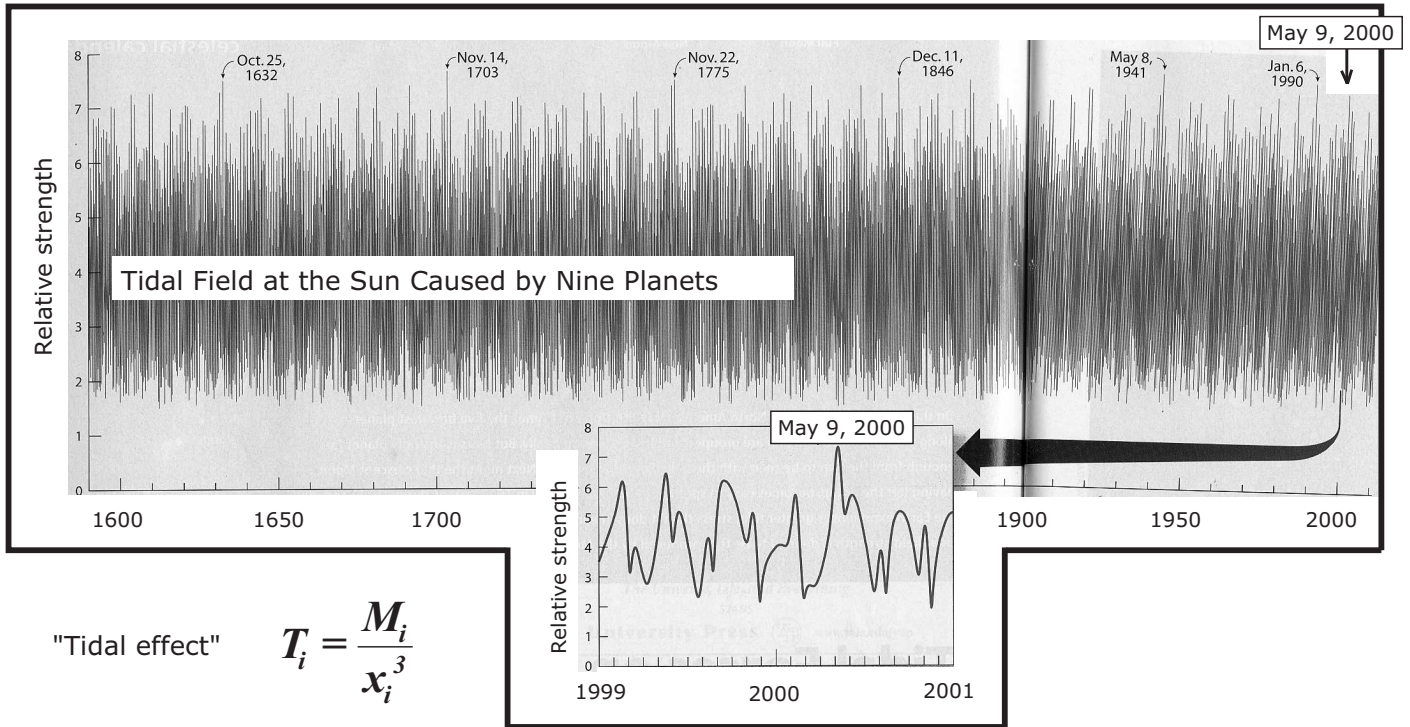
Figure 18: Tides at the sun caused by the planets. The planets generate tidal forces on the sun. The main contributors to the tidal force at the sun are Jupiter, Venus, Mercury, and Earth+Moon. The earth also experiences a differential force due to the planets, although it is not significant, compared to the tidal effects generated by the moon and sun. The "tidal effect" at body A (in this case, the sun) due to a body i with mass M_i at a distance x_i from body A is defined above (see Section 2.7); each planet will have a tidal effect at the sun. After *Olson and Lytle* (2000).

19A

z′

North Pole
(spin axis)

particle (mass m)
on Earth's surface

$P(\phi_p, \theta_p, r_e)$

θ_p $\mathbf{r_e}$

θ_m

P

E

ϕ_p

ϕ_m

y′

Equator

x′

Earth
(mass M_e)

$\mathbf{d}$

M

Moon
(mass M_m)

$M(\phi_m, \theta_m, d)$

19B   The EMP plane (plane of Earth, moon, and particle mass)

P

$\mathbf{r_e}$

E

ψ

$\mathbf{d}$

M
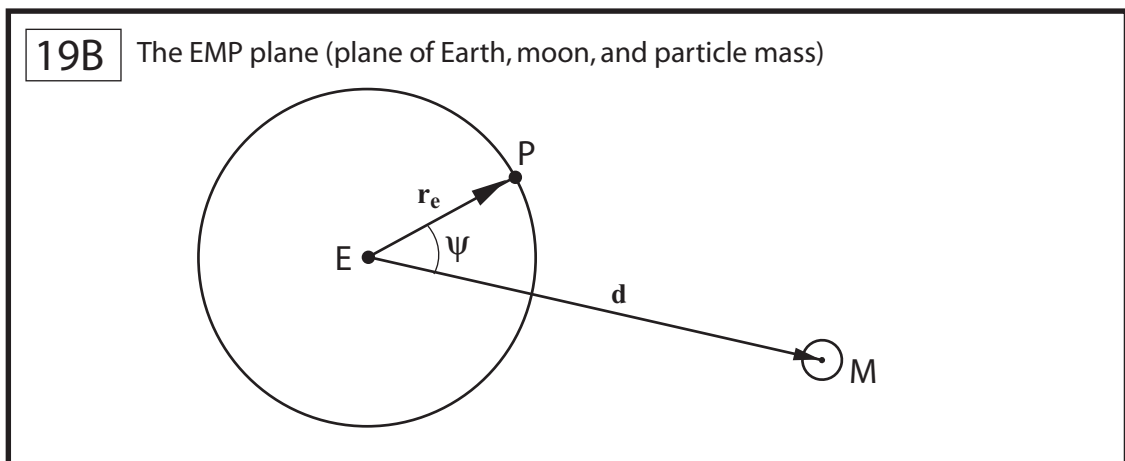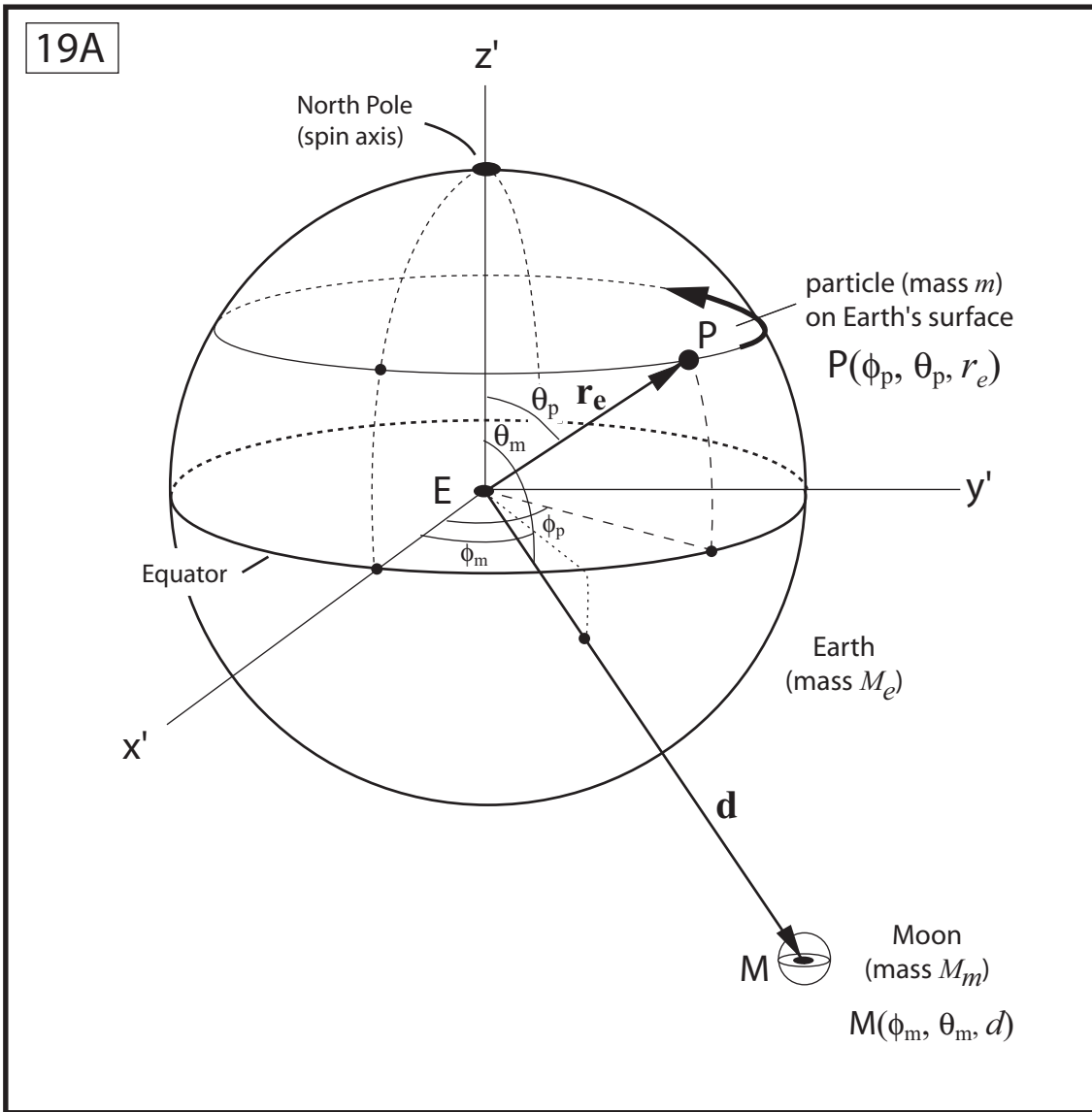
Figure 19:   A new configuration of 3D coordinates, incorporating the earth's rotation about its spin axis. Spin axis is vertical (z' axis); moon is not confined to the equatorial plane, as originally assumed (Figure 6). The angle between $\mathbf{r}_e$ and $\mathbf{d}$ is ψ. **A**. 3D view. **B**. 2D view. The viewing plane is not necessarily the view of the lunar orbital plane, as in Figure 7. See Section 2.8.
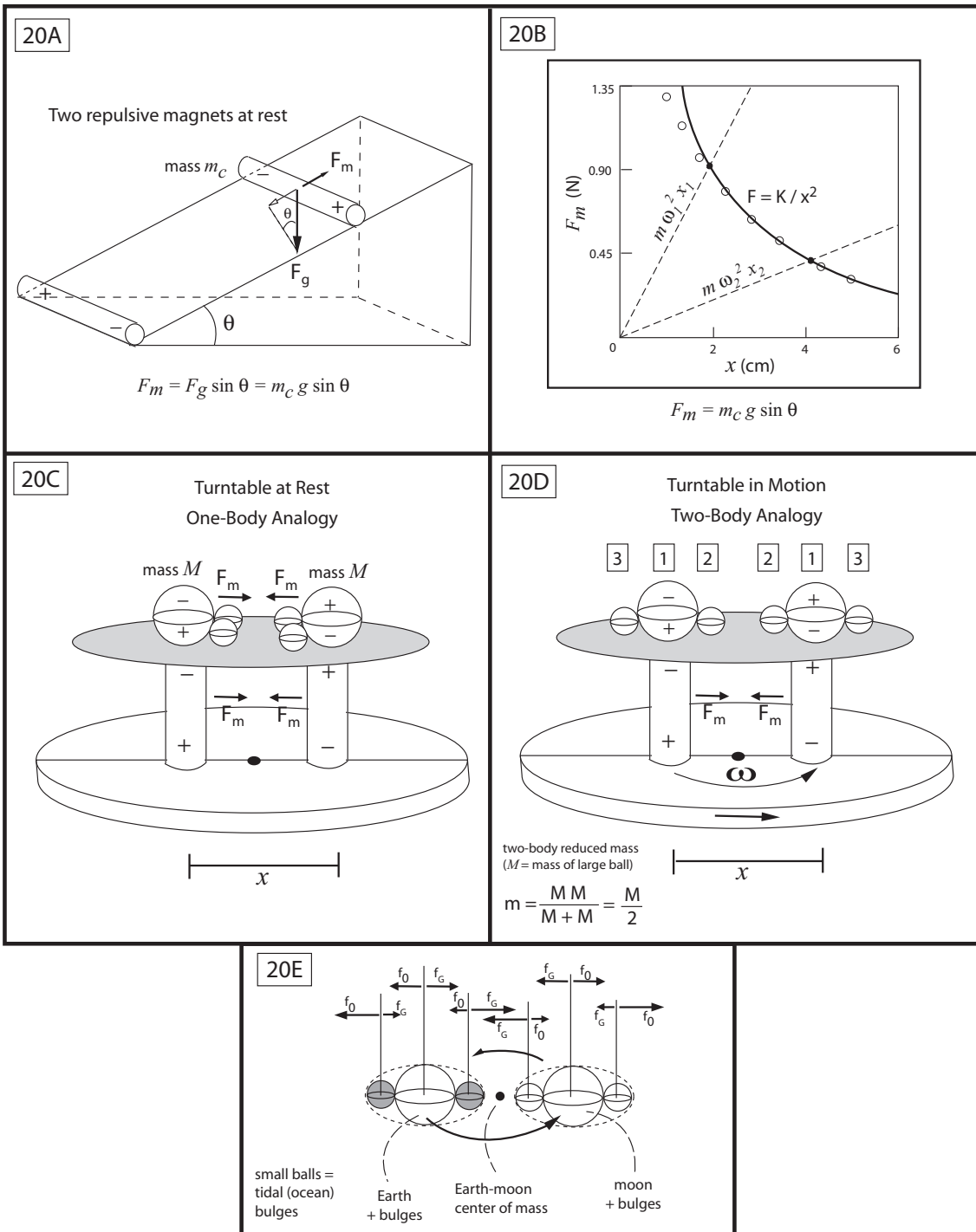
Figure 20: An experiment to demonstrate the tidal bulges using magnets (*White et al.*, 1993). **A**. Setup to determine the force between two magnets. **B**. Plot showing the inverse-square nature of the magnetic force, including experimental data points (*White et al.*, 1993). **C**. With the turntable at rest, the force between the magnets is similar to the one-body example (Figure 9). **D**. At angular speed ω, such that $m\omega^2 x = F_m$, as shown in B, the magnetic force between the large balls is equal to the centripetal acceleration. ① Magnetic force on large balls equals centrifugal force. ② Magnetic force on small balls exceeds centrifugal force. ③ Centrifugal force on small balls exceeds magnetic force. **E**. The earth–moon analogy, with force-per-mass arrows (relative acceleration) at points within the "earth" and the "moon".
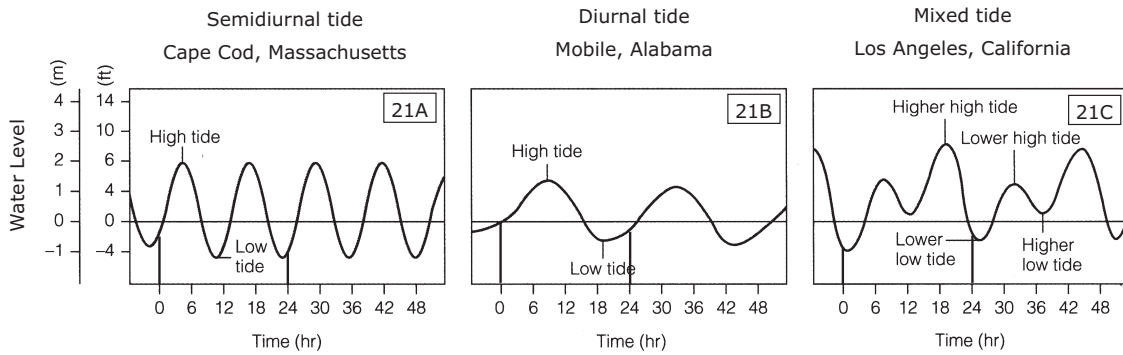
Figure 21: Three types of daily tidal patterns. The earth's rotation under the differential force of the moon and sun causes the semidiurnal and diurnal components of the tide. A semidiurnal tide has two rise-and-falls each day, while a diurnal tide has a single rise-and-fall per day. In coastal systems either one component may dominate (**A** or **B**) or a combination of the two components may occur (**C**). See global distribution in Figure 22. After *Garrison* (1998).
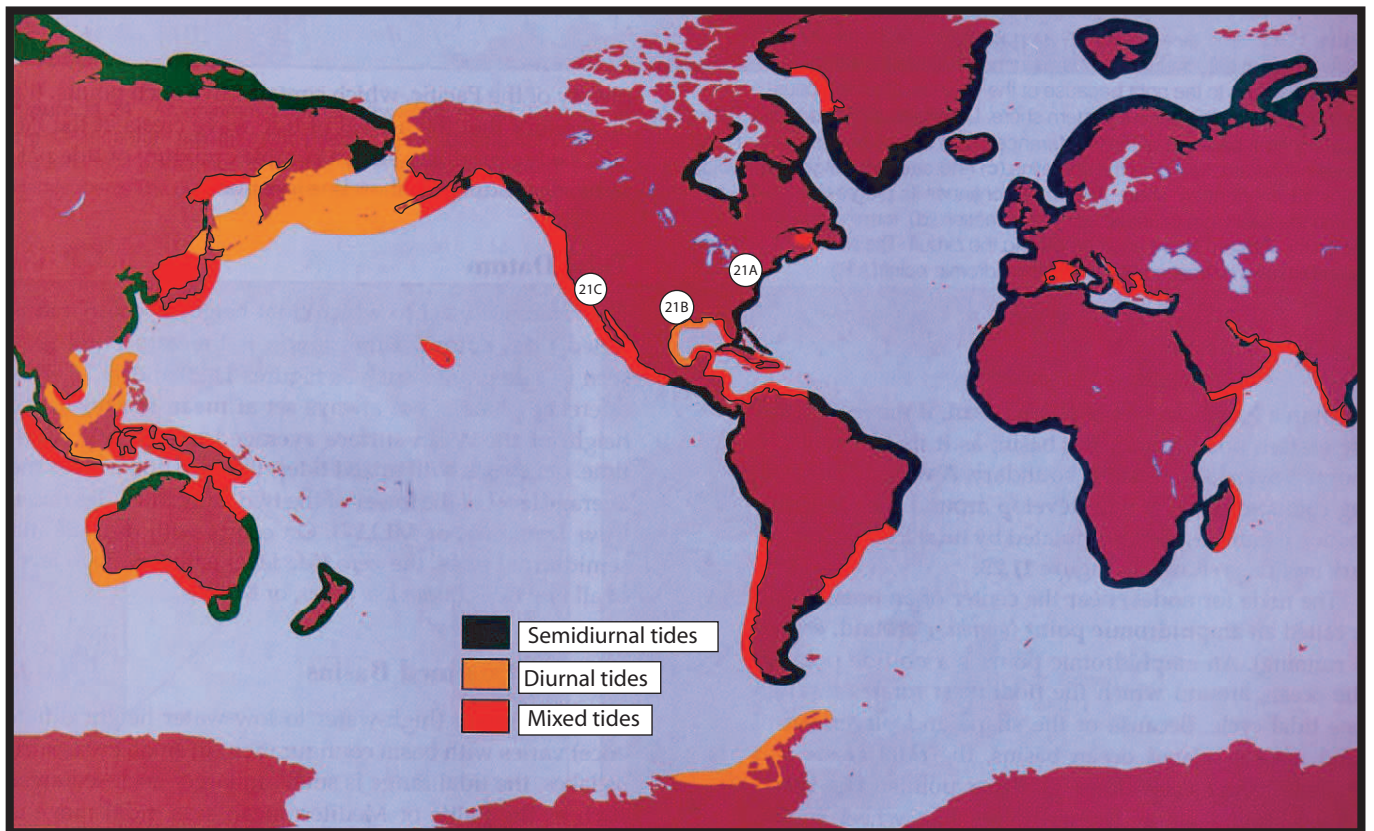

Figure 22: The worldwide geographic distribution of the three tidal patterns. Most of the world's coasts have semidiurnal tides. Note that the Atlantic coasts experience predominantly semidiurnal tides, although both the semidiurnal and the diurnal components are present, as shown in Figure 23. After *Garrison* (1998).
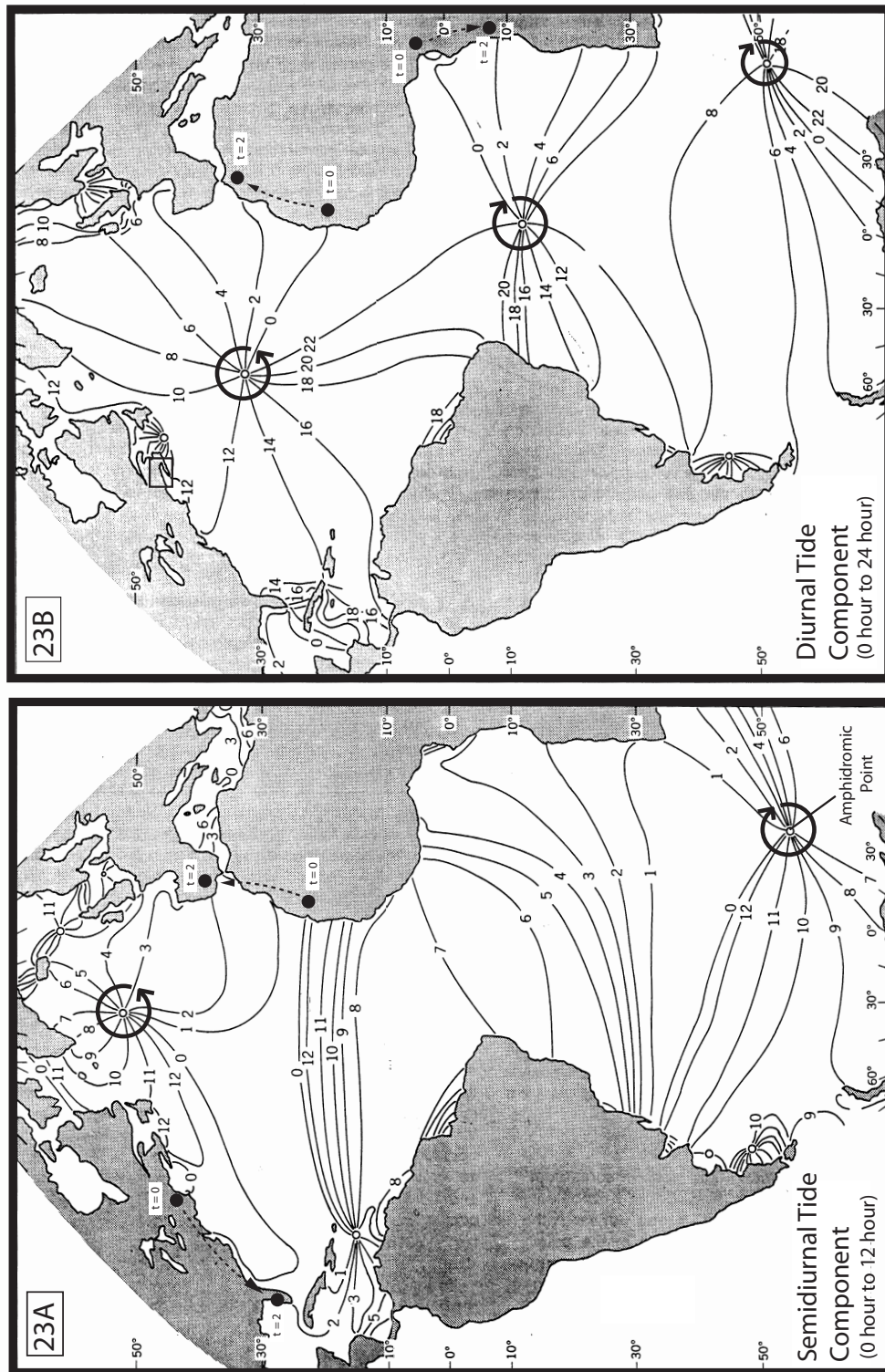
Figure 23: The propagation of the tidal wave components in the Atlantic Ocean (after *Strahler*, 1971). Lines indicate the high tide in lunar hours; time $t = 0$ is the moon's meridian passage (i.e., over the longitude marked by Greenwich, England). Cotidal lines represent the line of the high tide — the crest of the tidal wave — which one can imagine "starting" at $t = 0$. The tidal wave rotates counterclockwise in the northern hemisphere and clockwise in the southern hemisphere, always about a point that does not fluctuate with height, known as an *amphidromic point*. Solid circles indicate coastal regions experiencing high tide at $t = 0$, and then at $t = 2$. Positions of cotidal lines and amphidromic points are approximate. The semidiurnal (twice-a-day) and the diurnal (once-a-day) components together produce the resultant tidal wave.
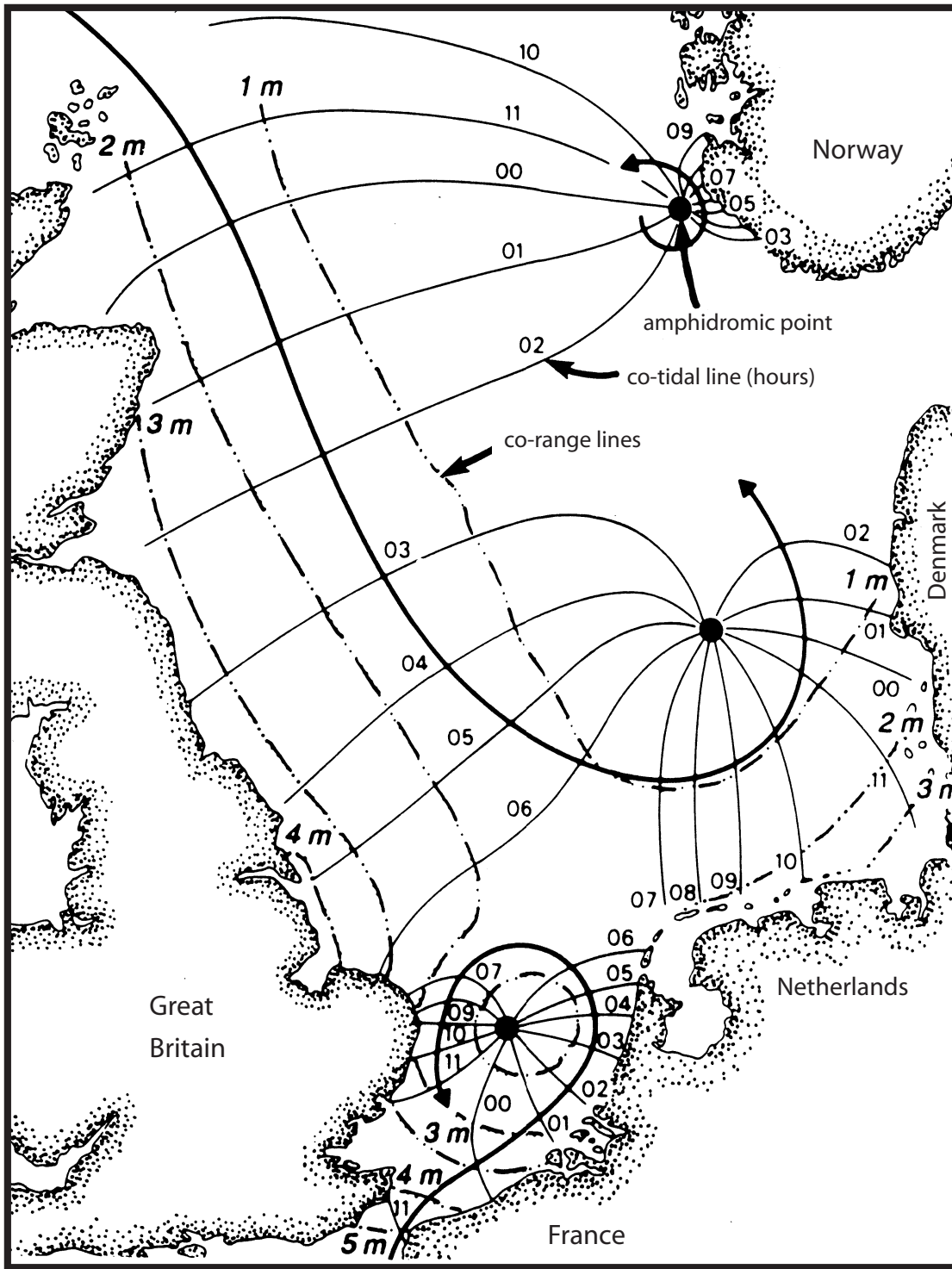
68

Figure 24: The propagation of the tidal wave in the North Sea (after *Dalrymple*, 1992). The solid cotidal lines show the times of high water in lunar hours and indicate the direction of propagation of the tidal wave. The tidal range (dotted co-range lines) increases outward from each of the three amphidromic points, points where the water level remains approximately constant (i.e., points that do not experience the tide). In each of the three cases, the sense of motion of the tidal wave is counterclockwise.
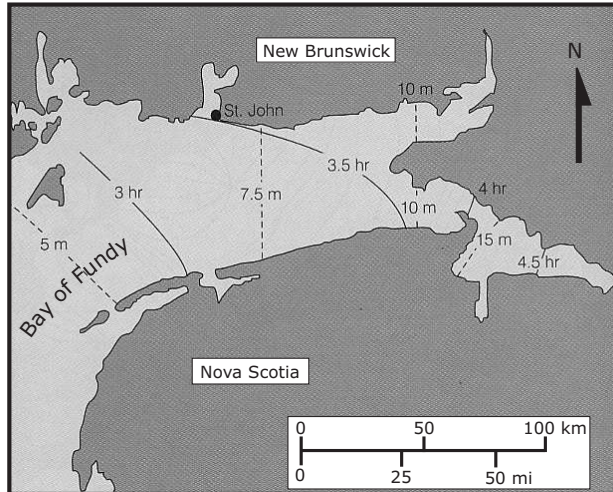
Figure 25: The world's largest tides: The Bay of Fundy. The largest tidal range on record was recorded in this bay (see box in Figure 23B) at 16 m (54 ft). One reason for the great range is that the resonant frequency of the Fundy basin is approximately equal to the frequency of the daily lunar tide. Dashed lines show the approximate tidal range; solid lines show the approximate high tide level at certain times (crest of the tidal wave). After *Garrison* (1998).
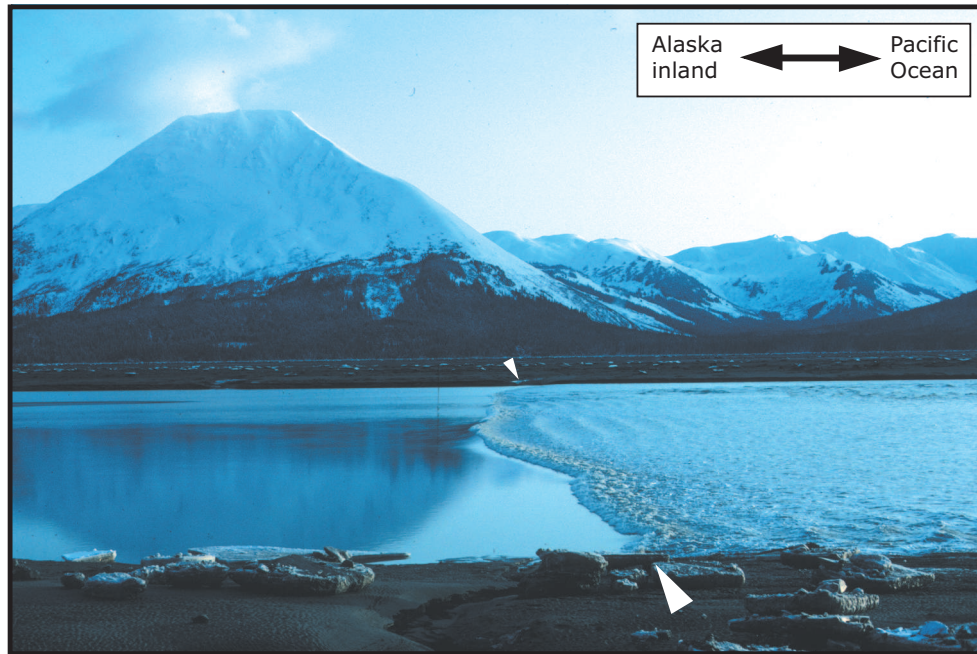

Figure 26: The tidal bore: a tidal wave in the true sense of the name. In certain areas, such as the Bay of Fundy or Cook Inlet, the incoming tide (the flood current) can be observed as an actual wave, known as a tidal bore. This tidal bore is from Cook Inlet, Alaska, March 9, 1993. The lunar phase was one day past full, generating spring tides (see Figure 16). The undisturbed water on the left will soon be overtaken by the incoming tidal wave. The wave was moving a few miles per hour; we drove alongside the road to watch it.
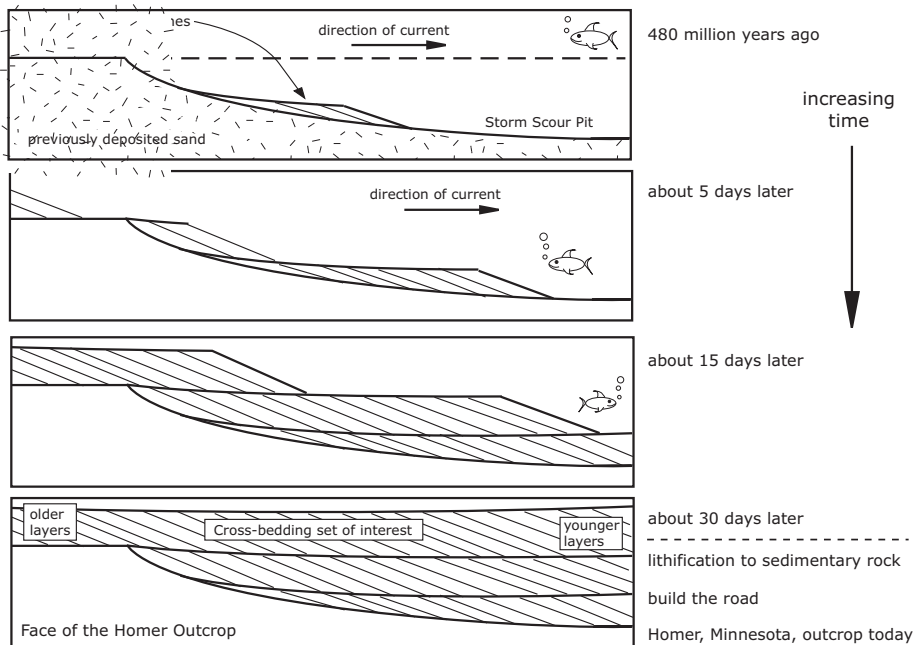
Figure 27: Cross-bedding: The preservation of underwater sand dune migration in the rock record. One way a migrating sand dune could be preserved in the rock record is if one dune, or a series of dunes, fills in a pit left by a storm. In the pit the energy of the water is much lower, and the dunes filling in the scour pit are protected from the more turbulent (erosive) currents above. Here, three advancing dunes, one right after the other, each form a cross-bedding set. This is the postulated mechanism for the formation of three cross-bedding sets at Homer, Minnesota.
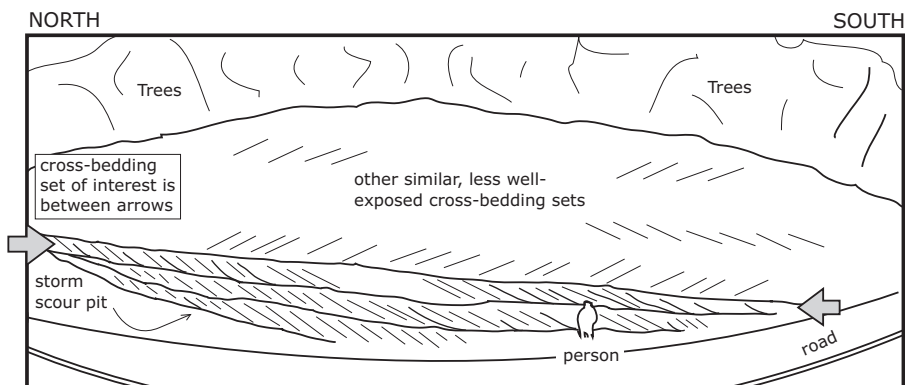

Figure 28: Roadside outcrop of the Jordan Sandstone near Homer, Minnesota. (line-sketch from a wide-angle lens photo). The schematic shown in Figure 27 shows how the cross-bedding patterns in the outcrop may have formed. The advancing side of the dune is the layer that is preserved in the rock record. Cross-bedding set of interest (between arrows) is well-exposed for 58 m (exposure is 95 m in total); the thickness of each cross-bedding layer was measured in order to try to determine whether tidal currents influenced deposition. As indicated by the height of the cross-bedding set (person for scale), the dunes were at least 1 m tall. Bold layers indicate thick layers of mud. See Figure 29 for a continental context.
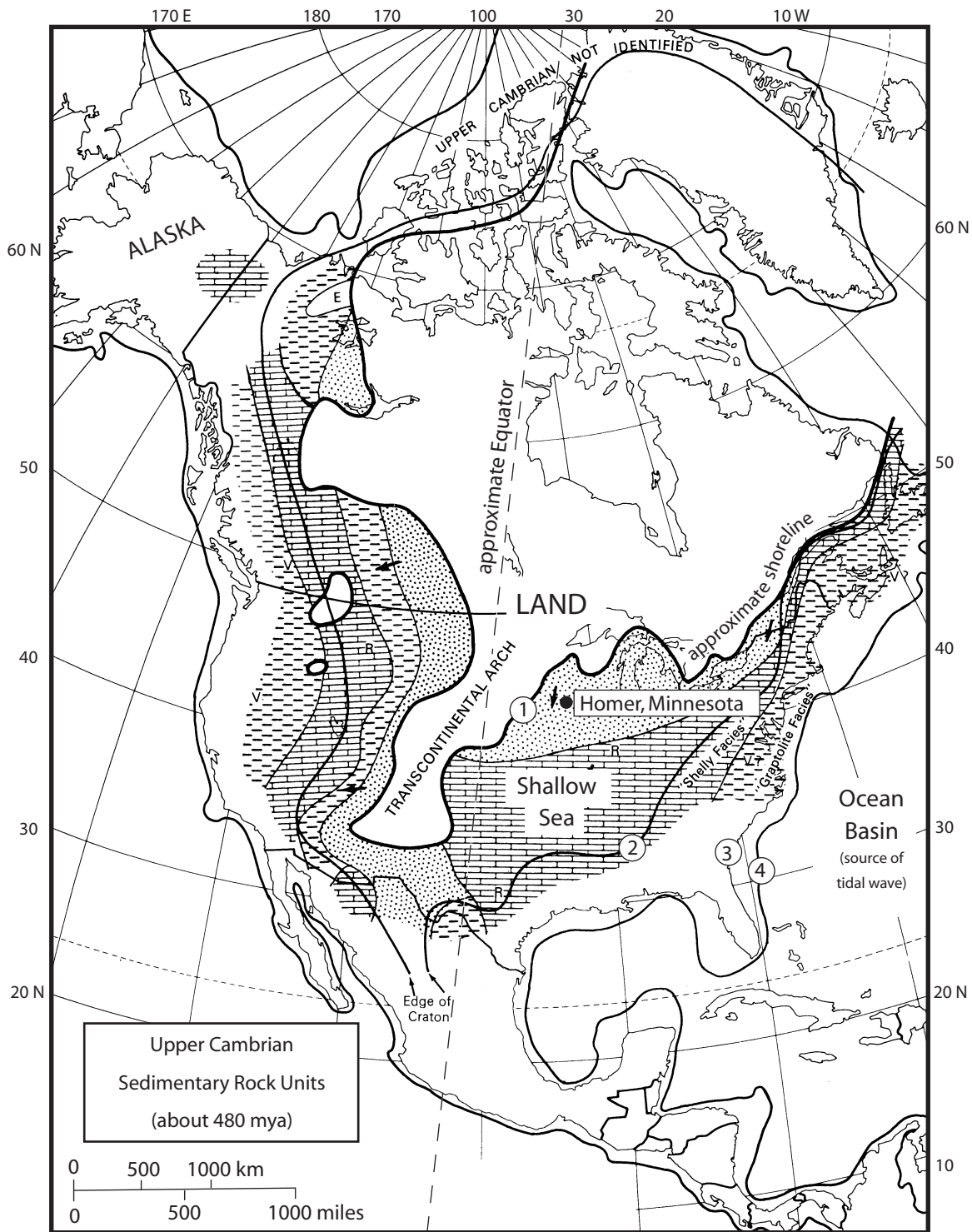
Figure 29: The submergence of North America during Upper Cambrian time: Context for the Homer, Minnesota, study. During Upper Cambrian time, a vast, presumably shallow (<500 m deep) sea covered much of North America, which was situated near the Equator and rotated from its present-day position (determined by paleomagnetic data and plate tectonic reconstructions). Tidal energy generated in the ocean basin apparently reached at least as far inland on the continent as Homer, Minnesota. ① = a very approximate shoreline during Cambrian time; ② = approximate continental margin during Cambrian time (edge of craton); ③ = present shoreline; ④ = present continental margin. Arrows indicate paleocurrent direction (south at Homer; see Figure 28). Sedimentary rock units include sandstone (stippled pattern; derived from deposited sand), limestone (bricks pattern; derived from $CaCO_3$ microfossils and precipitation), and shale (dashed pattern; derived from deposited mud). After *Dott Jr. and Batten* (1981).
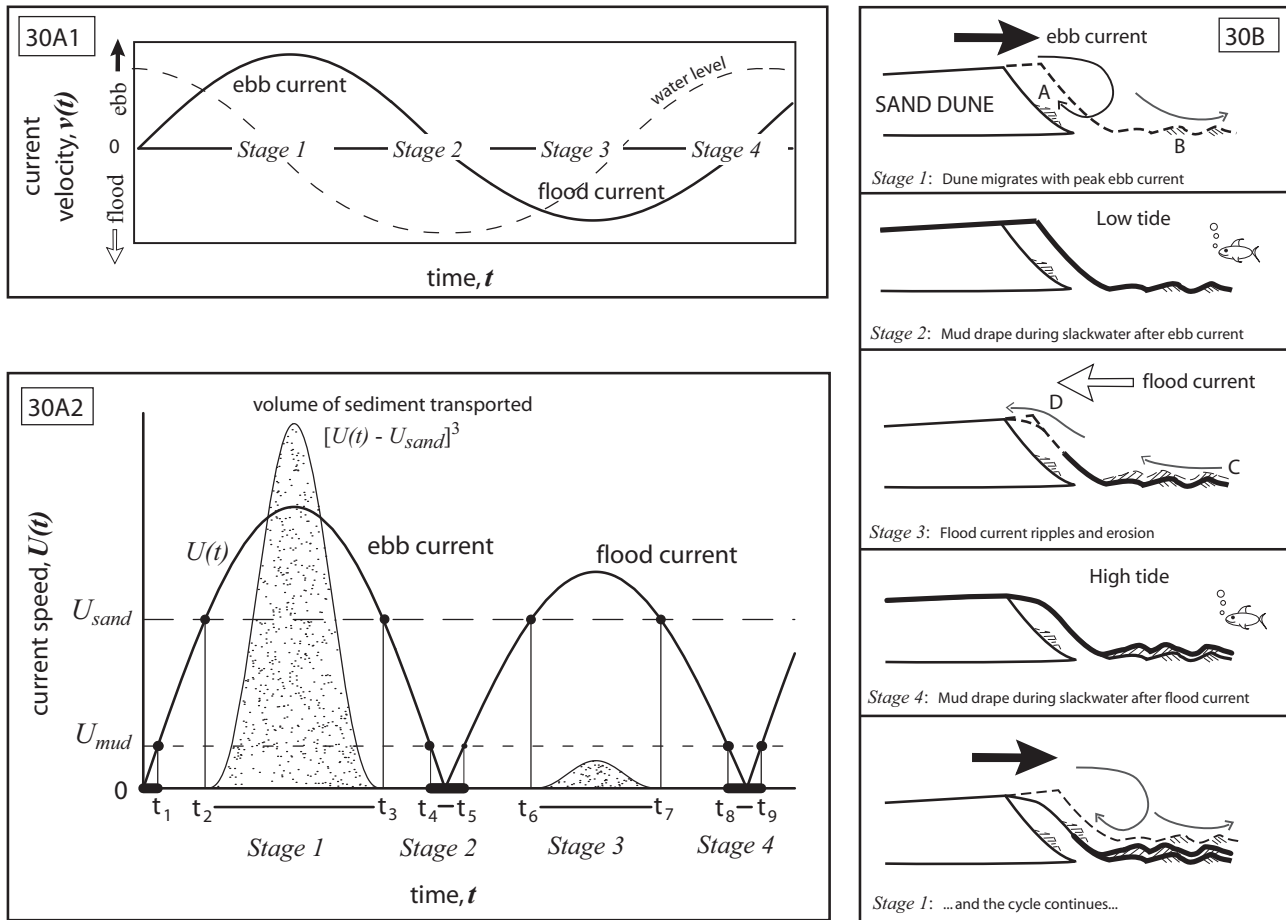
72

Figure 30: The ebb-flood cycle and the corresponding sediment deposition during the migration of a sand dune. **A1.** Velocity profile for the ebb-flood cycle, which may have a period of 12 hours (semidiurnal tidal cycle) or 24 hours (diurnal tidal cycle). In many systems, either the ebb or the flood may dominate; our profile is an ebb-dominated ebb-flood cycle. As indicated by the dashed line, low tide occurs during *Stage 2*, and high tide occurs during *Stage 4*. **A2.** Current speed profile and sediment volume transport profile for an ebb-dominated ebb-flood cycle. Sand is transported as bedload when the current speed $U(t)$ exceeds the threshold velocity of sand movement U_{sand}. The volume of sand transported is proportional to the stippled area under the curve $[U(t) - U_{\text{sand}}]^3$. Due to the asymmetry of the tidal currents, much more sand is transported by the peak ebb current (*Stage 1*) than by the peak flood current (*Stage 3*). Mud is deposited when the current speed drops below the threshold velocity of mud deposition U_{sand}. Periods of mud deposition are represented by the bold segments on the x-axis (*Stage 2* and *Stage 4*). Sand is not transported, nor is mud deposited, in the time intervals between stages. **B.** Schematic of sand dune migration during one ebb-dominated ebb-flood cycle. The dune is always underwater. During the peak ebb current stage, the dune migrates, and back-flow ripples (`A` in figure) form on the lower slipface due to eddy currents; co-flow ripples (`B`) form in the bottomset of the dune. During the peak subordinate current stage, ripples (`C`) migrate across the bottomset of the dune, and the mud and some of the sand from the upper slipface of the dune is eroded to form a reactivation surface (`D`). When the ebb current resumes (bottom of diagram, repeat *Stage 1*) at the start of a new ebb-flood cycle, mud is removed from the upper reaches of the dune. After *Nio and Yang* (1991); *Allen* (1982).
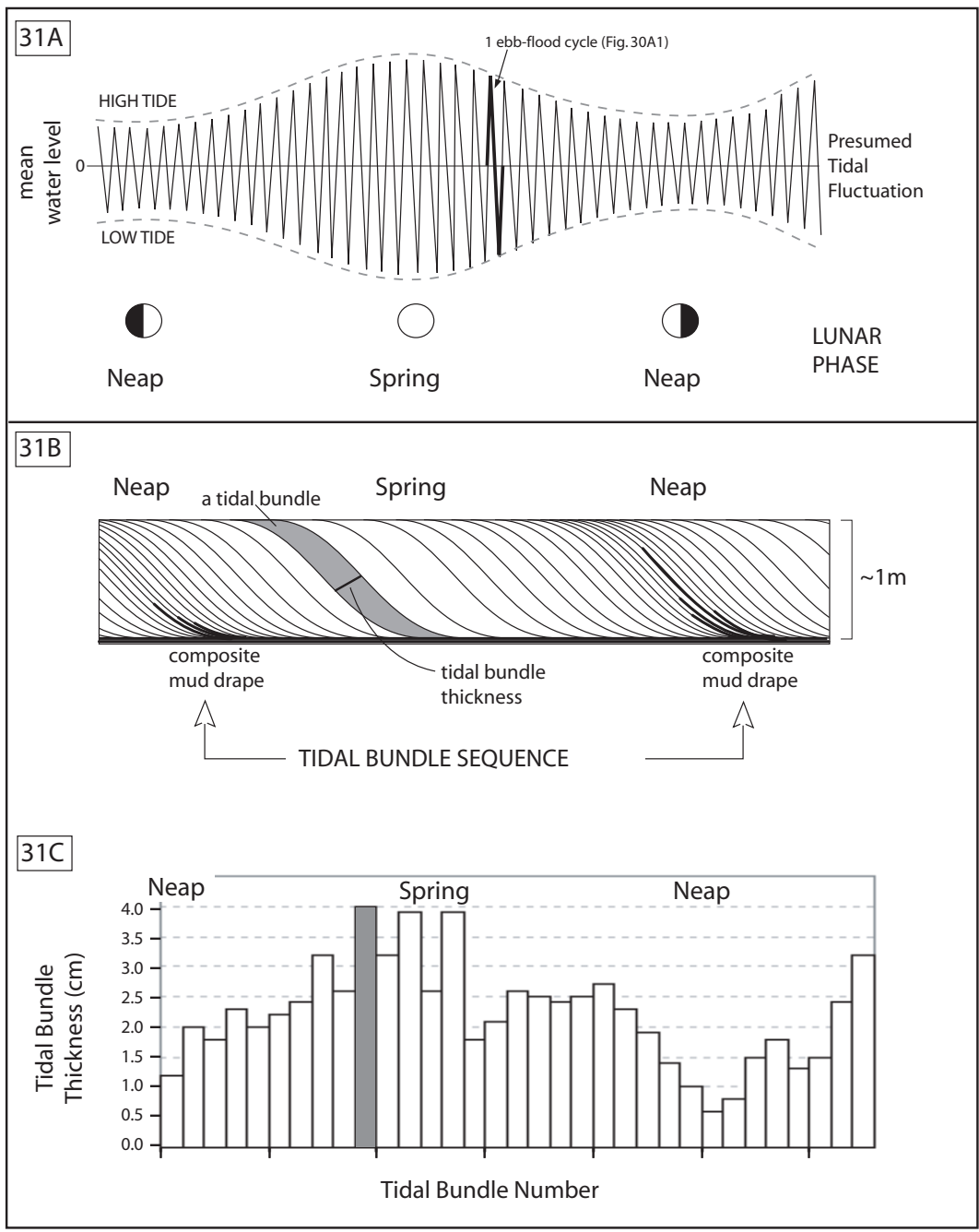
Figure 31: A tidal bundle sequence: the preservation of the neap-spring-neap tidal cycle in the rock record. **A**. Qualitative sketch of the presumed tidal fluctuation over a fortnightly period during the time of deposition (480 Ma) of the sands near Homer, Minnesota. The tidal fluctuation is greatest during spring tides and smallest during neap tides (see Figure 16). **B**. Schematic of a tidal bundle sequence at the Homer outcrop, such as the one in Figure 32A. The tidal bundle sequence is made up of a number of tidal bundles; it consists of the sediment deposited during a complete neap-spring-neap tidal cycle, whereas a tidal bundle consists of the sediment deposited during a complete ebb-flood cycle (Figure 30). A bundle sequence is recognized primarily as the interval between two composite mud drapes, whereas a tidal bundle is recognized as an individual sand lamina. **C**. Histogram (real data) of measured bundle thicknesses for the bundle sequence indicated in Figure 32D. Thicker bundles generally correspond to deposition during spring tides.
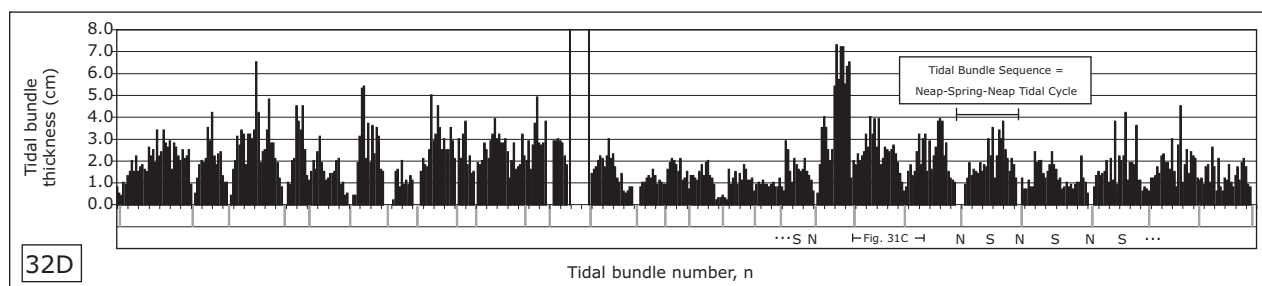
74
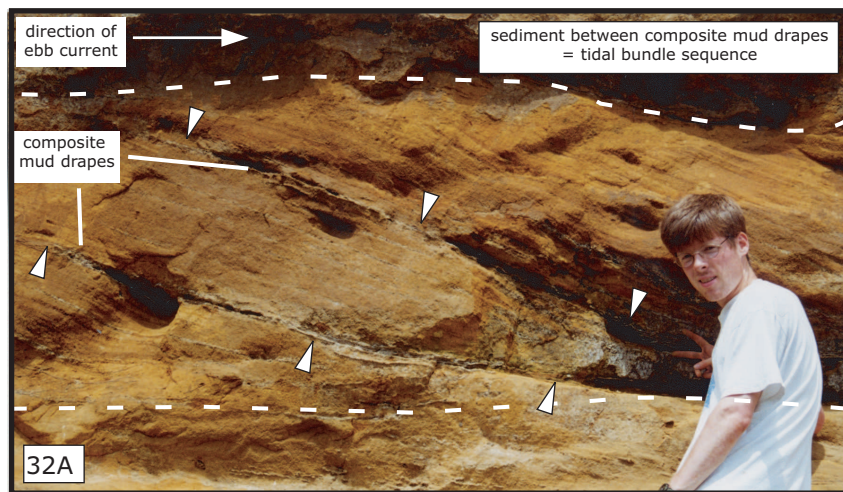
Tidal Bundle Sequence = Neap-Spring-Neap Tidal Cycle (14 days)
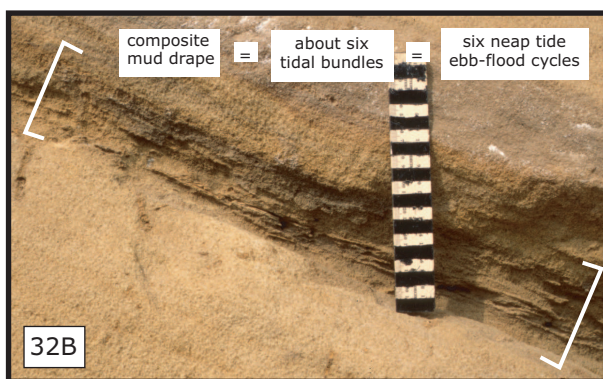
Thin Mud and Sand Layers = Neap Tide Deposition
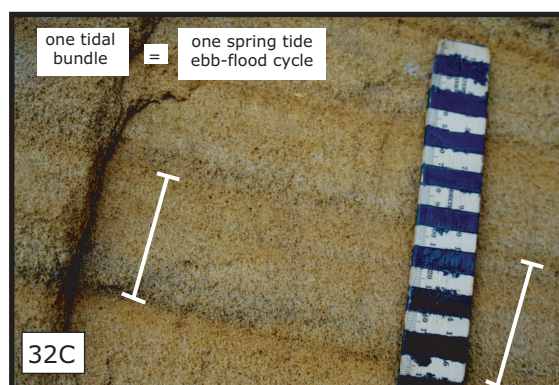
Thick Sand Layers = Spring Tide Deposition

Tidal Bundle Sequences at the Homer Outcrop = 26 Neap-Spring-Neap Tidal Cycles (13 Cambrian Months)

Figure 32: Evidence for the neap-spring-neap tidal cycle at the Homer, Minnesota, outcrop. **A**. A tidal bundle sequence contains the amount of sand and mud deposited during the fortnightly neap-spring-neap tidal cycle. At the Homer outcrop, they are recognized as the interval between two composite mud drapes (Figure 31B). **B**. Mud and thin sandy layers (very thin tidal bundles) are deposited during neap tides, forming composite mud drapes. **C**. Thick layers of sand are deposited during the spring tides, forming the thickest tidal bundles. **D**. Tidal bundle layer thicknesses for the 58-m section of cross-bedding at Homer (Figure 28). The thickening and thinning pattern of sandy layers, punctuated by periodic composite mud drapes, can be identified in this histogram of tidal bundle thickness. Tidal bundle number runs consecutively from $n = 1$ (oldest) to $n = 531$ (youngest); the gap in the histogram is a physical gap of poor exposure in the outcrop. Each black line corresponds to a tidal bundle; each gray line (below the x-axis) corresponds to the position of a composite mud drape. The volume of sediment between the composite mud drapes was deposited during a fortnightly neap-spring-neap tidal cycle. Tick mark spacing on x-axis is $n = 5$; N = neap tide, S = spring tide.

75

TIDAL BUNDLES

NEAP   SPRING   NEAP

mud drapes   mud drapes

SAND DUNE ADVANCE
(EBB TIDE DIRECTION)

salt marsh

coastal barrier

main ebb channel

flood channel

flood channel

isobath

tide-generated bedforms

EBB TIDAL DELTA

0   1   2 km

terminal

swash   platform

lobe

Potential deposition of
neap-spring-neap cycles
in distal setting

TIDAL RHYTHMITES

mud   silt   sand

SPRING

NEAP
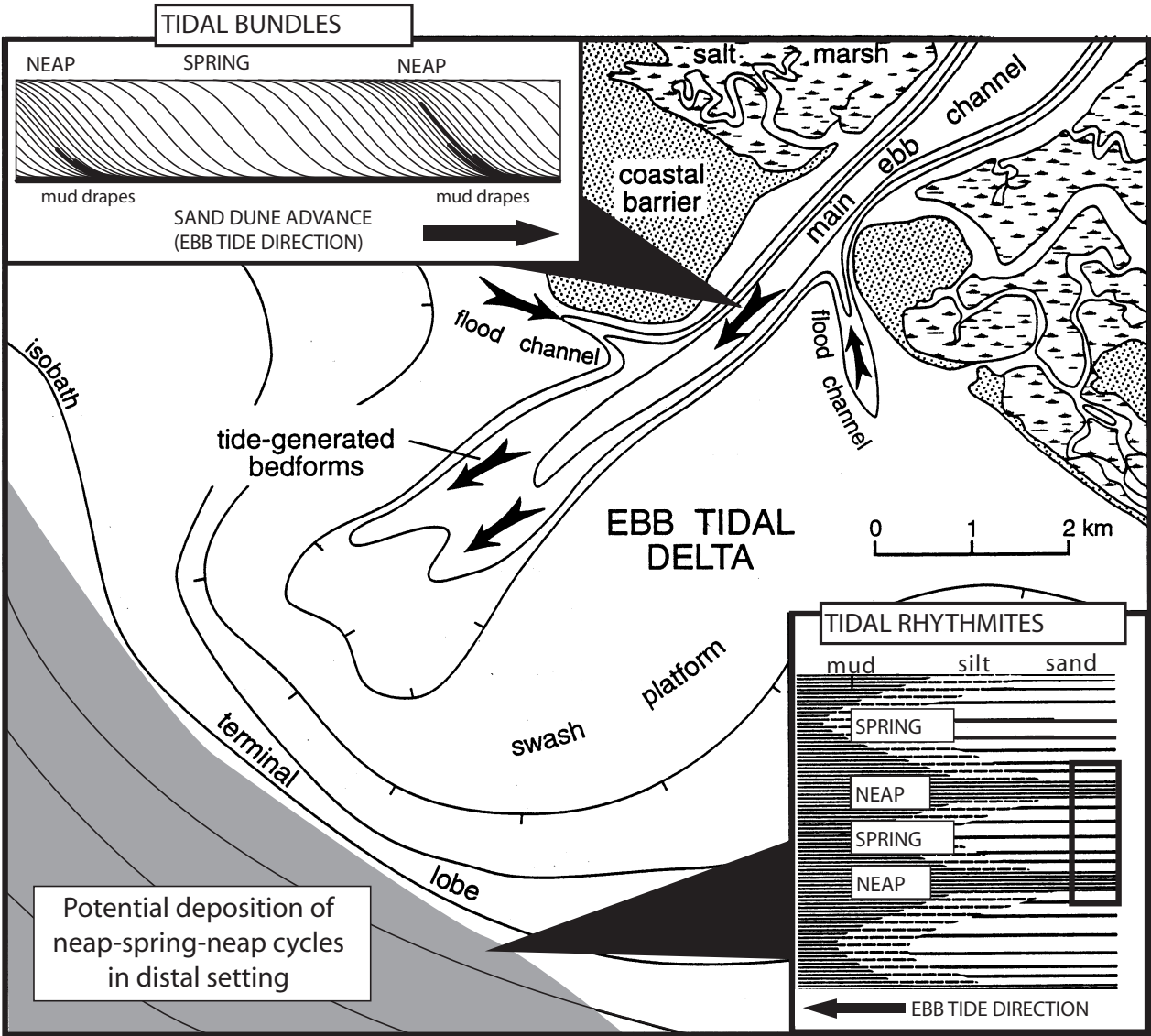
SPRING

NEAP

EBB TIDE DIRECTION

Figure 33: Coastal tidal setting for the daily deposition of sand and mud as tidal bundles and tidal rhythmites. The ebb tidal current (outgoing tide) dominates the main tidal channel, in which large sand dunes may migrate (top inset; Figure 31B). The dunes migrate the most during spring tides, which preserve thicker sandy layers known as tidal bundles. Mud will accumulate on the dunes during neap tides, which preserve mud drapes and thin sandy layers (tidal bundles). The fortnightly migration period of the dune preserves the neap-spring-neap cycle. In the quieter waters (gray region), mud and sand are deposited in thin, horizontal layers known as tidal rhythmites (bottom inset). Farthest offshore, only mud is deposited; closer in, the deposition of sand, silt, and mud is influenced by the daily tides and may preserve neap-spring-neap cycles (box in inset). Isobaths are depth contour lines. After *Williams* (2000).
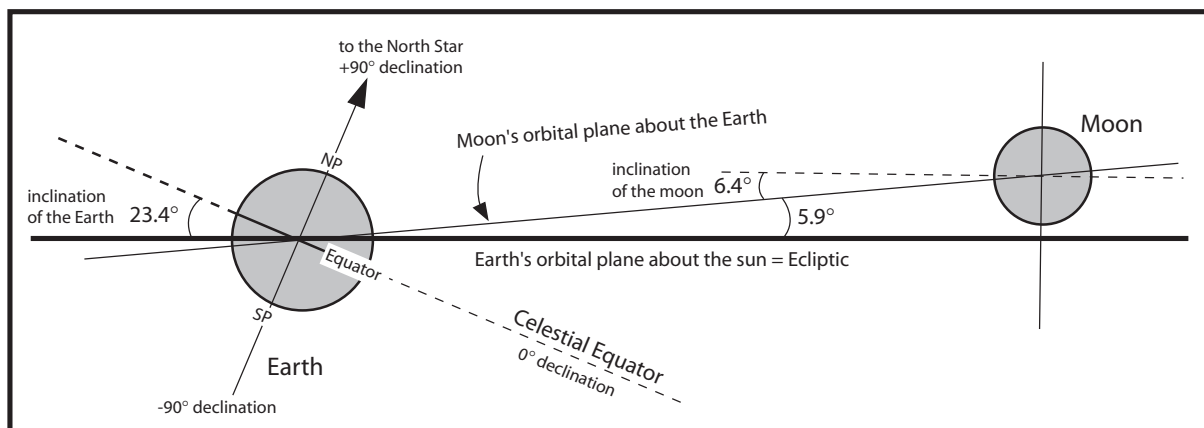
Figure 34: Declination and inclination in the earth–moon system. Declination is the angle between the object and the celestial equator. In this example, the declination of the moon is $23.4° + 5.9° = 29.3°$; the lunar declination varies over the course of the month. Inclination angles are fixed (on the monthly and yearly time scale). The inclination of the earth, or in other words, the changing declination of the sun, is the source of the seasons. Changing declinations of the sun and the moon give rise to various tidal cycles (even if the earth did not rotate).

The Semidiurnal Tidal Cycle (12 hours)

35A

EARTH (equatorial view)*

DOMINANT

MOON

SUBORDINATE

TIDAL BULGE

diurnal inequality = difference between dominant and subordinate tide

35B

Modern tides (water height)

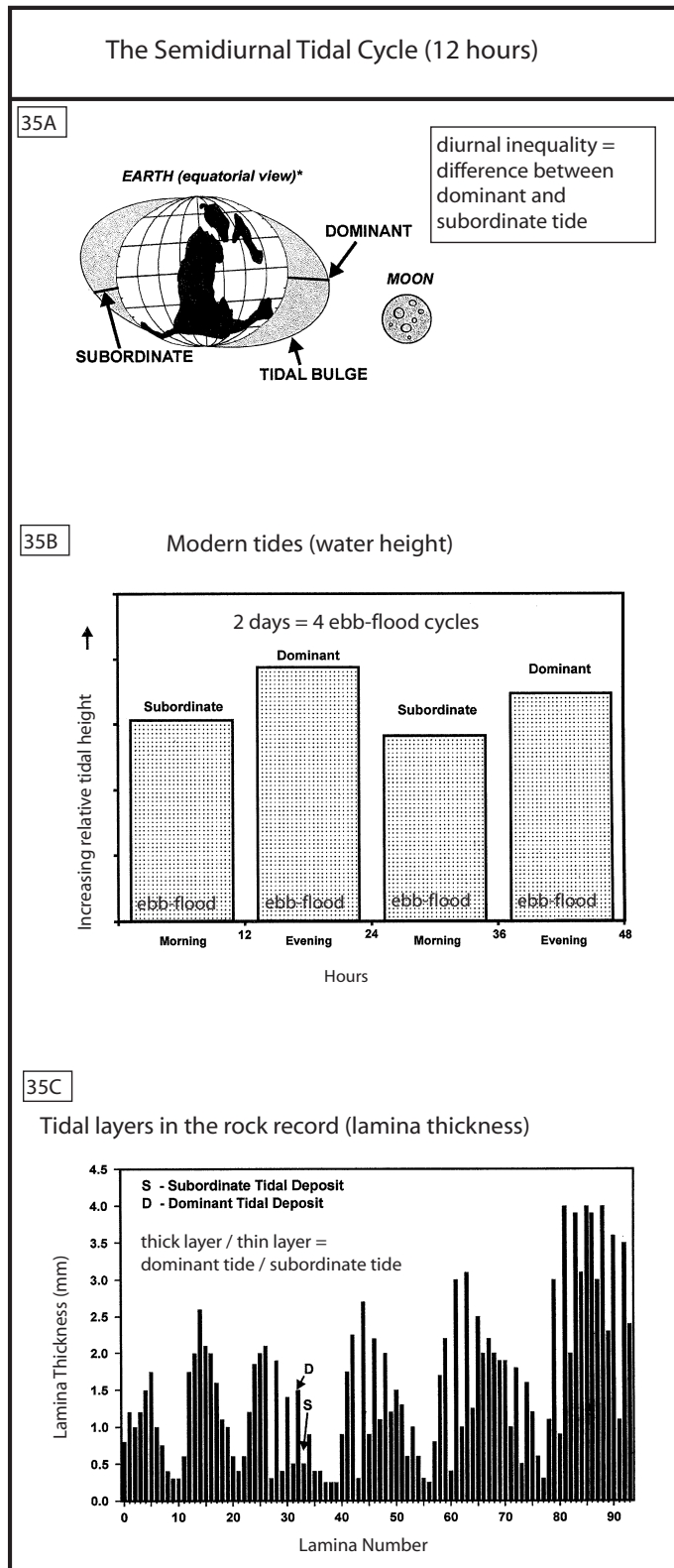2 days = 4 ebb-flood cycles

Dominant

Subordinate

Dominant

Subordinate

Increasing relative tidal height

ebb-flood   ebb-flood   ebb-flood   ebb-flood

Morning   12   Evening   24   Morning   36   Evening   48

Hours

35C

Tidal layers in the rock record (lamina thickness)

S - Subordinate Tidal Deposit
D - Dominant Tidal Deposit

thick layer / thin layer =
dominant tide / subordinate tide

Lamina Thickness (mm)

Lamina Number

Figure 35: The semidiurnal tidal cycle: evidence from modern tides and the rock record. **A**. The differential force due to the sun and the moon produce two bulges on opposite sides of the earth. **B**. The earth's daily rotation under the two tidal bulges causes the semidiurnal cycle. Because of the non-zero lunar declination, one tide (i.e., one ebb-flood cycle) tends to be higher (dominant) than the other (subordinate). **C**. Evidence of the daily cycle in the rock record, shown by the alternating thickness of 300-Ma sedimentary layers. After *Kvale et al.* (1999).
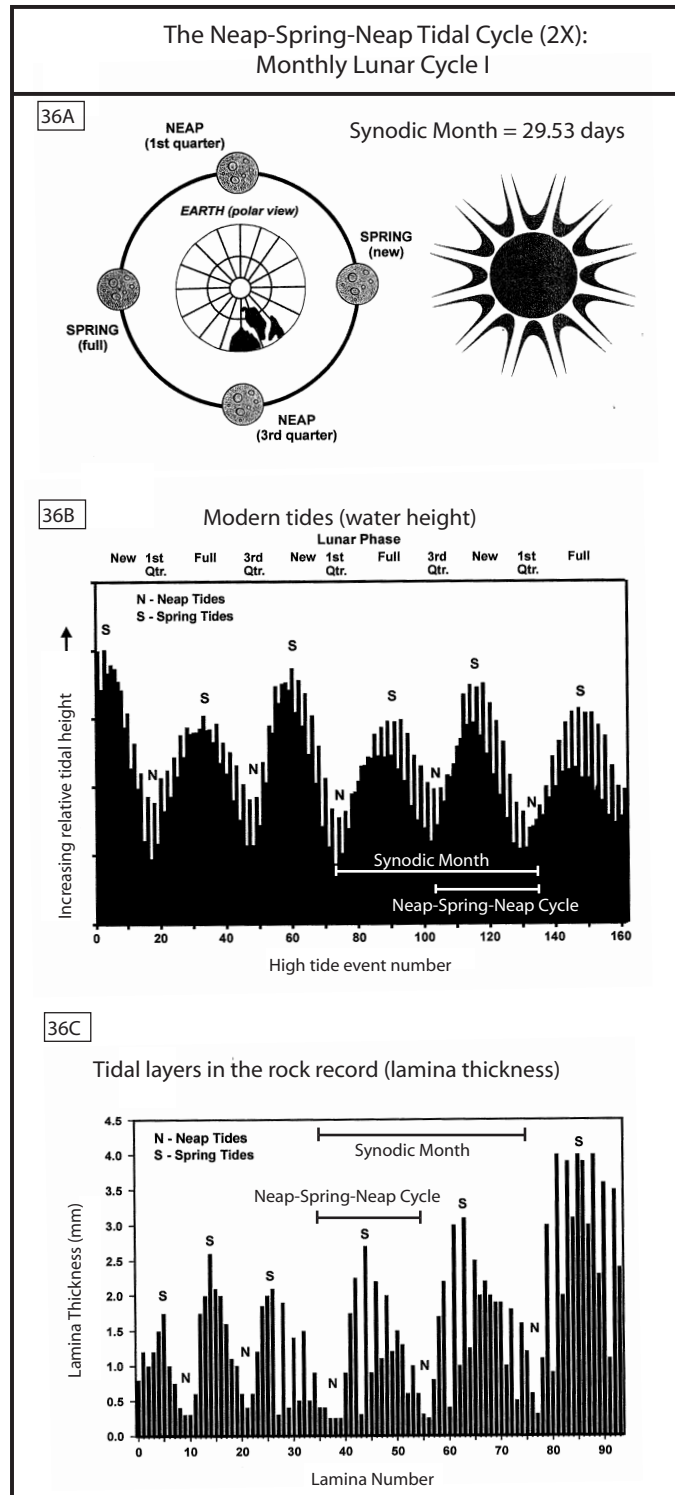
Figure 36: The neap-spring-neap tidal cycle (one half of lunar cycle I): evidence from modern tides and the rock record. There are two neap-spring-neap cycles per synodic month. **A**. Polar view of lunar orbit. Tides are highest at syzygy and lowest at quadrature (see Figure 16). **B**. Predicted high tides for Kwajalein Atoll, Pacific Ocean, showing the effects of changing lunar phase. **C**. Lamina thickness measurements, with the neap tides and spring tides labeled. Compare with Figures 36 and 37. After *Kvale et al.* (1999).
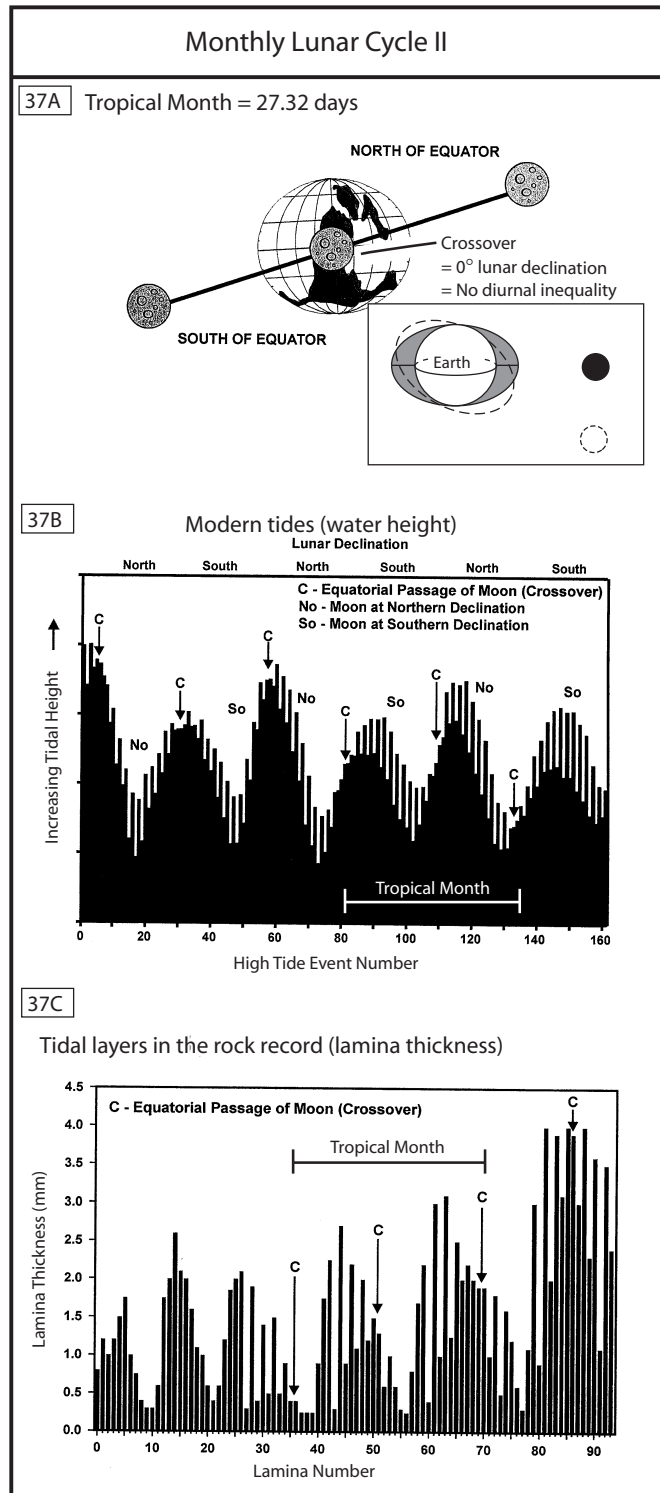
Figure 37: Monthly lunar cycle II: the tropical month. **A**. Edge-on view of the lunar orbital plane showing the moon at its extreme declinations and above the earth's equator in its lunar orbit (crossover). At crossover there is no difference between dominant and subordinate tides. **B**. Predicted high tides for Kwajalein Atoll, Pacific Ocean. Notice how the crossover position moves relative to the spring tides. **C**. Evidence of crossover in lamina thickness measurements from a sedimentary rock. After *Kvale et al.* (1999).
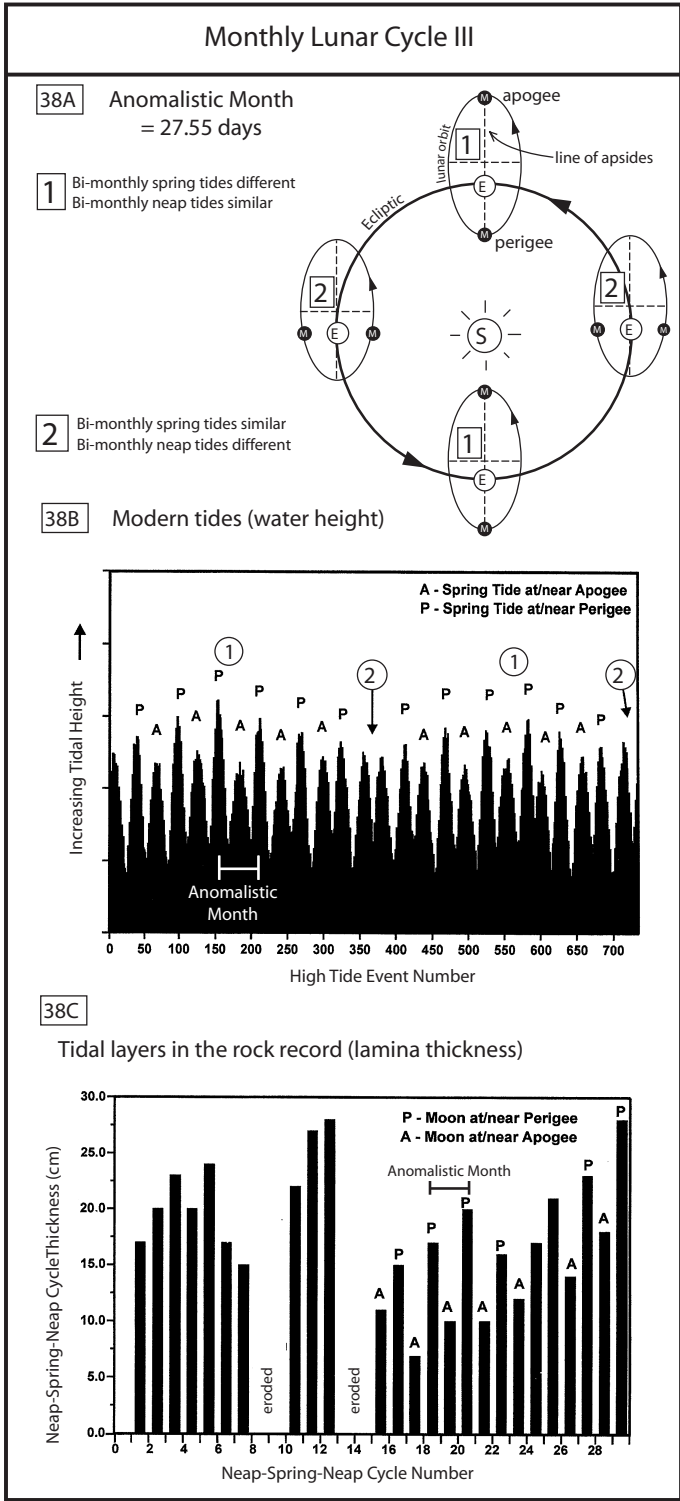
Figure 38: Monthly lunar cycle III: the anomalistic month. **A**. Polar view of the lunar orbital plane showing the moon at perigee and apogee. The tides are strongest when the moon is closest (perigee). **B**. Predicted high tides for Saint John's, New Brunswick (1991), showing the effects of several anomalistic months (see Figure 25). The pattern in the semimonthly inequality makes it possible to distinguish this from the neap-spring-neap cycle. **C**. Evidence of the phase flip from neap-spring-neap cycle thickness measurements. B and C after *Kvale et al.* (1999).
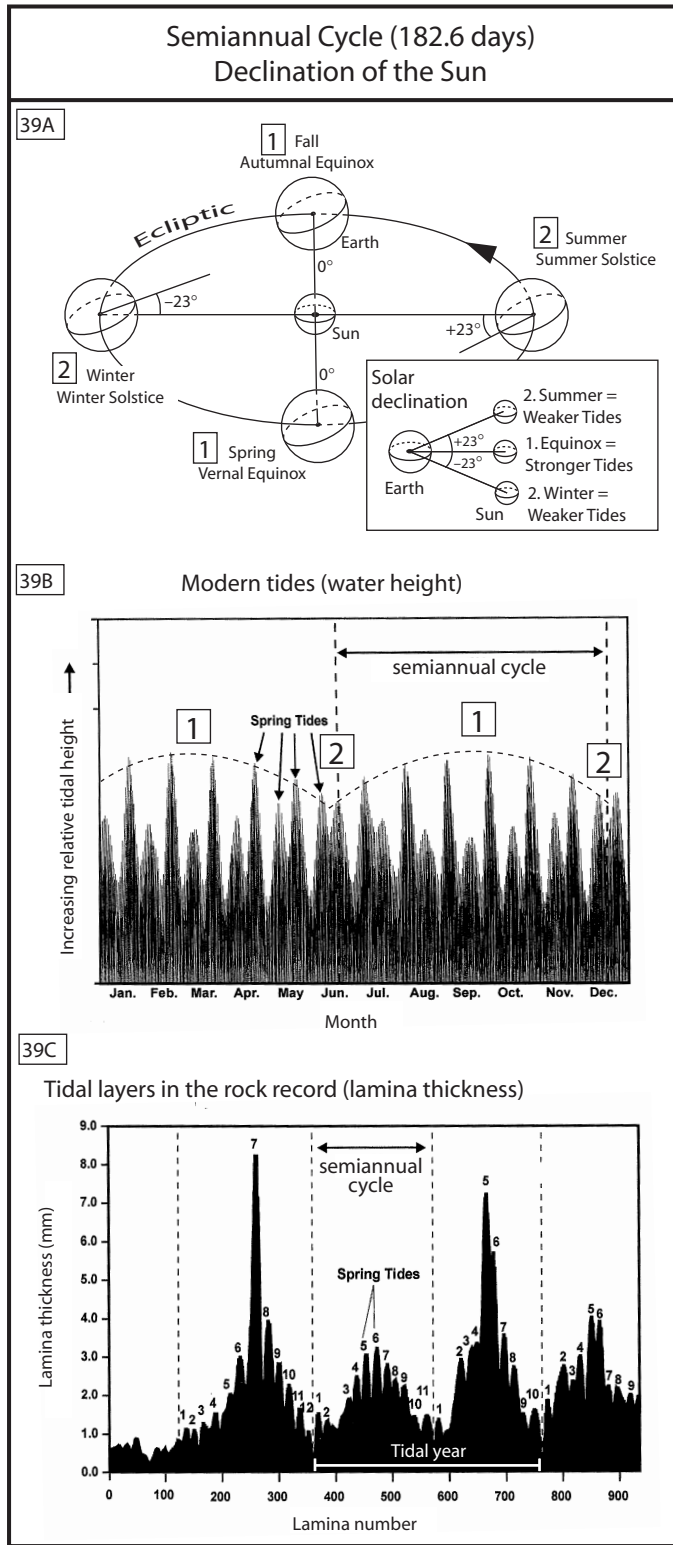
Figure 39: The semiannual cycle. **A**. The declination of the sun over the course of the year produces the semi-annual cycle (182.6 days). **B**. Predicted high tides for Saint John's, New Brunswick (1991) (see Figure 25), showing the semiannual cycle (dashed lines). The timing of the semiannual cycle is much more complicated than solar-declination-0° = highest-spring-tides, as suggested here. **C**. The semiannual cycle in the sedimentary record is more prominent than the tide charts because the volume of sediment responds as a cubic function to the water level (Figure 30A2). B and C after *Kvale et al.* (1999).
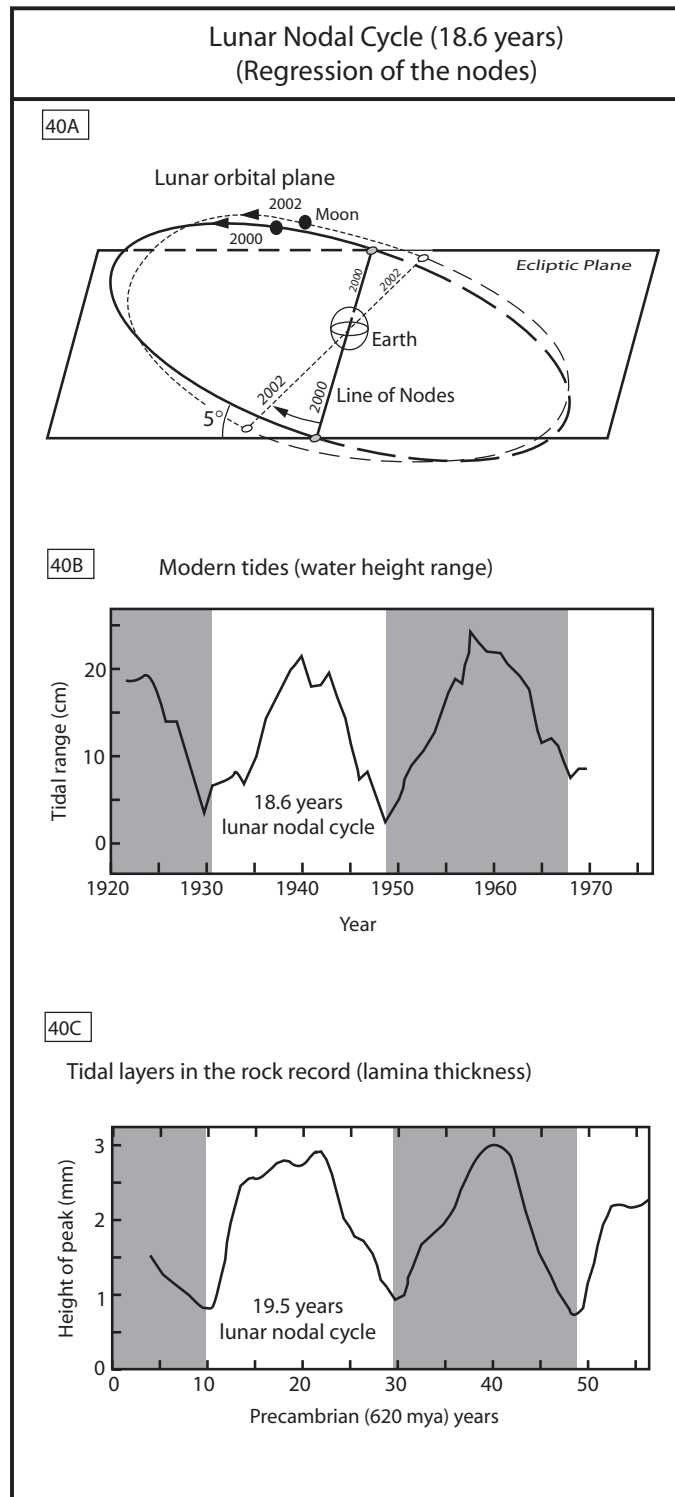
Figure 40: The lunar nodal cycle (regression of the nodes). **A**. Schematic of the regression of the nodes, which accounts for the 18.6-year lunar nodal cycle (present-day value). See also Figure 34. **B**. Annual mean tidal range for Boston for 1922–1970, which is dominated by the lunar nodal cycle. **C**. Evidence for the lunar nodal cycle from the rock record. The 60-year Elatina (620 Ma) rhythmite record reveals two complete lunar nodal cycles. Plotted here is a smoothed curve of the neap-spring-neap cycle thicknesses. B and C after *Williams* (2000).

Precambrian rocks with rhythmite layers

41E

1 neap-spring-neap tidal cycle = 13 days

N N N S S S

1 cm

1 ANNUAL OSCILLATION (of sea level) = 26 neap-spring-neap tidal cycles = 1 solar year

MONTHLY INEQUALITY of neap-spring-neap tidal cycles

41F

Apogee Perigee Apogee Perigee Apogee

N S N S N

1 ebb-flood tidal cycle = 1 day

1 NEAP-SPRING-NEAP tidal cycle = 13 days

1 cm

Neap-Spring-Neap Fortnightly Cycles

41A — Rock Record (600 mya) Lamina Thickness

annual oscillation 26.1

semiannual tidal cycle 13.1

harmonics (beats) 8.7 6.6

monthly inequality 2.15

Frequency (1/cycles): 0.00, 0.10, 0.20, 0.30, 0.40, 0.50
Period or wavelength (neap-spring cycles): 20, 10, 6, 4, 3, 2

Ebb-Flood Daily Cycles

41C — Rock Record (600 mya) Lamina Thickness

annual oscillation 333

neap-spring-neap tidal cycles 12.5 11.9 11.2 11.0

semiannual tidal cycle 159

anomalistic month (lunar ellipticity) 25.8 22.4

103

13.5 13.0 10.3

Frequency (1/laminae): 0.00, 0.05, 0.10
Period or wavelength (diurnal laminae): 100, 20, 10

41B — Modern Ocean Tides Maximum Water Height

annual oscillation 24.4

semiannual tidal cycle 12.5

monthly inequality 2.15

Frequency (1/cycles): 0.00, 0.10, 0.20, 0.30, 0.40, 0.50
Period (synodic fortnightly cycles): 20, 10, 6, 4, 3, 2

41D — Modern Ocean Tides Maximum Water Height

256 annual oscillation

neap-spring-neap tidal cycle 1/2 synodic month (lunar phase)

anomalistic month (lunar ellipticity) 26.9

1/2 tropical month (lunar declination) 13.5

semiannual tidal cycle 146

14.6

Frequency (1/days): 0.00, 0.05, 0.10
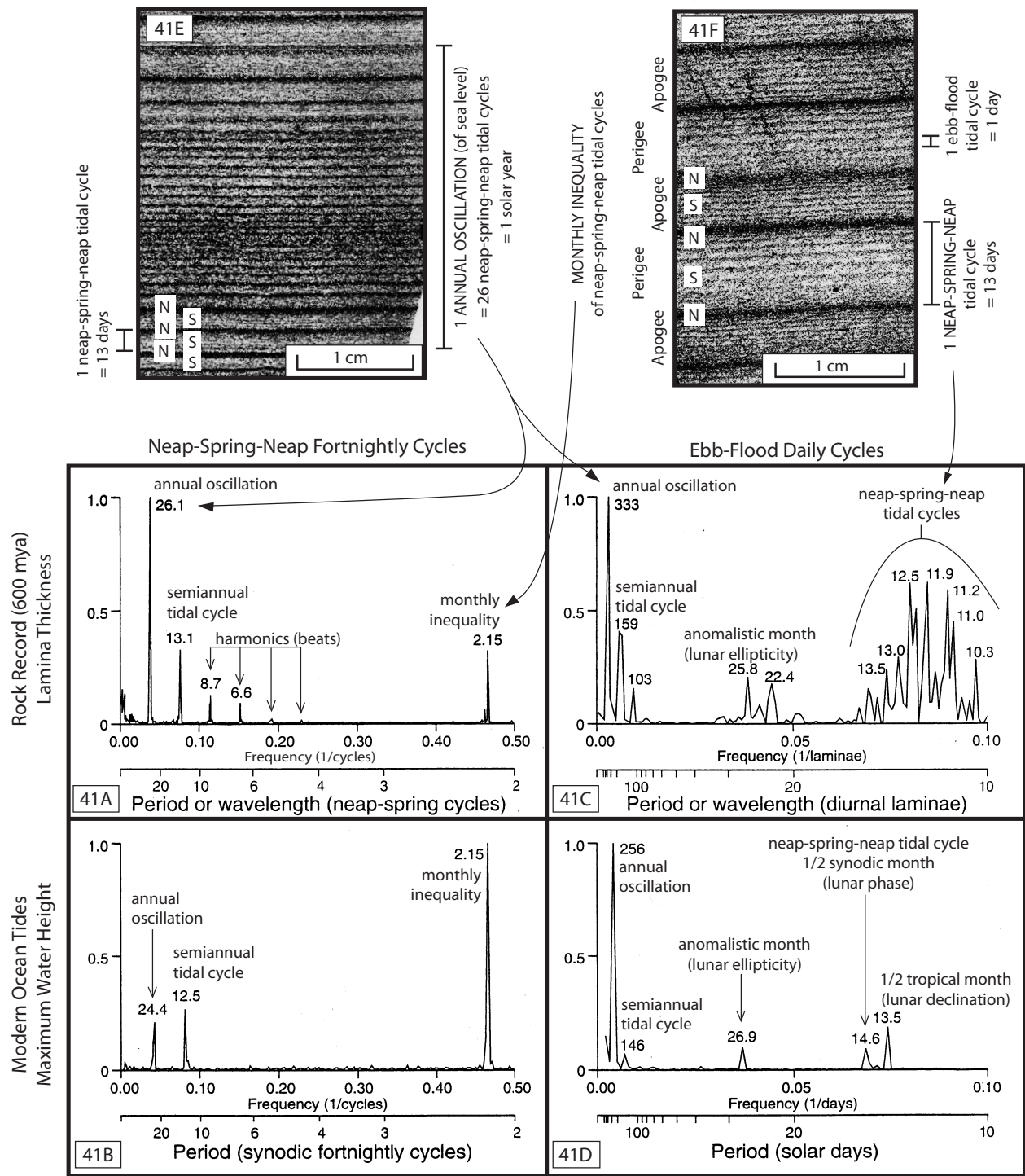Period (solar days): 100, 20, 10

Figure 41: Fourier transform spectra for ancient tidal sequence data (rock record) and modern tidal sequence data (tidal charts). Power spectral densities are normalized to unity for the strongest peak in each spectrum. Top row is data from Precambrian (ca. 620 Ma) rocks with tidal rhythmite layers (**A**, 60-year record = 1580 neap-spring-neap cycle thicknesses; **C**, 4.2-year record = 1337 diurnal lamina thicknesses); bottom row is from ocean tidal charts (**B**, 20-year record; **D**, 2.8-year record). Left column is fortnightly neap-spring-neap cycles: neap-spring-neap cycle thickness of laminae (**A**) or the average of the two highest readings for each spring tide period (**B**). Right column is daily ebb-flood cycles: diurnal laminae thickness (**C**) or the the average of the two highest daily readings (**D**). Top (**E**, **F**) shows photos of the actual rhythmite cores, corresponding to the cycles. Both the rock record and the tidal charts reveal the expected frequencies with sharp spectral peaks. See the labeled tidal cycles in Figures 36–39; see *Williams* (2000) for information on the annual oscillation. After *Williams* (2000).
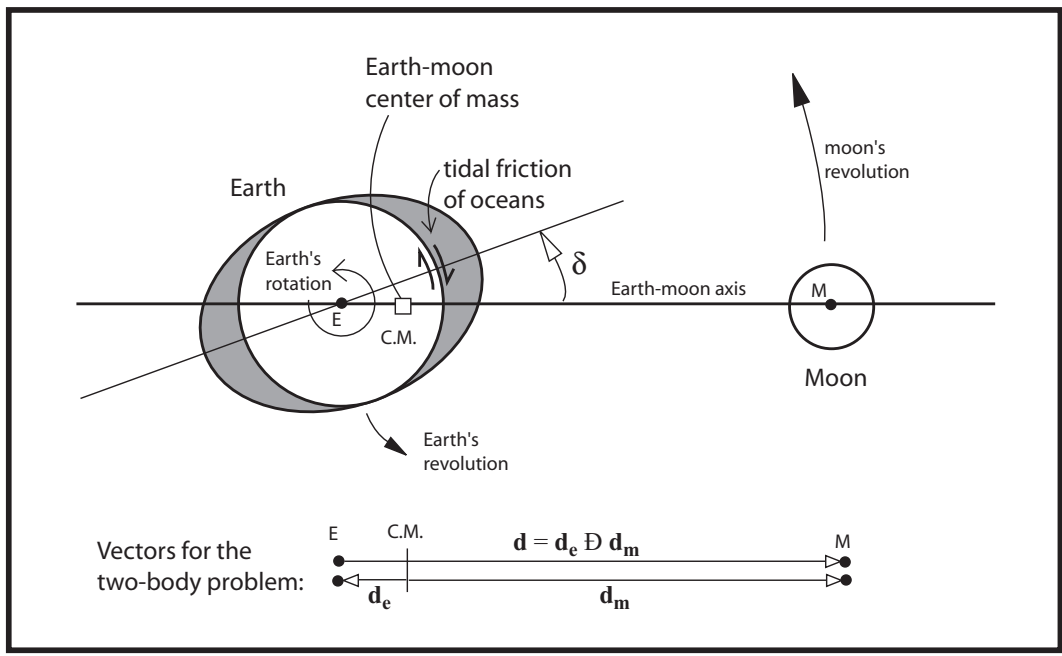
Figure 42: Conservation of angular momentum of the earth–moon system. The rotating earth spins the ocean tidal bulges in front of the earth–moon axis by an angle δ. The moon exerts a torque on the bulges, which slows the earth's rotation. The loss in the earth's rotational angular momentum is accompanied by a gain in net orbital angular momentum of the earth–moon system. See Section 5.1.
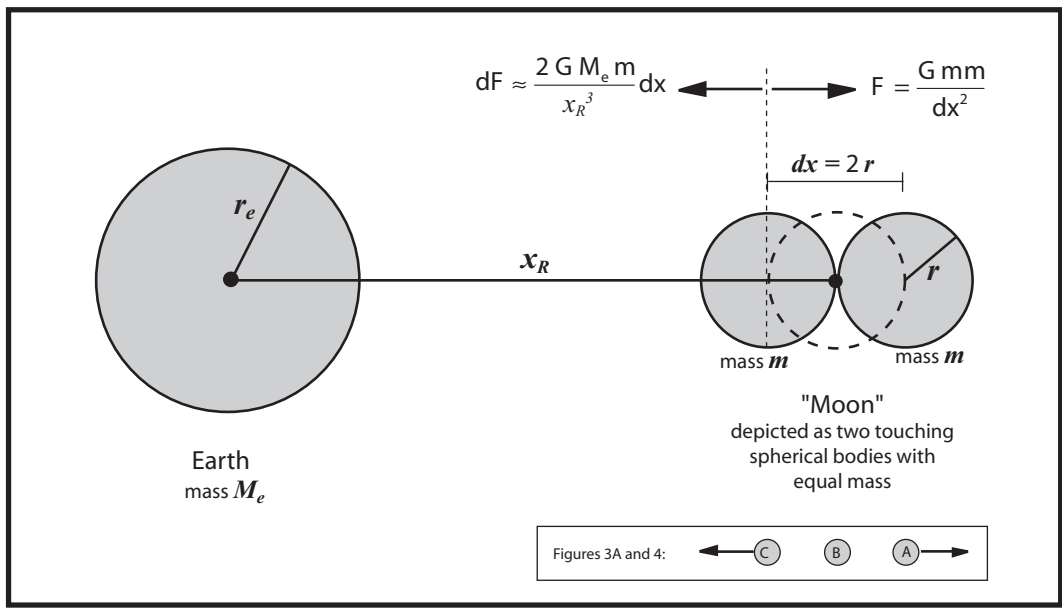

Figure 43: Configuration for determining the Roche limit. The moon is depicted as two spherical bodies touching each other. At an earth-"moon" distance of the Roche limit (x_R), the mutual gravitational attraction of the two moon-masses is equal to the differential force due to the earth. The earth exerts a greater force on the near moon-body than on the far moon-body. If the "moon" comes any closer to the earth, it will be pulled apart by the differential force, just like the balls in Figure 3A (inset). See Section 5.2.
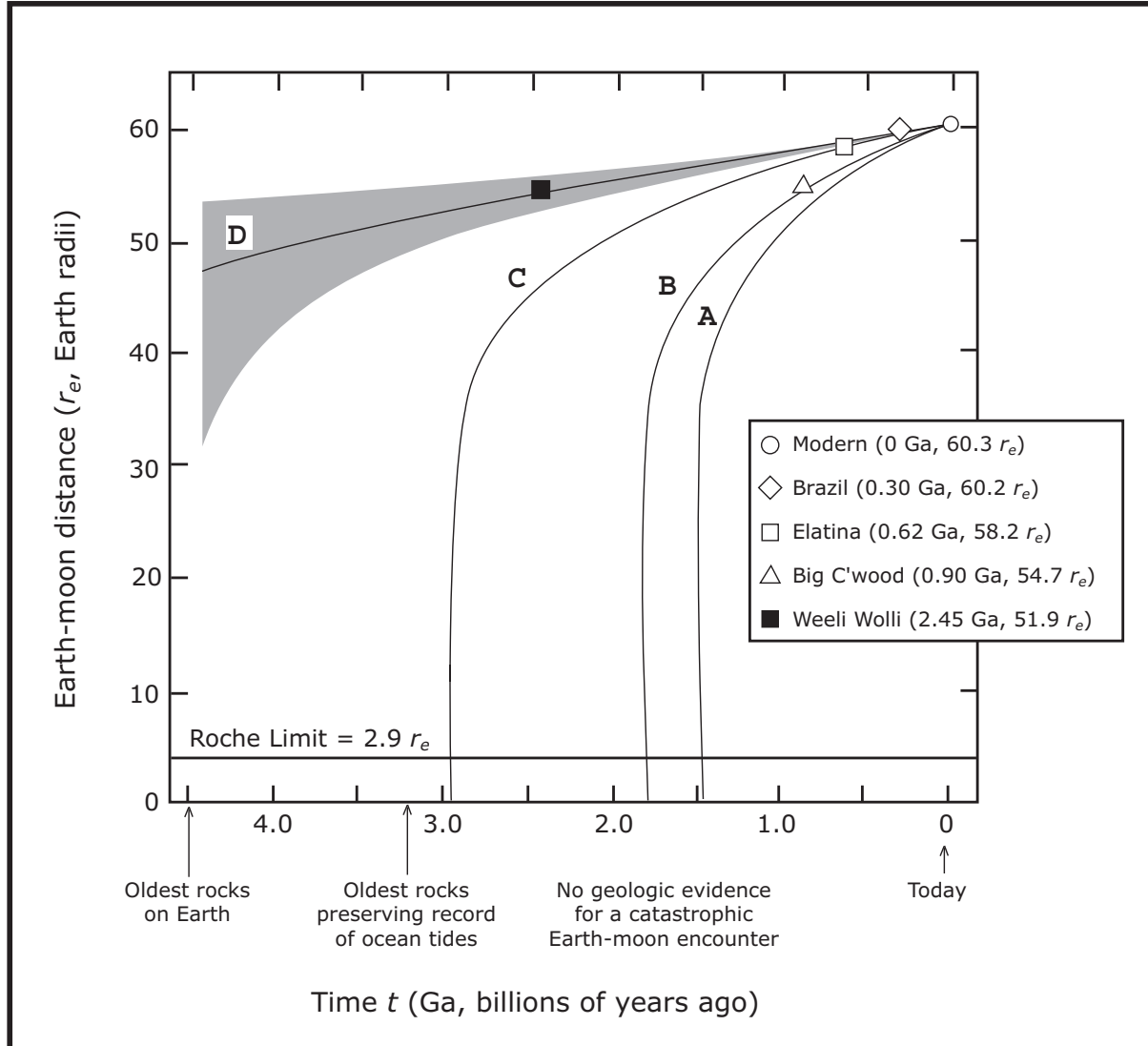
Figure 44: Earth–moon distance over the course of the earth's history, as suggested by different rates of tidal energy dissipation (after *Williams*, 2000). Four tidal energy dissipation rate curves based on geologic data combined with modern measurements. Geologic data points are from *Williams* (1989a, 2000) (□), *Sonett and Chan* (1998) (△), and *Kvale and Archer* (1990); *Kvale et al.* (1999) (◇). Curves **A**, **B**, and **C** predict a close earth–moon encounter within the last three billion years. The Roche Limit (Section 5.2) is the distance from the earth where the moon would be torn apart by differential force (Edouard Roche, 1820–1883). **A**. Curve based on the present lunar recession of 3.82 cm/yr, which is determined from interferometric laser measurements (*Dickey et al.*, 1994). **B**. Curve based on a mean lunar recession rate of 3.16 cm/yr over the past 0.5 billion years, which is determined from paleontological data (*Lambeck*, 1980); the Big Cottonwood datum coincides with this curve. **C**. Curve consistent with Elatina datum (see Figure 41). **D**. Curve consistent with Elatina datum and the preferred Weeli Wolli datum; shaded area shows the error region for the curve, based on the Weeli Wolli datum. This curve is the only one that does not predict a catastrophic close encounter between the moon and earth. See Section 5.4.
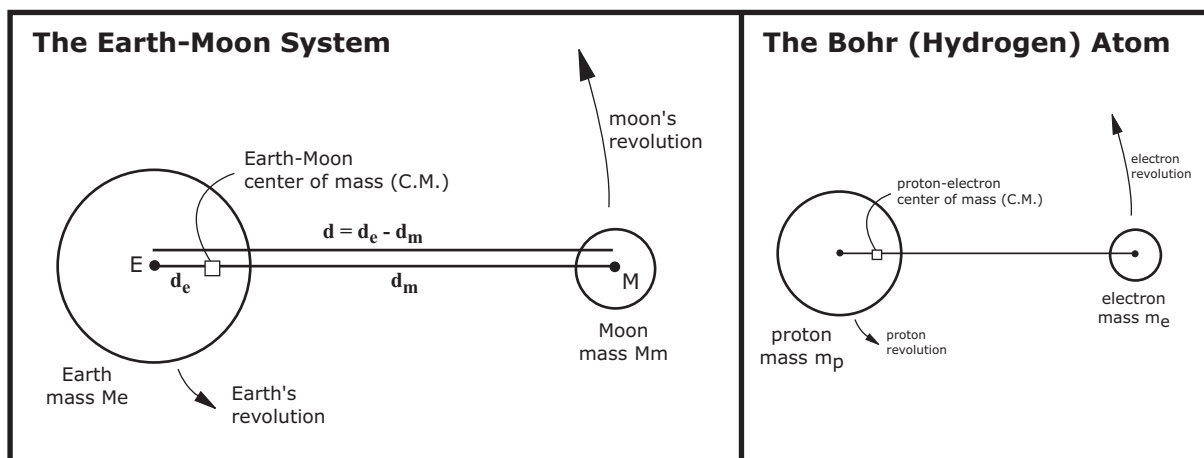
Figure 45: The two-body problem configuration. The earth and the moon, attracted by a gravitational force, revolve about a common center of mass, their period of revolution being about 28 days. The proton and the electron in the Bohr atom, attracted by an electrostatic force, revolve about a common center of mass. Relative sizes and distances are exaggerated in both cases. See Appendix B.

References

Alexander, C. R., R. A. Davis, and V. J. Henry (Eds.), *Tidalites: Processes and Products*, SEPM, Tulsa, Oklahoma, Special Publication 61, 1998.

Allen, J. R. L., Mud drapes in sand wave deposits: a physical model with application to the Folkestone Beds (early Cretaceous, southeast England), *Phil. Trans. Roy. Soc. London A, 306*, 291–345, 1982.

Allen, J. R. L., *Principles of Physical Sedimentology*, Allen and Unwin, London, 1985.

Archer, A. W., Hierarchy of controls on cyclic rhythmite deposition: Carboniferous basins of eastern and mid-continental U.S.A., in *Tidalites: Processes and Products*, edited by C. R. Alexander, R. A. Davis, and V. J. Henry, SEPM, Tulsa, Oklahoma, Special Publication 61, 1998.

Archer, A. W., and M. S. Hubbard, Highest tides of the world, in *Extreme Depositional Environments: Mega End Members in Geologic Time*, edited by M. A. Chan and A. W. Archer, pp. 151–173, Geol. Soc. Am., Boulder, Colo., Special Paper 370, 2003.

Arons, A. B., Basic physics of the semidiurnal lunar tide, *Am. J. Phys., 47*, 934–937, 1979.

Barger, V. D., and M. G. Olsson, *Classical Mechanics: A Modern Perspective*, McGraw-Hill, New York, 1973.

Bose, P. K., R. Mazumder, and S. Sarkar, Tidal sandwaves and related storm deposits in the transgressive Protoproterozoic Chaibas Formation, India, *Precambrian Res., 84*, 63–81, 1997.

Byers, C. W., and R. H. Dott Jr., Sedimentology and depositional sequences of the Jordan Formation (Upper Cambrian), northern Mississippi Valley, *J. Sed. Res., B65*, 289–305, 1995.

Chan, M. A., E. P. Kvale, A. W. Archer, and C. P. Sonett, Oldest direct evidence of lunar-solar tidal forcing encoded in sedimentary rhythmites, *Geology, 22*, 791–794, 1994.

Chapman, S., and R. S. Lindzen, *Atmospheric Tides: Thermal and Gravitational*, Reidel, Dordrecht, The Netherlands, 1970.

Clark, S., Epeiric tides, Undergraduate thesis, Carleton College Geology Dept., Northfield, Minnesota, 25 p., 1982.

Condie, K. C., *Plate Tectonics and Crustal Evolution*, Butterworth Heinemann, Oxford, 1997.

Cook, A. H., *Gravity and the Earth*, Wiley, New York, 1969.

Crawford Jr., F. S., *Waves*, McGraw-Hill, New York, 1968.

Dalrymple, R. W., Tidal depositional systems, in *Facies Models: Response to Sea Level Change*, edited by R. G. Walker and N. P. James, pp. 195–218, Geol. Assoc. Canada, 1992.

Danby, J. M. A., *Fundamentals of Celestial Mechanics*, 2 ed., Willmann-Bell, Richmond, Virginia, 1988.

Darwin, G. H., *The Tides and Kindred Phenomena in the Solar System*, John Murray, London, 1898.

Desplanque, C., and D. J. Mossman, Bay of Fundy tides, *Geosci. Can., 28*, 1–10, 2001.

Dickey, J. O., et al., Lunar laser ranging: A continuing legacy of the Apollo program, *Science, 265*, 482–490, 1994.

Dott Jr. , R. H., and R. L. Batten, *Evolution of the Earth*, McGraw-Hill, New York, 1981.

Dronkers, J. J., *Tidal Computations in Rivers and Coastal Waters*, North-Holland Pub., Amsterdam, 1964.

Eriksson, K. A., and E. L. Simpson, Quantifying the oldest tidal record: The 3.2 Ga Moodies Group, Barberton Greenstone Belt, South Africa, *Geology, 28*, 831–834, 2000.

Fenies, H., A. de Resseguier, and J. P. Tastet, Intertidal clay-drape couplets (Gironde estuary, France), *Sedimentology*, *46*, 1–15, 1999.

Fowles, G. R., *Analytical Mechanics*, Holt, Rinehart, and Winston, New York, 1962.

French, R., and F. Greenaway (Eds.), *Science in the Early Roman Empire: Pliny the Elder, his Sources and Influence*, Croom Helm, London, 1986.

Gamow, G., *The Tides*, Anchor Books, Garden City, New York, 1962.

Garrison, T., *Oceanography: An Invitation to Marine Science*, 3 ed., Wadsworth, Belmont, Calif., 1998.

Good, R. H., Tides and densities, *Am. J. Phys.*, *44*, 793–794, 2000.

Griffiths, D. J., *Introduction to Electrodynamics*, 3 ed., Prentice Hall, Upper Saddle River, New Jersey, 1999.

Harper, C., *Introduction to Mathematical Physics*, Prentice-Hall, Englewood Cliffs, New Jersey, 1976.

Harrison, J. C. (Ed.), *Earth Tides*, Van Nostrand Reinhold, New York, 1985.

Hartmann, W. K., *Moons & Planets*, 4 ed., Wadsworth, Belmont, Calif., 1999.

Horsfield, E., Cause of the earth tides, *Am. J. Phys.*, *44*, 793–794, 1976.

Irwin, M. L., General theory of epeiric clear water sedimentation, *Am. Assoc. Petroleum Geol. Bull.*, *49*, 445–459, 1965.

Kaufmann III, W. J., and R. A. Freedman, *Universe*, 6 ed., Freeman, New York, 1999.

Keulegan, G. H., and W. C. Krumbein, Stable configuration of bottom slope in a shallow sea and its bearing on geological processes, *Trans. Am. Geophys. Union*, *30*, 855–861, 1949.

Kibble, T. W. B., *Classical Mechanics*, 3 ed., Longman Scientific, Harlow, England, 1985.

Korgen, B. J., Seiches, *Am. Sci.*, *83*, 330–341, 1995.

Kvale, E. P., and A. W. Archer, Tidal deposits associated with low-sulfur coals, Brazil Fm. (Lower Pennsylvanian), Indiana, *J. Sed. Petrology*, *60*, 563–574, 1990.

Kvale, E. P., A. W. Archer, and H. R. Johnson, Daily, monthly, and yearly tidal cycles within laminated siltstones of the Mansfield Formation (Pennsylvanian) of Indiana, *Geology*, *17*, 365–368, 1989.

Kvale, E. P., H. R. Johnson, C. P. Sonett, A. Archer, and A. Zawistoski, Calculating lunar retreat rates using tidal rhythmites, *J. Sed. Res.*, *69*, 1154–1168, 1999.

Lamb, H., *Hydrodynamics*, 6 ed., Dover, New York, 1945.

Lambeck, K., *The Earth's Variable Rotation: Geophysical Causes and Consequences*, Cambridge U. Press, New York, 1980.

Marchuk, G. I., and B. A. Kagan, *Ocean Tides: Mathematical Models and Numerical Experiments*, Pergamon Press, Oxford, UK, 1984.

Marchuk, G. I., and B. A. Kagan, *Dynamics of Ocean Tides*, Kluwer, Dordrecht, The Netherlands, 1989.

Marion, J. B., and S. T. Thorton, *Classical Dynamics of Particles and Systems*, 4 ed., Saunders, Forth Worth, Texas, 1995.

Melchior, R., *The Earth Tides*, Pergamon, Oxford, 1966.

Misner, C. W., K. S. Thorne, and J. A. Wheeler, *Gravitation*, Freeman, San Francisco, Calif., 1973.

Newton, I., *The Principia: Mathematical Principles of Natural Philosophy*, U. Calif. Press, Berkeley, Trans. I. B. Cohen and A. Whitman (1999), 1687.

Nio, S. D., and C. S. Yang, Diagnostic attributes of clastic tidal deposits: a review, in *Clastic Tidal Sedimentology*, edited by D. G. Smith, G. E. Reinson, B. A. Zaitlin, and R. A. Rahmani, pp. 3–28, Can. Soc. Petroleum Geologists, Memoir 16, 1991.

Ohanian, H. C., *Gravitation and Spacetime*, 1 ed., Norton, New York, 1976.

Olson, D. W., and T. E. Lytle, Tidal forces on May 5, 2000, *Sky & Telescope*, pp. 109–111, 2000.

Pugh, D. T., *Tides, Surges, and Mean Sea-Level: A Handbook for Engineers and Scientists*, Wiley, New York, 1988.

Reineck, H.-E., and I. B. Singh, *Depositional Sedimentary Environments with Reference to Terrigenous Clastics*, 2 ed., Springer Verlag, Berlin, 1980.

Rosenburg, G. D., How long was the day of the dinosaur? And why does it matter?, in *Dinofest International: Proceesings of a Symposium Sponsored by Arizona State University*, edited by D. L. Wolberg, E. Stump, and G. D. Rosenburg, pp. 493–512, The Academy of Sciences, Philadelphia, Penn., 1997.

Runkel, A. C., Deposition of the uppermost Cambrian (Croixan) Jordan Sandstone, and the nature of the Cambrian-Ordovician boundary in the Upper Mississippi Valley, *Geol. Soc. Am. Bull.*, *106*, 492–506, 1994.

Schureman, P., *Manual of Harmonic Analysis and Prediction of Tides*, U.S. Gov. Printing Office, Washington, D.C., 1941.

Seligmann, P., and M. Steinberg, Simple hydrodynamic treatment of ocean tides, *Am. J. Phys.*, *43*, 1106–1108, 1975.

Sonett, C. P., and M. A. Chan, Neoproterozoic Earth-Moon dynamics: Rework of the 900 Ma Big Cottonwood Canyon tidal rhythmites, *Geophys. Res. Letters*, *25*, 539–542, 1998.

Sonett, C. P., E. P. Kvale, A. Zakharian, M. A. Chan, and T. M. Demko, Late Proterozoic and Paleozoic tides, retreat of the Moon, and rotation of the Earth, *Science*, *273*, 100–104, 1996.

Stacey, F. D., *Physics of the Earth*, 3 ed., Brookfield, Brisbane, Australia, 1992.

Strahler, A. N., *The Earth Sciences*, Harper & Row, New York, 1971.

Symon, K. R., *Mechanics*, 2 ed., Addison-Wesley, Reading, Mass., 1961.

Taff, L. G., *Celestial Mechanics*, Wiley, New York, 1985.

Tape, C. H., C. A. Cowan, and A. C. Runkel, Tidal bundle sequences in the Jordan Sandstone (Upper Cambrian) at Homer, Minnesota, in *Stratigraphy and Sedimentology of Cambrian Strata in West Central Wisconsin and Southeastern Minnesota: Field Trip Guidebook for the 30th Annual Meeting of the Great Lakes Section of the Society for Sedimentary Geology, Sept 23, 2000*, edited by K. G. Havholm, J. B. Mahoney, and A. C. Runkel, pp. 47–55, 2000.

Tape, C. H., C. A. Cowan, and A. C. Runkel, Tidal-bundle sequences in the Jordan Sandstone (Upper Cambrian), southeastern Minnesota, U.S.A.: Evidence for tides along inboard shorelines of the Sauk epicontinental sea, *J. Sed. Res.*, *73*, 354–366, 2003.

Taylor, J. R., and C. D. Zafiratos, *Modern Physics for Scientists and Engineers*, Prentice Hall, Englewood Cliffs, New Jersey, 1991.

Tipler, P. A., *Physics for Scientists and Engineers*, 3 ed., Worth, New York, 1991.

Tsantes, E., Note on the tides, *Am. J. Phys.*, *42*, 330–333, 1974.

Visser, M. J., Neap-spring cycles reflected in Holocene subtidal large-scale bedform deposits: a preliminary note, *Geology*, *8*, 543–546, 1980.

Volland, H., *Atmospheric Tidal and Planetary Waves*, Kluwer, Dordrecht, The Netherlands, 1988.

Walker, J. C., and K. J. Zahnle, Lunar nodal tide and distance to the moon during the Precambrian, *Nature*, *320*, 600–602, 1986.

Wells, M. R., P. A. Allison, G. J. Hampson, M. D. Piggott, and C. C. Pain, Modelling ancient tides: the Upper Carboniferous epi-continental seaway of Northwest Europe, *Sedimentology*, *52*, 715–735, 2005.

White, G., T. Mondragon, D. Slaughter, and D. Coates, Modelling tidal effects, *Am. J. Phys.*, *61*, 367–370, 1993.

Wilhelm, H., W. Zürn, and H.-G. Wenzel (Eds.), *Tidal Phenomena*, Springer-Verlag, Berlin, 1997.

Williams, G., Geological constraints on the Precambrian history of earth's rotation and the moon's orbit, *Rev. Geophysics*, *38*, 37–59, 2000.

Williams, G. E., Sunspot periods in the late Precambrian glacial climate and solar-planetary relations, *Nature*, *291*, 624–628, 1981.

Williams, G. E., Solar affinity of sedimentary cycles in the late Precambrian Elatina Formation, *Aust. J. Phys.*, *38*, 1027–1043, 1985.

Williams, G. E., Late Proterozoic tidal rhythmites in South Australia and the history of the earth's rotation, *J. Geol. Soc. London*, *146*, 97–111, 1989a.

Williams, G. E., Precambrian tidal sedimentary cycles and Earth's paleorotation, *Trans. Am. Geophys. Union*, *70*(3), 33,40–41, 1989b.

Wong, C. W., *Introduction to Mathematical Physics*, Oxford U. Press, New York, 1991.

Zeilik, M., and E. v. P. Smith, *Introductory astronomy and astrophysics*, Saunders College Pub., Philadelphia, Penn., 1987.